A Study of Gas Streaming in Deep Fluidized Beds

By

Shayan Karimipour

A Thesis Submitted to the College of

Graduate Studies and Research

In Partial Fulfillment of the Requirements

For the Degree of Doctor of Philosophy

In the Department of Chemical Engineering

The University of Saskatchewan

Saskatoon

Permission to Use

In presenting this thesis in partial fulfillment of the requirements for a Postgraduate degree from the University of Saskatchewan, I agree that the Libraries of this University may make it freely available for inspection. I further agree that permission for copying of this thesis in any manner, in whole or in part, for scholarly purposes may be granted by the professor who supervised my thesis work or, in his absence, by the Head of the Department or the Dean of the College in which my thesis work was done. It is understood that any copying or publication or use of this thesis or parts thereof for financial gain shall not be allowed without my written permission. It is also understood that due recognition shall be given to me and to the University of Saskatchewan in any scholarly use which may be made of any material in my thesis.

Requests for permission to copy or to make other use of material in this thesis in whole or part should be addressed to:

Head of the Department of Chemical Engineering

The University of Saskatchewan

Saskatoon, Saskatchewan S7N 5A9

Canada

Abstract

Recent studies have shown that, in a sufficiently deep gas-solid fluidized bed of Geldart A particles, gas streaming may occur causing gas to bypass a large portion of the particle bed. Since this is a newly observed phenomenon in fluidized beds, there is uncertainty and lack of information about the various aspects of the streaming flow. The objective of the current project was to investigate the streaming phenomenon with a combination of experimentation and modeling. In the experimental part, pressure fluctuations as a measure of the fluidized bed hydrodynamics were used to study the influence of different parameters on the behavior of a deep fluidized bed. Pressure fluctuations have been measured at 8 axial locations from 4 to 150 cm above the gas distributor for bed depths and gas velocities ranging from 0.4 to 1.6 m and 0.04 to 0.20 m/s (equal to 10 to 50 times minimum fluidization velocity), respectively. Two particle size distributions with Sauter mean diameters of 48 μm and 84 μm and two distributor plates with differing percentage open area were also tested for each bed depth and gas velocity. Analysis of pressure fluctuations in the time and frequency domains, in combination with visual observations revealed that streaming flow emerges gradually at bed depths greater than 1 m. Increased gas velocity and fines content act to delay the onset of streaming, but can not completely eliminate it over the range of velocities examined. The two different distributor designs had no measurable effect on the streaming flow. The results of this study are provided in the first chapter of the present report.

In order to further investigate the nature of streaming flow, several known cases, including a forced stream (imposing a stream flow by cutting a side of distributor) and

jetting flows (60 m/s and 31 m/s) were designed and conducted, in addition to the natural streaming flow in deep beds. Results indicated that the natural streaming most closely resembles the case of imposed stream in the bed with the presence of primary gas flow through the distributor. The case of jet flows with no additional gas resembles the severe streaming that might happen in very deep beds with the existence of completely non-fluidized regions. Application of supporting jets in addition to the main gas flow could enhance the fluidization quality to some extent, however, not enough to provide a normal fluidization. Wavelet analysis of the pressure fluctuations showed that in deep fluidized beds, bubbling activity with a dominant frequency approximately the same as the typical value reported in the literature (3-4 Hz) coexist with the streaming flow, although with a minor contribution. Wavelet findings suggested that the streaming flow can be considered to form by increasing the relative importance of one of the available stream of bubbles compared to others with increasing bed depth. The results of this study are provided in the second chapter of this report.

Further study of streaming flow was undertaken with computational fluid dynamic (CFD) simulation of the deep fluidized bed. CFD simulation of fine Geldart A particles has met with challenges in the open literature and various modifications have been proposed to be able to model fluidized beds of these particles. In the present work, the commercial CFD codes FLUENT and MFIX were initially tested for the modeling of deep fluidized bed of Geldart A particles. However, simulation results did not show any sign of streaming flow in the fluidized bed. Subsequently, the commercial CFD code BARRACUDA^{TM} that has been claimed by the developers to be appropriate for this purpose, was tested. Due to the

lack of data on the performance of this code, a simple case of modeling a freely bubbling fluidized bed of Geldart A particles was attempted first. For this purpose, four different simulation cases, which included three different numerical grid sizes and two drag models with a realistic particle size distribution were designed and tested. The simulated bed expansion, bubble size distribution, rise velocity and solid fraction were compared with commonly accepted correlations and experimental data from the literature. The results showed a promising predictive capability of the code without the need for modifying the drag model or other constitutive relations of the model. The third chapter of the report presents the simulation results of this study.

The BARRACUDA code was then used for simulating the deep fluidized bed of Geldart A particles. However, similar to the previous CFD codes tested, instead of streaming flow, bubbling fluidization was predicted. Therefore, a phenomenological model was developed to better understand streaming flow. It was assumed that the deep bed is comprised of two streaming and non-streaming zones. According to the model results, the stream represents a zone of much lower pressure drop compared to other parts of the bed, which can be a possible reason for the formation and stability of the streaming flow inside the fluidized bed. The model results showed that increasing the bed depth enhances the streaming flow, while increasing the gas velocity improves the uniformity of the bed and decreases the streaming severity. Streaming flow was found to be less severe for larger particle sizes. All of these trends agree with experimental findings. These findings provide the content of the fourth and final chapter of this report.

Acknowledgements

The completion of my PhD program would not have been possible without invaluable support and guidance of my supervisor, Prof. Todd Pugsley who truly believed in my potential and provided me with opportunities throughout my research and endeavors. I would like to express my sincere gratitude to him.

I would like to thank all of my friends in the Chemical Engineering Department of the University of Saskatchewan, specially my colleagues Zhiguo Wang and Mike Wormsbecker, who enriched my learning by sharing their wealth of knowledge with me.

I recognize and appreciate the assistance of the support staff and faculty at the Department of Chemical Engineering, specially my committee members, Profs: G. Hill, M. Nemati, A. Phoenix, and Prof. R. Johanson from the Department of Electrical Engineering for their valuable advices and proficiency in keeping me on track.

Financial support from the University of Saskatchewan is also gratefully acknowledged.

Table of Contents

List of Tables

List of Figures

CHAPTER 1 – Introduction

Contribution to Overall Study

This chapter provides insight regarding fluidization and the relevant theory related to this thesis. First, the concept of fluidization is explained along with its importance to the chemical process industry. Second, the chapter then goes on to present fundamental fluidization theory and its relevance to the present study. Finally, the motivation of this thesis is presented, along with the underlying objectives.

1.1. Fluidization

The Winkler coal gasifier can be considered as the first large scale industrial application of fluidized bed technology; the gasifier was first operated in 1926 (Kunii and Levenspiel, 1991). The single largest application of fluidized bed technology is the Fluid Catalytic Cracking (FCC) process. FCC originated from a collaboration between Standard Oil engineers (now Exxon) and two Massachusetts Institute of Technology (MIT) professors in 1942 (Wilson, 1997). The FCC process cracks heavier crude oil fractions into lighter, value-added products in the gasoline boiling range. Today, fluidized beds have found many applications in physical and chemical industrial processes. Some

of the major physical applications include drying of powders, granulation, dust/particle filtration, coating of pharmaceutical tablets, heat exchangers, boilers, and adsorption (Pain et al., 2001). The applications where the solid acts as catalyst or heat sink, such as in oil cracking for manufacturing of various chemical substances, production of different polymeric material, and those where solids undergo a phase change, such as in coal combustion or coal gasification are some examples of chemical applications of fluidized beds (Lim et al., 1995). Fluidized beds are used in the chemical process industries mostly because of the excellent gas-solid contacting, which greatly enhances the chemical reactions and heat and mass transfer (Kuipers et al., 1992).

1.1.1. Fluidization Regimes

When a fluid enters a vessel containing a bed of solid particles, different contact regimes can be established in the vessel (Kunii and Levenspiel, 1991). These regimes are arranged tentatively in order of increasing the superficial gas velocity. Fig. 1.1 presents a regime diagram illustrating those regimes. At very low fluid velocities, the fluid percolates through the void spaces (interstices) between particles without disturbing the bed and no visual change in the state of the bed occurs. With increasing fluid velocity, the solids start to vibrate but still maintain the same height as the bed at rest. This is called a fixed bed. In the fixed bed the particles are in direct contact with each other, supporting each other's weight. If the increase in velocity continues, the bed expands and particles remain suspended in a way that the drag force imparted by the upward fluid is equal to the weight of the particles. This is known as minimum fluidization. The state of the system has some fluid-like properties and is called a *fluidized bed*.

After the minimum fluidization, the behavior of a fluidized bed differs depending whether the fluid is a gas or liquid. In liquid-solid systems, a smooth progressive expansion of the bed occurs in which large scale instabilities and heterogeneities such as formation of bubbles are not observed. This behavior is typically observed when the fluid and solids have similar densities. In gas-solid systems, the appearance of bubbles imposes a great deal of instability in the system after minimum fluidization. This is called the bubbling regime. It should be mentioned that in group A particles there is a short period of bed expansion without formation of bubbles until the velocity at which bubble first appear (minim bubbling velocity) is reached.

If the bed is sufficiently deep and the column diameter is small, the bubbles may coalesce and create bubbles as large as the vessel diameter with the solid particles flowing down as a thin layer near the vessel wall. This is known as the slugging regime (Kunii and Levenspiel, 1991). If the particles are fluidized at a high enough gas flowrate, the upper surface of the bed disappears and, instead of bubbles, a turbulent motion of solid clusters and voids of gas of various sizes and shapes is observed. Beds under these conditions are called turbulent beds. With further increases of gas velocity, the rate of particle entrainment with gas increases and extreme turbulence and extensive refluxing of dense packets and strands of particles occurs. This regime is called fast fluidization. Eventually the fluidized bed becomes an entrained bed in which disperse, dilute or lean phase fluidized bed exists, which leads to a pneumatic transport of solids.

I all of these fluidization regimes all regions of the bed are similarly subject to the gas flow from the distributor and the phenomena that occur due to the fluidization are probable to occur all over the cross section.

1.1.2. Geldart Classification

The fluidized behavior of solid particles depends on their size and density. Geldart (1973) classified powders into four groups according to their fluidization properties at ambient conditions. A schematic diagram of the Geldart's particle classification chart is provided in Fig. 1.2. He categorized his observations by particle diameter versus the density difference between the fluid and particles and identified four classes of particles.

Group A particles, known as aeratable particles

- Usually fluidize easily, with normal bubbling fluidization at low gas velocities
- Bubbling bed fluidization at higher gas velocities
- Showing maximum stable bubble size with less than 10 cm diameter
- Gross circulation of solids

Group B particles, known as sand-like particles

- Form bubbles as soon as the gas velocity exceeds minimum fluidization
- Form large bubbles with no maximum stable bubble size

Group C particles, known as cohesive particles

- Hard to fluidize with a tendency to create slugs in small diameter fluidized beds

- Have tendency to form channels with no fluidization in large beds due to high interparticle cohesive forces

Group D particles, known as spoutable

- Particles are either very large or very dense
- Form bubbles which coalesce rapidly and grow large
- Form slugs when the bubble size approaches the bed diameter
- Form a spouting regime and particles may be blown out with a jet in a spouting motion

1.2. Streaming Phenomenon in Deep Fluidized Beds

Recent studies have shown that, in a sufficiently deep bed of Geldart's Group A particles (Geldart, 1973) gas bypassing may occur when the flow rate of the fluidizing gas is increased beyond the minimum fluidization velocity (Wells, 2001; Karri et al., 2004; Issangya et al., 2007). When this phenomenon occurs, the fluidizing gas bypasses the bed in the form of streams of gas, leaving a large fraction of the bed unfluidized or poorly fluidized. Since many industrial fluidized bed processes might work with deep beds, gas streaming is a potential problem that can decrease the efficiency of these chemical and physical fluidized bed processes.

With the exception of the previously cited works (Wells, 2001; Karri et al., 2004; Issangya et al., 2007), there is little discussion of streaming flow in the open literature. This may be attributed to the fact that laboratory scale fluidized beds are typically not

operated with sufficient bed depth for streams to appear (Karri et al., 2004). Some previous researchers have reported the presence of non-uniformity in the radial gas distribution (Rowe et al., 1978; Farag et al., 1997). However, they have not considered it as an important phenomenon to be separately studied. For instance, Farag et al. (1997) conducted experiments in 0.3 and 0.5 m columns with 160 cm bed of FCC particles and observed an axi-symmetric bubble flow "in spite of the careful design of the grid and frequent checks of column verticality". They have attributed this to the influence of the return of particles from the cyclone dipleg. They noticed that increasing the bed temperature enhanced the uniformity of the radial bubbling activity.

The concept of gas streaming was first reported in the literature by Wells (2001). He performed experiments in large scale units with up to 2.5 m diameter and 5 m bed depth and observed streaming flow under conditions that were expected to lead to operation in the bubbling regime. He studied the effects of fines content (particles smaller than 44 μm), distributor design, anti-static agents, baffles, and bed depth. Presumably due to restrictions surrounding the publication of industrial data, details of his findings were limited; however he reported no influence of the various parameters, with the exception of bed depth and baffles. The streaming phenomenon was attributed to gas compression caused by the pressure head of the deep bed over the distributor. The onset of streaming corresponded to an increase in the emulsion suspension density above that at minimum fluidization. The bed then defluidized and gas streaming occurred. Wells (2001) concluded that when the ratio of the density at minimum fluidization to the density of the emulsion phase becomes less than some critical value for a given bed depth, streaming

occurs. This ratio was calculated using the equation of Abrahamsen and Geldart (1980). However, his criterion was not a direct function of the operating condition such as bed depth and gas velocity. Instead, the emulsion phase density was a function of voidage at minimum bubbling and pressure at the surface of fluidized bed.

Karri et al. (2004) investigated the formation of streaming flow in a column of 0.3 m inner diameter and 4.9 m height, and tried to characterize different aspects of this phenomenon. They used FCC particles with average diameter of 70 μm and a static bed depth of 2 m. They found that the standard deviation of pressure drop in a bed exhibiting streaming was much greater than a uniformly fluidized bed. They also reported that for all combinations of operating conditions investigated, the addition of a sufficient amount of fines to the bed of Geldart's Group A particles was able to delay the streaming. This was contrary to the findings of Wells (2001). Karri et al. (2004) also evaluated the use of baffles and found that using two baffles located vertically with a distance of 0.76 cm apart can eliminate the streaming flow. The value of 0.76 cm was found by continuously withdrawing the particles from a fluidized bed with deep bed of particles until the signatures of streaming disappears. The bed depth at this stage was found to be 0.76 m.

Issangya et al. (2007) performed another study in a 0.9-m-diameter and 6.1 m tall test unit. They used FCC catalyst particles with fines contents of 3 and 12% and median particle diameters of 80 and 74 μm, respectively, and gas velocities up to 0.5 m/s. Tests with higher gas velocities were done in another unit. They applied four pressure transducers mounted at four radial positions across axial heights spanning 61 cm to detect

the presence of streaming flow. They attributed the significantly higher magnitudes of differential pressure fluctuations to the passage of streaming flow in front of the pressure transducer. They also concluded that the maximum in the plot of standard deviation of the pressure fluctuation measured across the entire bed *versus* gas velocity, which has been shown in the literature to be an indication of the transition between the bubbling to turbulent fluidization regimes, is not present for deep beds that are subject to streaming. They also used a bubble probe and related the non-uniformity of the radial bubble distribution to the streaming phenomenon. The maximum in the graph of standard deviation of pressure fluctuation *versus* gas velocity has been reported in the literature as the transition point between bubbling and turbulent regimes (Bi and Grace, 1995a, 1995b). The absence of this peak has been introduced as an indication of streaming in deep beds by Issangya et al. (2007) is contrary to the earlier findings of Ellis (2003). Ellis (2003) performed a comprehensive study on the bubbling-turbulent transition velocity in fluidized beds of FCC particle with 75 μm diameter and 1560 kg/m^3 density with bed depth and gas velocity of as high as 1.5 m and 1.2 m/s, respectively. She reported that although by increasing the bed depths the location of maximum shifts to the higher gas velocities, it is always present in the graph. Since her study was focused on the effect of the bubbling/turbulent transition point, there is not any reference to streaming in her work. The gas velocities used in the present work are much less than the transition point, thus, the present work remains neutral in this debate.

1.3. Pressure Measurement

Probably the most widespread measurement technique in fluidized beds is the pressure measurement. Research tools such as electrical capacitance tomography (ECT) and x-ray densitometry and imaging techniques are feasible to determine fluidized bed hydrodynamics through local voidage profiles in laboratory scale fluidized bed units, but have not been proved to be sufficient for monitoring larger scale units. Pressure fluctuation measurements have great potential to be used as a means of monitoring fluidized bed processes due to its simplicity and ease of application. Pressure fluctuations in fluidized beds are generated by temporary variations in the bed voidage (Saxena and Waghmare, 2000). These variations originate from a variety of phenomena that occur during fluidization process such as bubble formation, coalescence, splitting, eruption at the surface, etc. (van Ommen, 2001). Compression waves of various magnitudes created by these phenomena propagate and attenuate throughout the fluidized bed.

1.4. Computational Fluid Dynamics (CFD) Modeling of Dense Fluidized Beds

Although CFD modeling of single phase systems is now a common task, using CFD tools for modeling multiphase systems is still far from perfected. This is due in part to the difficulties encountered in describing the interactions between different phases. The systems containing solids are usually the most complex and challenging ones in the field of multiphase flows. According to the literature (van Wachem et al., 2001; Goldschmidt et al., 2001; Sinclair and van Wachem, 2004), the CFD models of particle-laden flows are divided into two major groups: Lagrangian and Eulerian models. In the Lagrangian models, also called Discrete Element Method (DEM), the particles paths and trajectories

are calculated based on the Newtonian laws of motion (Goldschmidt et al., 2001). The interactions between the particles are described either by a potential force soft-particle dynamics (Tsuji et al., 1993) or by collisional force hard particle dynamics (Hoomans et al., 1996).

The potential of easily changing the physical properties of the particles (e.g., size or density) and exploring the local physical phenomena related to the particle flow behavior is one of the important advantages of the Lagrangian approach. However, the Lagrangian approach consumes a large amount of computer memory and long calculation time is needed to track each of the single particles. Hence, Lagrangian approach seems not to be convenient for the simulation of dense-phase particle-laden flows, especially systems of industrial scale.

Eulerian models, also called Two Fluid Models (TFM), consider the particle and fluid phases as two interpenetrating continua and solve the Navier-Stokes equations as the governing equations for each phase. Since these equations were originally derived for fluids, several additional terms are included in these equations to be able to describe the behavior of the solid particles as a fluid. The kinetic theory of granular flow (Goldschmidt et al., 2001; Farrell et al., 1986; Kim et al., 1993) is the leading tool in calculating the solid phase properties. In this theory, a separate energy balance associated with the particle velocity fluctuations that results from particle interactions (the so-called "granular energy balance") is solved in conjunction with the particle continuity and momentum balances (Sinclair and van Wachem, 2004).

Although mathematical models have been able to provide acceptable results for the modeling of coarser particles (Goldschmidt et al., 2001; Taghipour et al., 2005; Boemer et al., 1997), attempts at the simulation of finer Geldart A class of powders have encountered some significant challenges (McKeen and Pugsley, 2003; Makkawi et al., 2006). This difficulty arises due to the relative importance of interparticle cohesive forces compared with the gravitational forces when dealing with Geldart A powders (e.g. Massimilla and Donsi, 1976). According to Molerus (1982), cohesive forces can be neglected for the larger group B and D particles. Massimilla and Donsi (1976) found that the cohesion force between particles of 40–100 μm diameters might be very high compared to the particle weight. Therefore, neglecting cohesive forces in CFD models of dense fluidized beds of Geldart A particles can lead to over-prediction of bed expansion by as much as 100% (McKeen and Pugsley, 2003; Makkawi et al., 2006). In fact, by neglecting these forces the underlying assumption is that mainly the collisional effects control individual particle-particle contacts, thus a large part of the remaining dynamic energy of the particles is consumed for propelling the particles towards the top of the bed.

McKeen and Pugsley (2003) were among the early researchers who reported this over-prediction of bed expansion. They argued that interparticle forces lead to the formation of particle clusters with a corresponding reduction in gas-solid drag. They found that by scaling the drag model of Gibilaro et al. (1985) with a fractional constant equal to 0.25, realistic bed expansion and bubble properties were predicted. Incorporation of equations for the interparticle cohesive forces was attempted by Kim and Arastoopour (2002), who

extended the kinetic theory of granular flow to cohesive particles by modifying the solid distribution equation. However, the final expression for the particulate stress was complex and difficult to incorporate into the current CFD models. Neither their model nor the model of McKeen and Pugsley (2003) considered the size distribution of particles in the fluidized bed.

As pointed out by Grace and Sun (1991), particle size distribution has a significant influence on the bed expansion. Therefore, considering the size distribution of the particles in the computational models might eliminate the problem of over-prediction of the bed expansion. However, the presence of different types and sizes of particles complicates the modeling process because separate continuity and momentum equations must be solved for each size and type (Risk, 1993; Gidaspow, 1994). As a result, these models have been only used for up to three solid phases in the literature, due to the computational limitations.

The multiphase Particle in Cell (PIC) approach (Andrews and O'Rourke, 1996; Snider et al., 1998; Snider, 2001; Karimipour and Pugsley, 2009), which is essentially an Eulerian-Lagrangian model, provides a numerical scheme in which particles are grouped into computational parcels each containing a number of particles with identical density, volume and velocity, located at a specific position. The evolution of the particle phase is governed by solving a Liouville equation for the particle distribution. The result of this procedure is a computational technique for multiphase flow that can handle particle loadings ranging from dilute to dense with a distribution of particle types and sizes.

1.5. Project Motivation

Streaming flow in deep beds is a relatively new phenomenon reported in the literature in fluidized beds and there is still a great deal of uncertainty and contradiction between results of different investigations. For instance, while Wells (2001) found no effect of fines content, others (Karri et al., 2004; Issangya et al., 2007) reported an influence of fines on the streaming flow. The mathematical work presented by Wells (2001) to predict the onset of streaming flow does not a have a functional dependency on conditions such as bed depth and gas velocity and seems not to be able to predict the presence of streaming for various cases. These facts indicate that further experimental and theoretical work is still required to shed light on this phenomenon. The present work attempted to verify the presence of the streaming flow, to find the differences between the hydrodynamics of fluidized beds with different bed depths, and to investigate the possible reasons for these differences and their relationship to the presence of streams. For this purpose, a combination of experimental and mathematical modeling has been employed.

1.6. Objectives

The main objective of the present PhD project was to perform a comprehensive study on the various aspects of the gas streaming phenomenon in deep fluidized beds of Geldart A particles. This main objective was achieved by a combination of experimental and modeling work. The detail of the sub-objectives of the project can be summarized as follows:

1. Experimental study of the general characteristics of deep beds (chapter 1).

   a. Design and construction of a 0.3 m diameter by 3.3 m tall cold model fluidized bed.
   b. Calibration and installation of the pressure transducers across the fluidized bed.
   c. Measurement of pressure fluctuations for different conditions of bed depth, gas velocity, particle size, and distributor design.
   d. Comparative study of the effect of these different conditions on the fluidized bed hydrodynamics using pressure fluctuations time series.

2. Experimental study of the nature of streaming flow (chapter 2).
   a. Measurement of pressure fluctuations for various conditions of bed depth, gas velocity, particle size, and distributor design for different cases of forced streaming flow and jet flows.
   b. Assessment of the tendency for streaming in these different cases.
   c. Wavelet decomposition analysis to investigate the detail of the phenomena that participate in the observed streaming flow.
3. Modeling study of the streaming flow in deep fluidized bed (chapters 3 and 4).
   a. CFD simulation using available commercial codes.
   b. Phenomenological modeling of the deep bed.

1.7. References

Abrahamsen, A.R., Geldart, D., 1980. Behaviour of gas-fluidized beds of fine powders part I. Homogeneous expansion, Powder Technology 26, 35-46.

Andrews, M.J., O'Rourke, P.J., 1996. The multiphase particle-in-cell (MP-PIC) method for dense particulate flows, International Journal of Multiphase Flow 22, 379-402.

Bi, H.T., Grace J.R., 1995a. Effect of measurement method on the velocities used to demarcate the onset of turbulent fluidization, The Chemical and Biochemical Engineering Journal 57, 261-271.

Bi, H.T., Grace J.R., 1995b. Flow regime diagrams for gas-solid fluidization and upward transport, International Journal of Multiphase Flow 21, 1229-1236.

Boemer, A., Qi, H., Renz, U., 1997. Eulerian simulation of bubble formation at a jet in a two-dimensional fluidized bed. International Journal of Multiphase Flow 23, 927-944.

Ellis, N., 2003. Ph.D. Dissertation, Hydrodynamics of gas-solid turbulent fluidized beds, University of British Columbia, Canada.

Farag, H.I., Mejdell, T., Hjarbo, K., Ege, P., Lysberg, M., Grislingas, A., De Lasa, H., 1997. Fibre optic and capacitance probes in turbulent fluidized beds, Chemical Engineering Communication 157, 73-107.

Farrell, M., Lun, C., Savage, S., 1986. Simple kinetic theory for granular flow of binary mixtures of smooth, Inelastic, Spherical Particles. Acta Mechanica 63, 45-60.

Geldart, D., 1973. Types of gas fluidization. Powder Technology 7, 285-292.

Gibilaro, L., Di Felice, R., Waldram, S., 1985. Generalized friction factor and drag coefficient correlations for fluid-particle interactions. Chemical Engineering Science 40, 1817-1823.

Gidaspow, D., 1994. Multiphase flow and fluidization: Continuum and kinetic theory description. Academic Press, Boston.

Goldschmidt, M., Kuipers, J., van Swaaij, W., 2001. Hydrodynamic modelling of dense gas-fluidised beds using the kinetic theory of granular flow: effect of coefficient of restitution on bed dynamics. Chemical Engineering Science 56, 571-578.

Grace, J., Sun, G., 1991. Influence of particle size distribution on the performance of fluidized bed reactors. Canadian Journal of Chemical Engineering 69, 1126-1134.

Hoomans, B., Kuipers, J., Briels, W., van Swaaij, W., 1996. Discrete particle simulation of bubble and slug formation in a two-dimensional gas-fluidised bed: A hard sphere approach. Chemical Engineering Science 51, 99-118.

Issangya, A., Knowlton, T., Karri, S.B.R., 2007. Detection of gas bypassing due to jet streaming in deep fluidized beds of group A particles. In: Fluidization XII, Berruti, F., Bi, X., Pugsley, T. (Eds.), Vancouver, British Columbia, Canada, May 13-17.

Karimipour, S., Pugsley, T., 2009. Application of the particle in cell approach for the simulation of bubbling fluidized beds of Geldart A particles. 7th International Conference on Computational Fluid Dynamics in the Minerals and Process Industries, Melbourne, Australia, December 9-11.

Karri, S.B.R., Issangya, A.S., Knowlton, M., 2004. Gas bypassing in deep fluidized beds. In: Fluidization XI, Arena, U., Chirone, R., Miccio, M., Salatino, P. (Eds.), Ischia (Naples), Italy, May 9-14.

Kim, S., Woodcock, L., 1993. Kinetic theory of granular shear flow: constitutive relations for the hard-disk model. Journal of Statistical Physics 71, 143-162.

Kim, H., Arastoopour, H., 2002. Extension of kinetic theory to cohesive particle flow. Powder Technology 122, 83-94.

Kuipers, J., van Duin, K., van Beckum, F., van Swaaij, W., 1992. A numerical model of gas-fluidized beds. Chemical Engineering Science 47, 1913-1924.

Kunii, D., Levenspiel, O., 1991. Fluidization Engineering, 2nd edition, Butterworth-Heinemann, Boston, USA.

Lim, K., Zhu, J., Grace, J., 1995. Hydrodynamics of gas–solid fluidization. International Journal of Multiphase Flow 21, 141-193.

Makkawi, Y., Wright, P., Ocone, R., 2006. The effect of friction and inter-particle cohesive forces on the hydrodynamics of gas-solid flow: A comparative analysis of theoretical predictions and experiments. Powder Technology 163, 69-79.

Massimilla, L., Donsi, G., 1976. Cohesive forces between particles of fluid-bed catalysts. Powder Technology 15, 253-260.

McKeen, T., Pugsley, T., 2003. Simulation and experimental validation of freely bubbling bed of FCC catalyst. Powder Technology 129, 139-152.

Molerus, O., 1982. Interpretation of Geldart type A, B, C and D powders by taking into account interparticle forces. Powder Technology 33, 81-87.

Pain, C. Mansoorzadeh, S. de Oliveira, C. Goddard, A., 2001. Numerical modelling of gas-solid fluidized beds using the two-fluid approach. International Journal for Numerical Methods in Fluids 36, 91-124.

Risk, M., 1993. Mathematical modeling of densely loaded, particle laden turbulent flows. Atomization and Sprays 3, 1-27.

Rowe, P.N., L. Santoro, J.G. Yates, 1978. The division of gas between bubble and interstitial phases in fluidized beds of fine powders. Chemical Engineering Science 33, 133-140.

Saxena, S.C., Waghmare, B., 2000. Investigation of pressure fluctuation history records of gas-solid fluidized beds. International Journal of Energy Research 24, 495-502.

Sinclair, J., van Wachem, B., 2004. Modeling particle-laden flows: A research outlook. AIChE Journal 50, 2638-2645.

Snider D.M, O'Rourke P.J., Andrews M.J., 1998. Sediment flow in inclined vessels calculated using a multiphase particle-in-cell model for dense particle flows. International Journal of Multiphase Flow 24, 1359-1382.

Snider D.M., 2001. An incompressible three-dimensional multiphase particle-in-cell model for dense particle flows. Journal of Computational Physics 170, 523-549.

Taghipour, F., Ellis, N., Wong, C., 2005. Experimental and computational study of gas-solid fluidized bed hydrodynamics. Chemical Engineering Science 60, 6857-6867.

Tsuji, Y., Kawaguchi, T., Tanaka, T., 1993. Discrete particle simulation of two-dimensional fluidised bed. Powder Technology 77, 79-87.

van Ommen, J., Schouten, J., Coppens, M., van den Bleek, C., 2001. Monitoring of fluidized bed hydrodynamics to detect changes in particle size distribution. In: Fluidization X, Kwauk, M., Li, J., Yang, W.C. (Eds.), Beijing, China, May 20-25.

van Wachem, B., Schouten, J., van den Bleek, C., 2001. Comparative analysis of CFD models of dense gas-solid systems. AIChE Journal 47, 1035-51.

Wells, J., 2001. Streaming flow in large scale fluidization. AIChE Annual Meeting, Particle Technology Forum, Reno, Nevada, USA.

Wilson, J., 1997. Fluid Catalytic Cracking Technology and Operation, 1st edition, Pennwell Publishing, Oklahoma, USA.

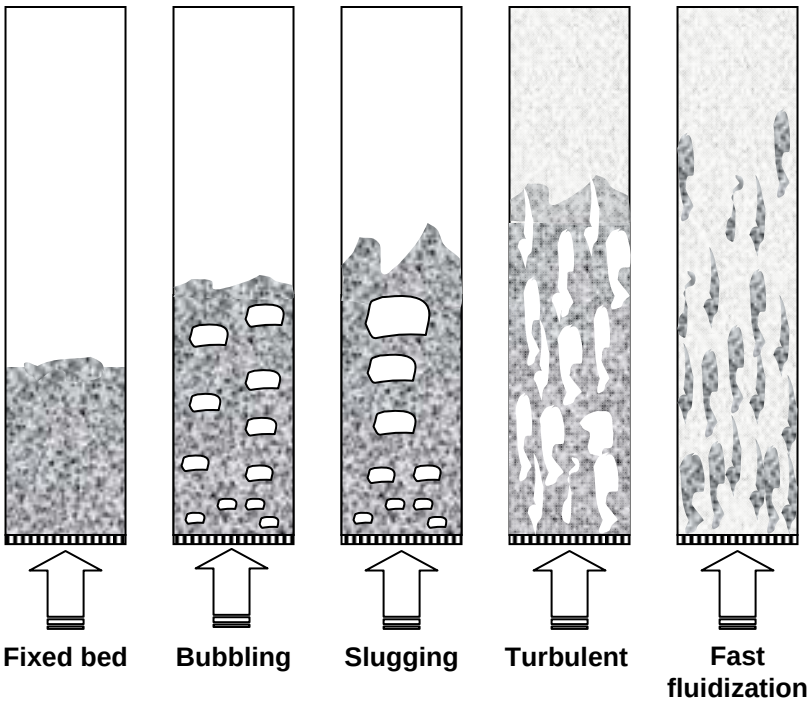

Figure 1.1. Different fluidization regimes that occur by increasing the gas velocity in fluidized beds

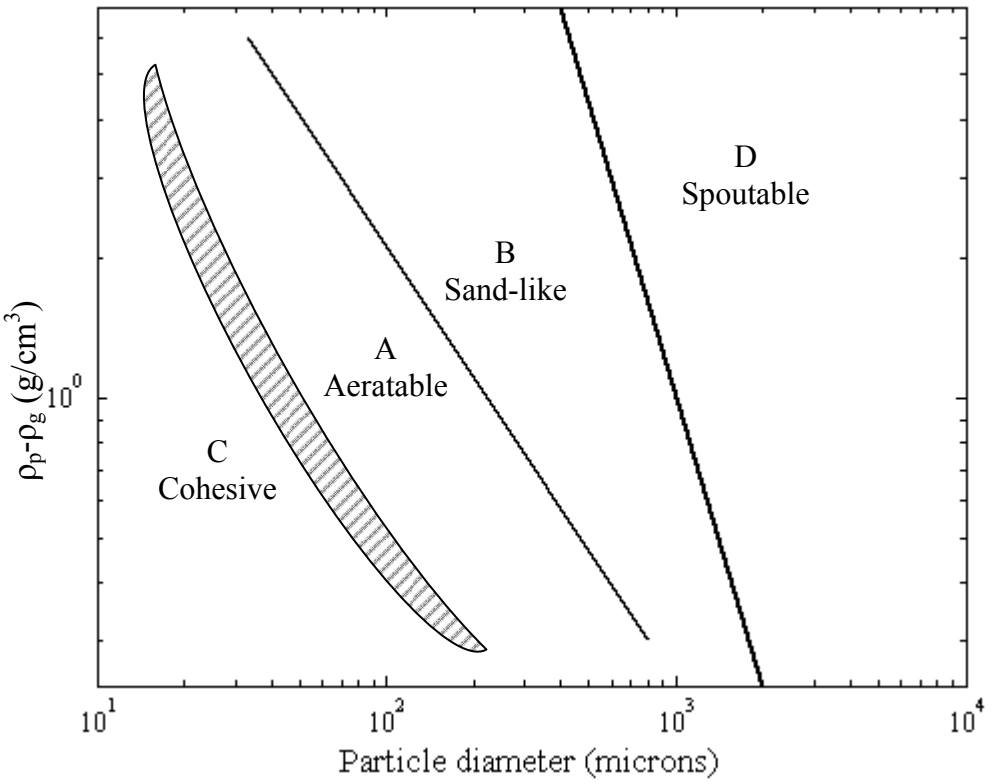

Figure 1.2. A schematic diagram of Geldart's particle classification chart

CHAPTER 2 - Study of Gas Streaming in a Deep Fluidized Bed Containing Geldart's Group A Particles

The contents of this chapter have been published in the journal ***Chemical Engineering Science***. It has been published in a version similar to what appears in this chapter.

Citation

S. Karimipour, T. Pugsley, Study of gas streaming in a deep fluidized bed containing Geldart's group A particles, ChemicalEngineeringScience65(2010) 3508-3517.

Contribution of PhD Candidate

The experiments performed for the purpose of this work were planned and performed by Shayan Karimipour. Todd Pugsley provided consultation regarding the experimental program. The programs for all of the data analysis were developed by Shayan Karimipour. All of the writing of the submitted manuscript was done by Shayan Karimipour with Todd Pugsley providing editorial guidance regarding the style and technical content of the manuscript.

Contribution of this Paper to the Overall Study

This paper investigates the characteristics of gas streaming in a deep fluidized bed containing Geldart A particles in a 30-cm ID cold flow unit. The objective of this work was to verify the presence of the streaming flow, find the differences between the hydrodynamics of fluidized beds with different bed depths, and explore the possible reasons for these differences and their relationship to the presence of streams.

2.1. Abstract

The nature of gas streaming in a deep fluidized bed containing Geldart's Group A powder has been investigated in a 30-cm ID cold flow unit. Pressure fluctuations have been measured at 8 locations from 4 to 150 cm above the gas distributor for bed depths and gas velocities ranging from 0.4 to 1.6 m and 0.04 to 0.20 m/s, respectively. In order to study the effect of fines content on gas streaming, two particle size distributions with Sauter mean diameters of 48 μm and 84 μm were tested for each bed depth and gas velocity. Two distributor plates with differing percentage open area were also tested for their influence on gas streaming. Analysis of pressure fluctuations in the time and frequency domains, in combination with visual observations show that streaming flow emerges gradually at bed depths greater than 1 m. Increased gas velocity and fines content act to delay the onset of streaming, but can not completely eliminate it over the range of velocities examined. The two different distributor designs had no measurable effect on the streaming flow.

2.2. Introduction

Fluidized beds have broad applications in many chemical, pharmaceutical, and mineral processing industries. Numerous studies have been carried out to characterize the hydrodynamics of fluidized beds. Several techniques based on the measurement of the fluctuations of pressure (Johnsson et al., 1995; Svensson et al., 1996; Bai et al., 1997), voidage (Daw and Halow, 1991; Huilin et al., 1997; Bai et al., 1997; Ohara et al., 1999) and temperature (Kozma et al., 1996; Woo et al., 2001; Huilin et al., 2002) have been developed and used in the literature. Pressure transducers have been one of the most popular devices due to their simplicity and ease of implementation in industrial facilities. Tamarin (1964) and Hiby (1967) were one of the first researchers who attempted to determine the frequency of the pressure fluctuations using visual observations of the pressure signals. Kang et al. (1967) were among the first who used time series analysis techniques such as probability density functions, root mean square of pressure fluctuations, and power spectral density (PSD), to illustrate the time and frequency characteristics of the pressure fluctuations. Lirag and Littman (1971) included autocorrelation and cross-correlation functions to the analysis techniques used by Kang et al. (1967). The autocorrelation function was used to detect signs of periodic phenomena in the pressure fluctuations, while the cross-correlation function was used to calculate the time lag between the pressure fluctuations in the bed and in the plenum. This time lag was used to calculate the propagation velocity of the pressure wave. Fan et al. (1981) and Clark et al. (1991) also discussed similar applications of pressure fluctuations analysis in fluidized bed researches.

Investigating regime transitions in fluidized beds based on analysis of the time series of pressure data has been one of the major concerns of many researchers. Yerushalmi and Cankurt (1979) defined the transition velocity from bubbling to turbulent regime as the point where the standard deviation of pressure fluctuations reaches a peak. Regime transitions have also been identified by studying the changes that occur in the frequency distribution of PSD (Lirag and Littman, 1971; Canada et al., 1978; Satija and Fan, 1985; Johnsson et al., 1995; Svensson et al., 1996).

The study of pressure fluctuations has been widely continued until recent days. One of the important operating parameters that can greatly affect the fluidized bed hydrodynamics, and thus the in-bed pressure fluctuations, is the bed depth. Grace and Sun (1991) studied the effect of bed depths varied from 40 to 100 cm on the differential pressure fluctuations in a bed of FCC particles. They found that the transition velocity from bubbling to turbulent regime is almost independent of the bed depth. Similar results were reported by Satija and Fan (1985) and Jin et al. (1986). Falkowski and Brown (2004) studied the pressure fluctuations for a range of variables including bed depth in a fluidized bed of Geldart B and D particles to determine the effect of these parameters on the PSD graph. They reported that dominant frequency decreases with increasing the bed depth from 8.6 to 50.8 cm.

The bed depth, which is directly related to the material inventory of the fluidized bed, is indeed one of the important operating parameters in various applications of fluidized beds. Achieving specific efficiencies or throughput can lead to the necessity of employing

deep fluidized beds. In these cases, maintaining specified gas residence times, low particle entrainment, and a good fluidization quality possess special importance. Recent studies have shown that, in a sufficiently deep bed of Geldart's Group A particles (Geldart, 1973) gas bypassing may occur when the flow rate of the fluidizing gas is increased beyond the minimum fluidization velocity (Wells, 2001; Karri et al., 2004; Issangya et al., 2007). When this phenomenon occurs, the fluidizing gas bypasses the bed in the form of streams of gas, leaving a large fraction of the bed unfluidized or poorly fluidized. Since many industrial fluidized bed processes might work with deep beds, gas streaming is a potential problem that can decrease the efficiency of these chemical and physical fluidized bed processes.

With the exception of the previously cited works (Wells, 2001; Karri et al., 2004; Issangya et al., 2007), there is little discussion of streaming flow in the open literature. This may be attributed to the fact that laboratory scale fluidized beds are typically not operated with sufficient bed depth for streams to appear (Karri et al., 2004). At the same time, industrial units that may operate with very deep beds of particles are mostly made of steel columns that eliminate the possibility of visual observation of the inside of the column. Some previous researchers have reported the presence of non-uniformity in the radial gas distribution (Rowe et al., 1978; Farag et al., 1997). However, they have not considered it as an important phenomenon to be separately studied. For instance, Farag et al. (1997) conducted experiments in 0.3 and 0.5 m diameter columns with a 160 cm deep bed of FCC particles and observed an axi-symmetric bubble flow "in spite of the careful design of the grid and frequent checks of column verticality". They attributed this to the

influence of the return of particles from the cyclone dipleg. They noticed that increasing the bed temperature enhanced the uniformity of the radial bubbling activity.

The concept of gas streaming was first reported in the literature by Wells (2001). He performed experiments in large scale units with up to 2.5 m diameter and 5 m bed depth and observed streaming flow under conditions that were expected to lead to operation in the bubbling regime. He studied the effects of fines content (particles smaller than 44 μm), distributor design, anti-static agents, baffles, and bed depth. Presumably due to restrictions surrounding the publication of industrial data, details of his findings were limited; however he reported no influence of the various parameters, with the exception of bed depth and baffles. The streaming phenomenon was attributed to gas compression caused by the pressure head of the deep bed over the distributor. The onset of streaming corresponded to an increase in the emulsion suspension density above that at minimum fluidization. The bed then defluidized and gas streaming occurred. Wells (2001) concluded that when the ratio of the density at minimum fluidization to the density of the emulsion phase becomes less than some critical value for a given bed depth, streaming occurs. However, his criterion was not a direct function of the operating condition such as bed depth and gas velocity. Instead, the emulsion phase density was a function of voidage at minimum bubbling and pressure at the surface of the fluidized bed.

Karri et al. (2004) investigated the formation of streaming flow in a column of 0.3 m inner diameter and 4.9 m height, and tried to characterize different aspects of this phenomenon. They used FCC particles with average diameter of 70 μm and a static bed

depth of 2 m. They found that the standard deviation of pressure drop in a bed exhibiting streaming was much greater than a uniformly fluidized bed. They also reported that for all combinations of operating conditions investigated, the addition of a sufficient amount of fines to the bed of Geldart's Group A particles was able to delay the streaming. This was contrary to the findings of Wells (2001). Karri et al. (2004) also evaluated the use of baffles and found that two baffles separated vertically by a distance of 0.76 cm eliminated the streaming flow. The value of 0.76 cm was chosen because it corresponded to the maximum bed depth beyond which streaming occurred in a non-baffled bed.

Issangya et al. (2007) performed another study in a 0.9-m-diameter and 6.1 m tall test unit. FCC catalyst with fines contents of 3 and 12% and median particle diameters of 80 and 74 μm, respectively was used as the bed test material. Results for gas velocities up to approximately 1 m/s were reported. Four pressure transducers were mounted at four radial positions across axial heights spanning 61 cm to detect the presence of streaming flow. They attributed the larger differential pressure fluctuations measured by certain transducers to the passage of streams closer to that transducer. Issangya et al. (2007) also concluded that the maximum in the plot of standard deviation of the pressure fluctuation measured across the entire bed *versus* gas velocity, which has been shown in the literature to be an indication of the transition between the bubbling and turbulent fluidization regimes, is not present for deep beds that are subject to streaming. The absence of the maximum in the graph of standard deviation of pressure fluctuation *versus* gas velocity which is reported as an indication of streaming in deep beds by Issangya et al. (2007) is contrary to the findings of Ellis (2003). Ellis (2003) performed a comprehensive study on

the bubbling-turbulent transition velocity in fluidized beds of FCC particle with 75 μm diameter and 1560 kg/m^3 density with bed depth and gas velocity of as high as 1.5 m and 1.2 m/s, respectively. She reported that although by increasing the bed depths the location of the maximum shifts to the higher gas velocities, it is always present in the graph. Since her study was focused on the effect of the bubbling/turbulent transition point, there is not any reference to streaming in her work. The gas velocities used in the present work are much less than the transition point, thus, the present work remains neutral in this debate.

Streaming flow in deep beds is a relatively new phenomenon reported in the literature in fluidized beds and there is still a great deal of uncertainty and contradiction between results of different investigations. For instance, while Wells (2001) found no effect of fines content, others (Karri et al., 2004; Issangya et al., 2007) reported an influence of fines on the streaming flow. The mathematical work performed by Wells (2001) to predict the onset of streaming flow was not a direct function of the operating conditions such as bed depth and gas velocity and seems not to be able to predict the presence of streaming flow for various conditions. He also has not presented a comparative analysis between different bed depths to clarify the presence of streaming flow.

These facts indicate that further experimental and theoretical work is still required to shed light on this phenomenon. The objective of the present work is to verify the presence of the streaming flow, to find the differences between the hydrodynamics of fluidized beds with different bed depths, and to investigate the possible reasons for these differences and their relationship to the presence of streams. For this purpose, pressure fluctuations have

been used to perform a comparative analysis of the influence of different parameters on the fluidized bed behavior. The pressure fluctuations have been measured at several locations along the fluidized bed for various combinations of bed depth, gas velocity, particle size, and distributor design in a 0.3 m diameter column. Quantitative analysis methods in both the time and frequency domains have been used to extract and evaluate useful information regarding the fluidized bed behavior under these different conditions.

2.3. Experimental

Fluidized Bed

The fluidized bed unit was made of a cylindrical Plexiglas column with an inner diameter of 30 cm and height of 3.3 m (Fig. 2.1). The column was equipped with an internal cyclone and a dipleg to continuously return entrained particles to the bed during operation. The distance between the dipleg exit and the distributor was 0.19 m for all bed depths. The cyclone gas exit was connected with a flexible hose to a barrel with filter cloth stretched over openings on the top to prevent very fine particles from escaping into the surrounding room. In order to test the influence of distributor design, two different perforated plate distributors with open areas and orifice diameters of 0.54% and 1 mm and 2.15% and 2 mm, respectively were used. The former is referred to as the high pressure drop (HPD) distributor and the latter the low pressure drop (LPD) distributor. The holes on both distributors were arranged in a rectangular pitch. A very fine screen was glued on the distributor to prevent from weeping of particles into the wind-box. The fluidization air was supplied by a 50 hp Kaeser® positive displacement blower. The air flowrate was measured using an orifice plate and water manometer. To limit the effect of

electrostatic charges on the fluidized bed hydrodynamics, the outer periphery of the column was wrapped with aluminum strips and grounded properly in a way that still allowed visual observation of the system through the wall of the Plexiglas vessel.

Test Material

The bed material was fluid catalytic cracking (FCC) catalyst with a particle density of 1400 kg/m^3. Two catalyst size distributions were used: one with a Sauter mean diameter of 84 μm and the other with a Sauter mean of 48 μm. The particle size distributions of the two test powders, measured using a Mastersizer S Long Bench (Malvern, Worcestershire, UK), are provided in Fig. 2.2. The minimum fluidization velocity of the particles having a mean diameter of 84 μm was measured in previous experiments to be 0.004 m/s (McKeen and Pugsley, 2003). The minimum fluidization velocity for the finer particles was not available experimentally, and thus was calculated using the Wen and Yu (1966) equation to be equal to 0.0014 m/s.

Experimental Conditions and Instrumentation

The operating variables investigated in the present study and their ranges are summarized in Table 2.1. Pressure fluctuations were measured with reference to the atmosphere by Omega® differential pressure transducers mounted along the fluidized bed column. The axial positions of the pressure transducers are illustrated in Fig. 2.1, while model numbers and specifications of the transducers are provided in Table 2.2. The pressure transducers were flush-mounted to the internal wall of the fluidized bed with 15 cm long and 4.5 mm diameter stainless steel tubes covered by a 10 μm mesh at the tip to prevent particles from

entering the tube. Special care was taken to maintain the volume of the steel tube less than 2500 mm^3, as recommended by Johnsson et al. (2000), to reduce the damping effect of the tube on the pressure fluctuations. Pressure measurements were performed at a sampling frequency of 100 Hz, which is well above the major frequencies observed in fluidized bed pressure fluctuation power spectra (the dominant frequency is normally below 10 Hz (Johnsson et al., 2000). Sampling time was 5 min for all measurements. The data acquisition equipment was interfaced with a continuous data logging program built with LabVIEW® (National Instruments®, Austin, USA).

2.4. Analysis Methods

Time series of pressure fluctuations collected with the differential pressure transducers have been analyzed in the time and frequency domains. Key properties that are extracted from the time series through these analyses are briefly explained in the following sections.

2.4.1. Autocorrelation and Cross Correlation Functions

The autocorrelation function measures the correlation between successive observations in a single time series. It is calculated through a comparison between a times series and the delayed version of itself. The autocorrelation function is one at zero delay, and decreases with an increase in the delay value. For a times series containing different degrees of periodicity, the autocorrelation function shows an oscillatory behavior. The rate of decrease of the function is proportional to the rate of information loss in the system. Hence, the more vigorous the turbulence in the measurement region, the more rapid the

decrease of the autocorrelation function. The autocorrelation function is calculated from the following equation:

$$ACF = \frac{\sum_{i=1}^{n-k}(x_i - \overline{x})(x_{i+k} - \overline{x})}{\sum_{i=1}^{n}(x_i - \overline{x})^2} \tag{2.1}$$

The cross correlation function measures the correlation between two different time series. It compares a reference time series with the delayed versions of another time series and calculates a correlation coefficient for each pair of time series. The magnitude of the correlation coefficients is a measure of the similarity of the phenomena affecting regions where the time series are measured. If the magnitude is large, it can be concluded that those time series are highly correlated and the same phenomena is happening in both regions. The rate of decrease of the cross correlation function can be interpreted in the same manner as the autocorrelation function. A rapid decrease indicates that mostly local phenomena are affecting the two measurement regions. However, a slow decrease shows that a more global phenomenon or a phenomenon that prolongs from one measurement region to the other is predominant. The cross correlation function can be calculated using the following equation:

$$ACF = \frac{\sum_{i=1}^{n-k}(x_i - \overline{x})(y_{i+k} - \overline{y})}{\sqrt{\sum_{i=1}^{n}(x_i - \overline{x})^2}\sqrt{\sum_{i=1}^{n}(y_i - \overline{y})^2}} \tag{2.2}$$

2.4.2. Power Spectral Density and Coherency

Spectral analysis is a common tool for exploring the pressure fluctuations time series generated in a fluidized bed. This approach has been used in many previous works for determining bubble characteristics (e.g. Fan et al., 1983; van der Schaaf et al., 2002),

fluidization regime transitions [(e.g. Johnsson et al., 2000), and fluidization quality (e.g. van Ommen et al., 2000)]. Most of these applications rely on determining the major frequencies present in the time series and relating them to various physical phenomena in the system. This is usually done by calculating the PSD of the time series. In the present work, the PSD function of all time series is estimated with Welch's averaged periodogram method (Welch, 1967). It is computed for a window length of 1024 points and is averaged over the length of the time series. The window size is selected in such a way to eliminate the roughness of the PSD and at the same time, maintain the important features of it. This was done by choosing different values of window size and visual comparison of the PSDs calculated for each case. In order to avoid edge effects and reduce spectral leakage in PSD calculations, Hanning windowing has been applied to each window. The dominant frequency is considered as the frequency corresponding to the maximum power of the PSD function.

The coherency between time series from two successive measurement locations along the fluidized bed is calculated as a measure of similarity between the spectral activities happening in those locations. The coherency ranges from 0 to 1 and can be calculated using the formula below (van der Schaaf et al., 2002):

$$\gamma_{xy}^2(f) = \frac{\Phi_{xy}(f)\Phi_{xy}^*(f)}{\Phi_{xx}(f)\Phi_{yy}(f)} \tag{2.3}$$

where Φ_{xy} and Φ_{xy} are the power spectral density and cross power spectral density for x and y time series, respectively. A coherency of one indicates that phenomena with exactly the same frequency activity are present in the region of both measurement ports, although the PSD of each time series might be different from the other at that frequency. On the

other hand, a zero coherency means the existence of no spectral correlation between two time series at that specific frequency. It should be noted that the difference between coherency and the cross correlation function is that cross correlation compares the value of pressure in two time series and reports the extent of similarity in terms of a correlation coefficient. The coherency quantifies the similarity between variations of the pressure for two time series. This means that although the pressure may not be the same, the rate of variation might be similar.

2.5. Results and Discussions

2.5.1. Visual Observations

The use of a transparent Plexiglas vessel in the present study permitted us to make visual observations during experiments. This section is based on the observations made for the coarse FCC particles (3% fines content); however, it covers low and high gas velocities and both the HPD and LPD gas distributors. The observations showed that in the case of the 40 cm bed depth, bubbles were formed over the entire bed cross section and the entire bed appeared to be fluidized. For the 80 cm bed depth, some signs of preferential gas flow began to emerge; however, this was not severe enough to deteriorate the general fluidization quality and the entire cross section remained fluidized. The presence of streaming flow was clear for the 120 cm bed depth. In this case, the bed was divided into two regions with a diffuse boundary which changes due to the high turbulency of the gas flow. Most of the gas appeared to flow upward in a stream that formed just above the gas distributor and that constituted a small fraction of the bed cross-sectional area. In the remainder of the cross section near the distributor, particles were slowly flowing down. It

was further observed that the particles were entrained by the stream to the top of the bed and then moved downward in the dense region away from the streaming flow. Gas entering the bed through the distributor tended to preferentially migrate laterally and join the streaming flow, instead of flowing upward in the form of jets and then detaching to form bubbles, as is the case in a normal fluidized bed. It should be noted that the distributor plate was checked before and after the experiments to make sure that the distributor orifices were not plugged by fine particulate material. Although the stream could remain in one place for a longer time (typically less than two min), they generally tended to change their position around the column during the measurement period. At bed depths greater than 120 cm, the stream boundaries became more distinguished from the remainder of the bed.

The streams observed at low gas velocities are best described as a "trail" of bubbles and the stream passage was more unstable in nature. However, for higher velocities, the stream looked similar to a passage of particle-laden gas in a pipe. These streams were observed to mostly form at near-wall regions. This is probably due to the effect of wall to support and stabilize the stream in a specific place. It is worth mentioning that although the simultaneous presence of several gas streams has been reported in the literature (Karri et al., 2004; Issangya et al., 2007) the occurrence of more than one stream was rarely observed in the present work. Since the streams make the majority of gas to pass from a channel with lower cross sectional area, the velocity of the gas in the streams are expected to be much higher than the superficial gas velocity. This higher velocity may cause higher rates of particle entrainment compared to the normal bubbling beds.

2.5.2. Quantitative Analyses and Discussion

2.5.2.1. Effect of Bed Depth

The time series of pressure fluctuations measured at an axial position of 30 cm above the distributor for bed depths of 40 to 160 cm, superficial gas velocity of 35 U_{mf}, and the coarse FCC particles (3% fines content) are shown in Fig. 2.3. The autocorrelation coefficients calculated using these time series is presented in Fig. 2.4a. There are observable differences between the autocorrelations of the fluidized bed with different bed depths. There is a clear decrease in the periodicity of the autocorrelation function with increasing bed depth. For shallow beds, the periodic nature of the fluidized bed is characterized by bubbling activities with various sizes along the column. These bubbles that change faster compared to the gas stream produce higher frequency variations. With the onset of streaming flow at bed depths beyond 80 cm, smooth fluidization with uniform bubbling activity is compromised and the periodic variations of autocorrelation are gradually suppressed. This is clearly observable by lower domain and lower frequency oscillations in the autocorrelation graph for deep beds of 120 and 160 cm depths.

Another visible difference with increasing bed depth is the rate of decrease of the autocorrelation function. In the case of shallow bed depths, the autocorrelation coefficient decreases sharply. This can be attributed to the presence of various local phenomena arising from the coalescence and splitting of gas bubbles and to a lesser extent caused by

gas-particle and particle-particle interactions around the measurement point. However, since streaming is a more stable (albeit undesirable) phenomenon compared to the rigorous mixing present during bubbling fluidization, the autocorrelation coefficient corresponding to streaming decreases more slowly.

Fig. 2.4b provides the cross correlation of the pressure fluctuations for the first two successive measurement locations above the gas distributor (4 cm and 30 cm) for bed depths of 40 to 160 cm and gas velocity of 35 U_{mf}. As Fig. 2.4b shows, the correlation coefficient between adjacent locations is higher in deeper beds and also lasts longer. This suggests that the phenomenon that is affecting these two locations is changing with increasing bed depth and its spread over these adjacent measurement points increases the correlation coefficient between locations along the column. As mentioned for the case of the autocorrelation function, this is probably due to the gradual change of fluidized bed hydrodynamics from normal bubbling to severe streaming flow. Deterioration of the periodic nature of the fluidized bed with increasing bed depth can also be seen in the cross correlation graph.

Power spectral density (PSD) functions of the pressure fluctuations for different bed depths are shown in Fig. 2.4c. Dominant frequencies are apparent in the PSD graph at low bed depths and are equal to 4 Hz and 2.7 Hz for the 40 cm and 80 cm bed depths, respectively. Increasing the bed depth shifts the dominant frequency towards very low frequencies. The 120 cm bed exhibits local maxima at low frequencies, while the PSD function for the 160 cm bed follows an exponential decrease with no noticeable

maximum. It is well known from the fluidization literature that the dominant frequency is related to the major bubbling activity in the system. Increasing the bed depth shifts the bed from a bubbling fluidization regime to a regime dominated by streaming flow. Since the streams correspond to a lower variability compared to bubbling flow with a range of bubble sizes and rise velocities, the dominant frequency decreases when streams are formed. Stable streaming flow in the case of deeper beds behaves like the single phase flow of gas in a pipe, which shows a distribution of frequencies with low power without a clear dominant frequency.

The coherency between two pressure fluctuations time series measured at 4 cm and 30 cm above the gas distributor for different bed depths is plotted in Fig. 2.4d. As the plot illustrates, the maximum coherency value shifts towards lower frequencies with increasing bed depth. This indicates that most of the events affecting the fluidized behavior in deep beds are low frequency phenomena. For the 120 and 160 cm bed depths, the coherency rapidly decreases with frequency, which demonstrates that when streams are present, they produce very low frequency activity and there exist no other major phenomenon to increase the coherency at higher frequencies. In the case of lower bed depths, Fig. 2.4d depicts a maximum at frequencies corresponding to the typical dominant frequency in a bubbling bed.

It has been shown (Ellis, 2003) that the transition from the bubbling to the turbulent fluidization regime first starts at positions closer to the upper surface of a fluidized bed and then gradually, with increasing velocity, the transition works its way downward until

the entire bed is in turbulent fluidization. The extent of streaming flow at different axial positions in our 30 cm ID fluidized bed can be evaluated by comparing the pressure fluctuations corresponding to different positions above the gas distributor (Fig. 2.5). Fig. 2.5 represents the autocorrelation function of the pressure fluctuation for different positions along the fluidized bed for the case of 160 cm bed depth. There is a clear change in the autocorrelation function with increasing axial position above the distributor. By moving upward in the bed, the autocorrelation function tends to find its periodic nature, which resembles the fluidization behavior corresponding to bed depths of 40 and 80 cm in Fig. 2.4a. It can be concluded that even in the case of deep fluidized beds, the upper part of the bed encounters a better mixing condition, which is also in accordance with the visual observations.

2.5.2.2. Effect of Gas Velocity

The effect of gas velocity on the autocorrelation and the power spectral density are provided in Figs. 2.6 and 2.7. In general, increasing the gas velocity delays the streaming in a deep bed by providing extra gas to diffuse into the poorly fluidized regions. As can be seen from Figs. 2.6 and 2.7, increasing gas velocity does not have a great influence in the 40 cm bed, which indicates that in shallow beds, fluidization is well established at low velocities. This fact has also been reported by other researchers (Cui et al., 2000). Changes in the periodic nature of the bed with increasing velocity can be attributed to changes in bubble diameters and rise velocities as more gas is added to the bed. However, increasing the gas velocity causes a marked change in the case of deep-bed fluidization, although the condition is still far from the smooth fluidization seen in the shallower bed.

The change can be seen in the return of periodic oscillations, a more rapid decrease of the autocorrelation function and the suggestion of a dominant frequency in the PSD plot (albeit a lower dominant frequency than that associated with fully bubbling fluidization).

It is important to point out from Figs. 2.6 to 2.7 that the extent of the change in the autocorrelation function and the PSD trace in moving from 35 to 50 times the minimum fluidization velocity is far less than when moving from 10 to 35 times the minimum fluidization velocity. In addition, the plots at these higher velocities are still very dissimilar from those in the shallow bed. This signifies that for the range investigated here (up to 50 U_{mf} (=0.2 m/s)), increasing the fluidizing velocity in deep fluidized beds can not completely solve the maldistribution problem caused by streaming flow in the fluidized bed with coarse FCC particles and bed depth of 160 cm. Presumably, very high gas velocities might be effective in eliminating the streams, however this would lead to excessive entrainment and indeed a potential transition to the fast fluidization regime. Such experiments would require modification to our unit involving multistage cyclones and proper solids recycling.

2.5.2.3. Effect of Particle Size Distribution

The effect of the particle size distribution (i.e. fines addition) on the fluidized bed behavior in two bed depths of 40 cm and 160 cm and gas velocity of 10 U_{mf} in terms of PSD and autocorrelation coefficients is shown in Figs. 2.8 and 2.9. As can be seen in Fig. 2.8a and 9a, there is no observable difference for the 40 cm deep fluidized bed for the two particle sizes. As the autocorrelation plot of Fig. 2.8a shows, the periodic nature and the

level of the correlation between two fluidized beds of coarse and fine particles are minimally affected by the particle size distribution. The PSD graphs of Fig. 2.9a show the dominant frequency of 4 and 4.5 Hz for coarse and fine particles, respectively, which are quite close. However, the plots corresponding to the 160 cm bed depth, where it was established that streaming flow occurs, shows differences between the two particle sizes. The autocorrelation for fine particles in the deep bed, Fig. 2.8b, shows some levels of periodicity and a sharper drop-off rate, which are characteristics of normal fluidization. The difference between the fluidization of two particle sizes can also be seen in the PSD graph of Fig. 2.9b. As noted previously, in case of coarse particles, the PSD decreases exponentially and does not show a dominant frequency. However, the fluidized bed of fine particles exhibits local peaks at frequencies of roughly 2.5 and 3 Hz and are probably the outcome of the superposition of the bubbling and streaming phenomena in the bed. The general conclusion is that fines content has some influence on decreasing the severity of the streaming flow. This influence can be attributed to the effect of fines in loosening the boundary between bubbles and gas passages and the surrounding dense phase (Lockett and Harrison, 1967) that allows the gas to further diffuse into the surrounding regions. The effect of fines on decreasing the viscosity of the fluidized bed can also be an important factor in conducting an extra flow of gas into other parts of the fluidized bed (Geldart, 1972). Rowe et al. (1978) reported that the interstitial gas flow increased by three orders of magnitude with increasing fines content from 3% to 20% for particles originally having a mean diameter of 52 μm. It should be noted that the effect of fines in the range of operating conditions studied here (160 cm bed and gas velocity of 10 U_{mf})is still not sufficient to achieve a normal bubbling activity in the system.

2.5.2.4. Effect of Distributor

A plot of the distributor pressure drop as a function of gas velocity is provided in Fig. 2.10. As can be seen, the LPD and HPD distributors have very different pressure drops and are expected to exert a different influence on the bed hydrodynamics. The effect of distributor pressure drop on the fluidization quality for 40 and 160 cm bed depths, two gas velocities of 10 and 50 times minimum fluidization, and the coarse FCC particles (3% fines) are provided in Figs. 2.11 and 2.12, in terms of autocorrelation and PSD. For the 40 cm bed depth, both the low pressure drop (LPD) distributor and the high pressure drop (HPD) distributor exhibit similar autocorrelation functions. At high velocity, the oscillations are larger for the LPD distributor. Generally, the higher pressure drop provides a more uniform air distribution, thus promoting the formation of bubbles over the entire distributor and spread over wider frequencies. The formation of larger bubbles that easily coalesce and produce dominant bubbling activity is the reason for sharper peaks in the PSD graph of the LPD distributor at lower gas velocity. The graphs of both autocorrelation and PSD for the 160 cm bed which is subject to streaming flow do not show any significant effect of distributor design on the streaming phenomenon at both high and low velocities.

2.6. Conclusions

A series of experiments was conducted to study the effect of bed depth, superficial gas velocity, fines content, and distributor pressure drop on streaming flow in a 0.3-m diameter fluidized bed. The analysis of the pressure fluctuations time series for bed

depths ranging from 40 to 160 cm revealed that the normal bubbling fluidization is gradually compromised by increasing the bed depth. This conclusion is based on the gradual increase of the autocorrelation function, the decrease in the rate of decay of the autocorrelation function, and the disappearance of the dominant frequency in the PSD graph with increasing bed depth. The extent of streaming maldistribution was found to be non-uniform along the bed, with the quality of fluidization improving with increasing height above the distributor plate. Increasing the gas velocity from 10 to 50 U_{mf} was found to be able to delay the streaming flow, likely due to the additional gas diffusing into the poorly fluidized regions. This effect was observed to be more prominent when gas velocity was increased from 10 to 35 U_{mf} than when it was increased from 35 to 50 U_{mf}. The analyses illustrated that increasing the fines content from 3% to 20% can decrease the severity of the streaming flow. However, the improvement is not enough to solve the streaming problem. Finally, analyses did not show any significant effect of distributor design on the streaming phenomenon.

2.7. References

Bai, D., Bi, H.T. Grace J., 1997. Chaotic behavior of fluidized beds based on pressure and voidage fluctuations. AIChE journal 43, 1357-1361.

Bai, D., Issangya, A.S., Grace J., 1999. Characteristics of gas-fluidized beds in different flow regimes. Industrial and Engineering Chemistry Research 38, 803-811.

Canada, G.S., McLaughlin, M., Staub, F.W., 1978. Flow regimes and void fraction distribution in gas fluidization of large particles in beds without tube banks. AIChE Symposium Series 74, 14-26.

Clark, N.N., McKenzie, E.A., Gautam, M., 1991. Differential pressure measurements in a slugging fluidized bed. Powder Technology 67, 187-199.

Cui, H., Mostoufi, N., Chaouki, J., 2000. Characterization of dynamic gas-solid distribution in fluidized beds. Chemical Engineering Journal 79, 133-143.

Daw, C.S., Halow, J.S., 1991. Characterization of voidage and pressure signals from fluidized beds using deterministic chaos theory. In: Proceeding of 11th International Conference on Fluidized Bed Combustion. Anthony, E.J. (Ed.), American Society of Mechanical Engineers, New York.

Ellis, N., 2003. Ph.D. Dissertation, Hydrodynamics of gas-solid turbulent fluidized beds. University of British Columbia, Canada.

Falkowski, D., Brown, R.C., 2004. Analysis of pressure fluctuations in fluidized beds. Industrial and Engineering Chemistry Research 43, 5721-5729.

Fan, L.T., Ho, T.C., Hiraoka, S., Walawender, W.P., 1981. Pressure fluctuations in a fluidized bed. AIChE Journal 27, 388-396.

Fan, L.T., Ho T.-Ching, Walawender, W.P., 1983. Measurements of the rise velocities of bubbles, slugs and pressure waves in a gas-solid fluidized bed using pressure fluctuation signals. AIChE Journal 29, 33-39.

Farag, H.I., Mejdell, T., Hjarbo, K., Ege, P., Lysberg, M., Grislingas, A., De Lasa, H., 1997. Fibre optic and capacitance probes in turbulent fluidized beds. Chemical Engineering Communication 157, 73-107.

Geldart, D., 1972. The effect of particle size and size distribution on the behaviour of gas-fluidised beds. Powder Technology 6, 201-215.

Geldart, D., 1973. Types of gas fluidization. Powder Technology 7, 285-292.

Grace, J., Sun, G., 1991. Influence of particle size distribution on the performance of fluidized bed reactors. The Canadian Journal of Chemical Engineering 69, 1126-1134.

Hiby, J.W., 1967. Periodic phenomena connected with gas-solid fluidization. Proceedings of the International Symposium on Fluidization, The Netherlands University Press, Amsterdam, The Netherlands.

Huilin, L., Gidaspow, D., Bouiilard J., 1997. Dimension measurements of hydrodynamic attractors in circulating fluidized beds. Powder Technology 90, 179-185.

Huilin, L., Gidaspow, D., Bouiilard J., 2002. Chaotic behavior of local temperature fluctuations in a laboratory-scale circulating fluidized bed. Powder Technology 123, 59-68.

Issangya, A., Knowlton, T., Karri, S.B.R., 2007. Detection of gas bypassing due to jet streaming in deep fluidized beds of group A particles. In: Fluidization XII, Berruti, F., Bi, X., Pugsley, T. (Eds.), Vancouver, British Columbia, Canada, May 13-17.

Jin, Y., Yu, Z.Q., Wang, Z.W., Cai, P., 1986. In: Fluidization, Ostergaard V.K., Sorensen, A. (Eds.), Engineering Foundation, New York.

Johnsson, F., Svensson, A. Andersson, S., Leckner, B., 1995. Fluidization regimes in boilers, Fluidization VIII, Tours, pp. 129-136.

Johnsson, F., Zijerveld, R.C., Schouten, J.C., van den Bleek, C.M., Leckner, B., 2000. Characterization of fluidization regimes by time-series analysis of pressure fluctuations. International Journal of Multiphase Flow 26, 663-715.

Kang, W.K., Sutherland, J.P., Osberg, G.L. 1967. Pressure fluctuations in a fluidized bed with and without screen cylindrical packings. Industrial Engineering Chemistry Fundamentals 6, 499-504.

Karri, S.B.R., Issangya, A.S., Knowlton, M., 2004. Gas bypassing in deep fluidized beds. In: Fluidization XI, Arena, U., Chirone, R., Miccio, M., Salatino, P. (Eds.), Ischia (Naples), Italy, May 9-14.

Kozma, R., Kok, H., Sakuma, M., Djainal, D.D., Kitamura, M., 1996. Characterization of two-phase flows using fractal analysis of local temperature fluctuations. International Journal of Multiphase Flow 22, 951-968.

Lirag, R.C., Littman, H., 1971. Statistical study of the pressure fluctuations in a fluidized bed. AIChE Journal 67, 11-22.

Lockett, J. Harrison, D., 1967. The distribution of voidage fraction near bubbles rising in gas fluidized beds. Proceeding of the International Symposium on Fluidization, Drinkenburg, A.A.H. (Ed.) Netherland University Press, Amsterdam, pp. 257-270.

McKeen, T. Pugsley, T., 2003. Simulation and experimental validation of freely bubbling bed of FCC catalyst. Powder Technology 129, 139-152.

Ohara, H., Ji, H., Kuramoto, K., Tsutsumi, A., Yoshida, K., Hirama, T., 1999. Chaotic characteristics of local voidage fluctuation in a circulating fluidized bed. The Canadian Journal of Chemical Engineering 77, 247-252.

Rowe, P.N., L. Santoro, J.G. Yates, 1978. The division of gas between bubble and interstitial phases in fluidized beds of fine powders. Chemical Engineering Science 33, 133-140.

Satija, S., Fan, L.-S., 1985. Characteristics of slugging regime and transition to turbulent regime for fluidized beds of large coarse particles. AIChE Journal 31, 1554-1562.

Svensson, A., Johnsson, F., Leckner, B., 1996. Fluidization regimes in non-slugging fluidized beds: the influence of pressure drop across the air distributor. Powder Technology 86, 299-312.

Tamarin, A.I., 1964. The origin of self-excited oscillations in fluidized beds. International Journal of Chemical Engineering 4, 50-54.

van der Schaaf, J., Schouten, J.C., Johnsson, F., van den Bleek, C., 2002. Non-intrusive determination of bubble and slug length scales in fluidized beds by decomposition of the power spectral density of pressure time series. International Journal of Multiphase Flow 28, 865-880.

van Ommen, J.R., Coppens, M.O., van den Bleek, C.M., Schouten, J.C., 2000. Early warning of agglomeration in fluidized beds by attractor comparison. AIChE Journal 46, 2183-2197.

Welch, P.D., 1967. The use of a fast Fourier transform for the estimation of power spectra. IEEE Transactions, Audio and Electroacoustics AU-15, 70-73.

Wells, J., 2001. Streaming flow in large scale fluidization. AIChE Annual Meeting, Particle Technology Forum, Reno, Nevada, USA.

Wen, C.Y., Yu, Y.H., 1966. A generalized method for predicting the minimum fluidization velocity. AIChE Journal 12, 610-612.

Woo, K.J., Kim, J.S., Kang, Y., Kim, S.D., 2001. Effects of chaotic temperature fluctuations on the heat transfer coefficient in liquid-liquid-solid fluidized beds, Chemical Engineering Technology 24, 829-834.

Yerushalmi, J., Cankurt, N.T., 1979. Further studies of the regimes of fluidization. Powder Technology 24, 187-205.

2.8. Nomenclature

ACF autocorrelation function

f frequency (Hz)

H bed depth (m)

i counter

k counter

n time series length

CCF cross correlation function

T time series period (1/s)

U_0 superficial gas velocity (m/s)

x_i ith component of the x time series

$\overline{x}$ average of the x time series

y time series

$\overline{y}$ average of the x time series

Greek Letters:

Φ_{xx} power spectral density for x time series

Φ_{xy} cross power spectral density between x and y time series

Φ_{yy} power spectral density for y time series

γ_{xy} coherency between x and y time series

Table 2.1. The range of different variables studied in this work

Variable	**Range**
Bed depth (cm)	40, 80, 120, 160
U_0/U_{mf}	10, 35, 50
Fines content (particles with a diameter of less than 44 μm)	3%, 20%
Distributor	1 mm holes and 0.54% opening, 2 mm holes and 2.15% opening

Table 2.2. Specifications of the pressure transducers used in the present work

Model	**Type**	**Range**	**Accuracy**	**Response**	**Position on the column**
Omega PX143-2.5BD5V	Differential	-17.2 to 17.2 kPa	±1.5 FC	1 ms	130, 150 cm
Omega PX142-005D5V	Differential	0 to 34.5 kPa	±1.5 FC	1 ms	50-110 cm
Omega PX142-015D5V	Differential	0 to 103.4 kPa	±1.5 FC	1 ms	4, 30 cm

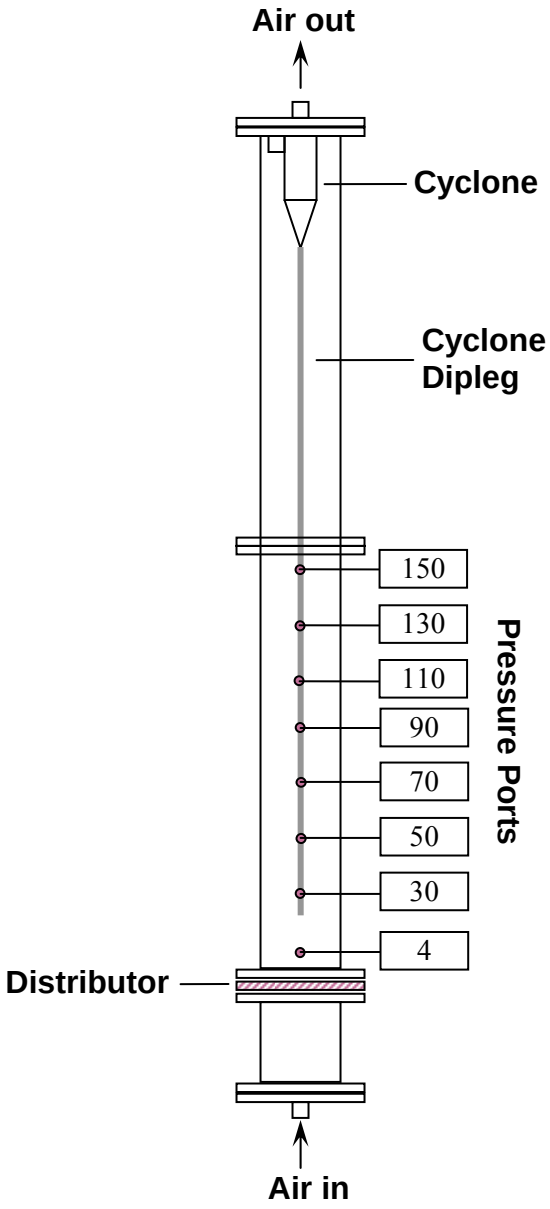

Figure 2.1. Schematic diagram of the fluidized bed used in the experiments depicting axial positions (in cm) of the pressure ports above the distributor.

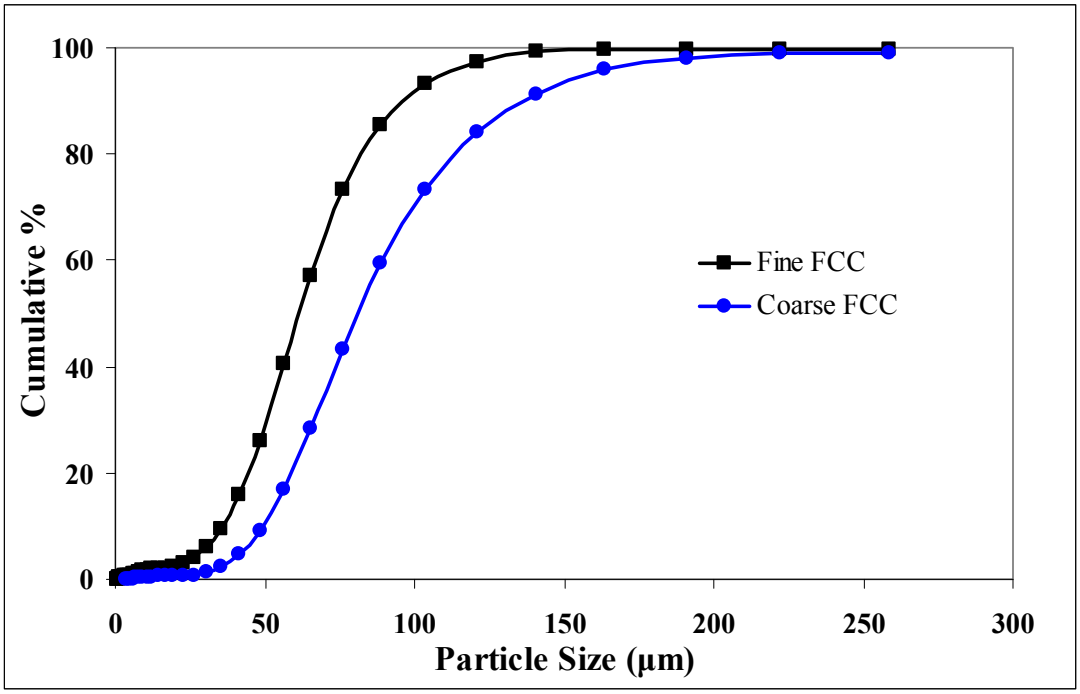

Figure 2.2. Particle size distribution of the FCC powders used in the experiments

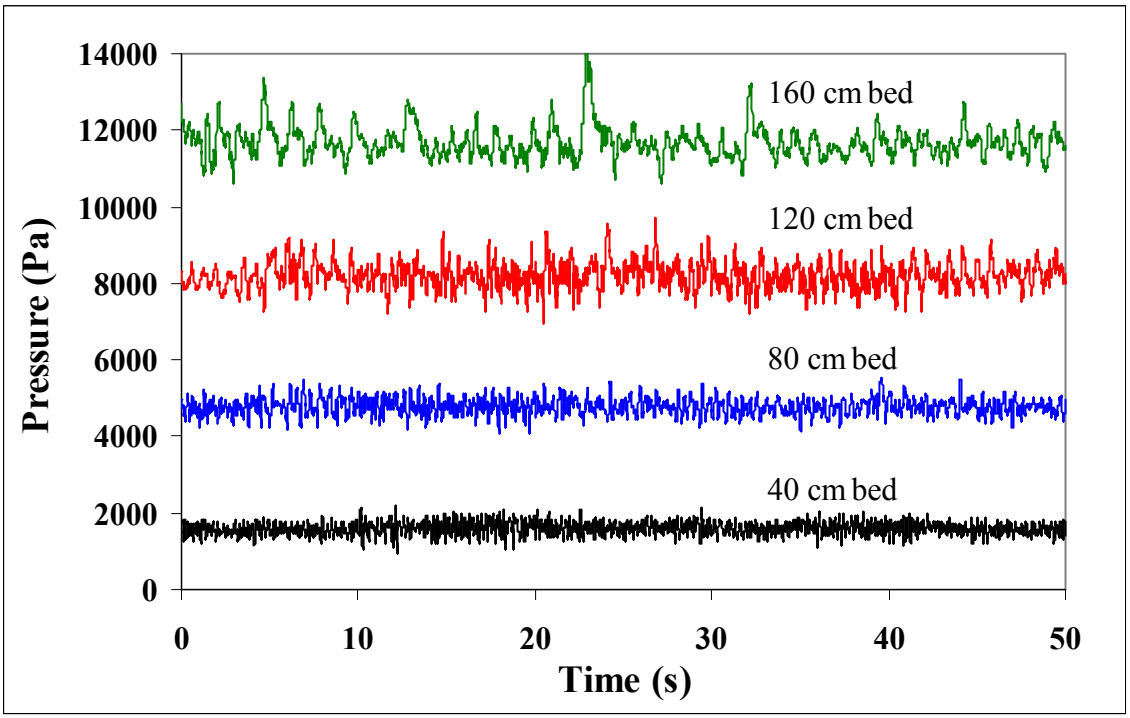

Figure 2.3. Time series of pressure fluctuations measured for different bed depths, coarse FCC (3% fines content), HPD distributor, U_0=35 U_{mf}. Pressure fluctuations correspond to an axial position of 30 cm above the distributor plate.

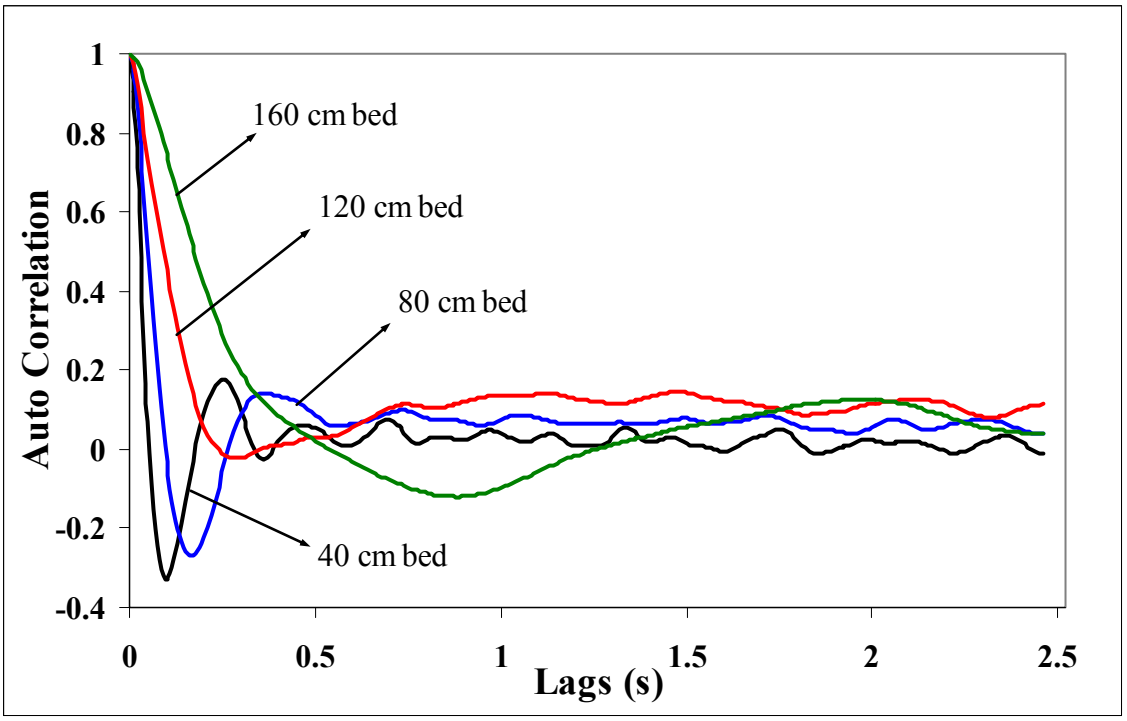

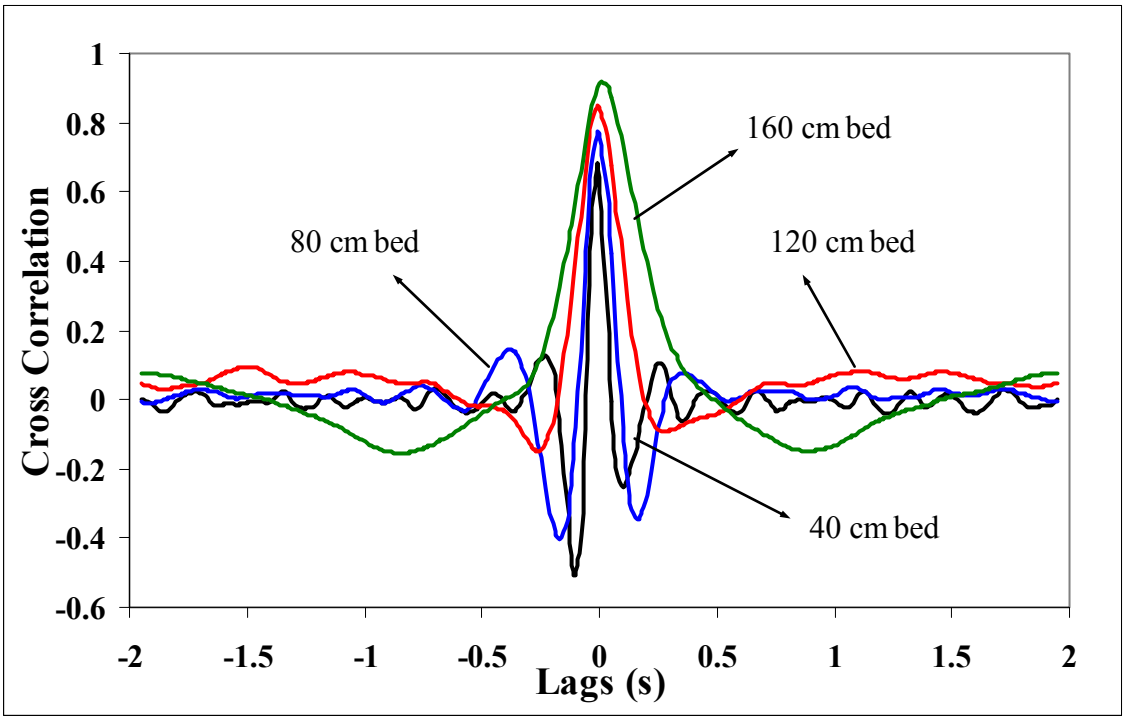

Figure 2.4. (a) Autocorrelation and (b) Cross correlation of pressure fluctuations for different bed depths, coarse FCC (3% fines content), HPD distributor, U_0=35 U_{mf}. Pressure fluctuations correspond to an axial position of 30 cm above the distributor plate.

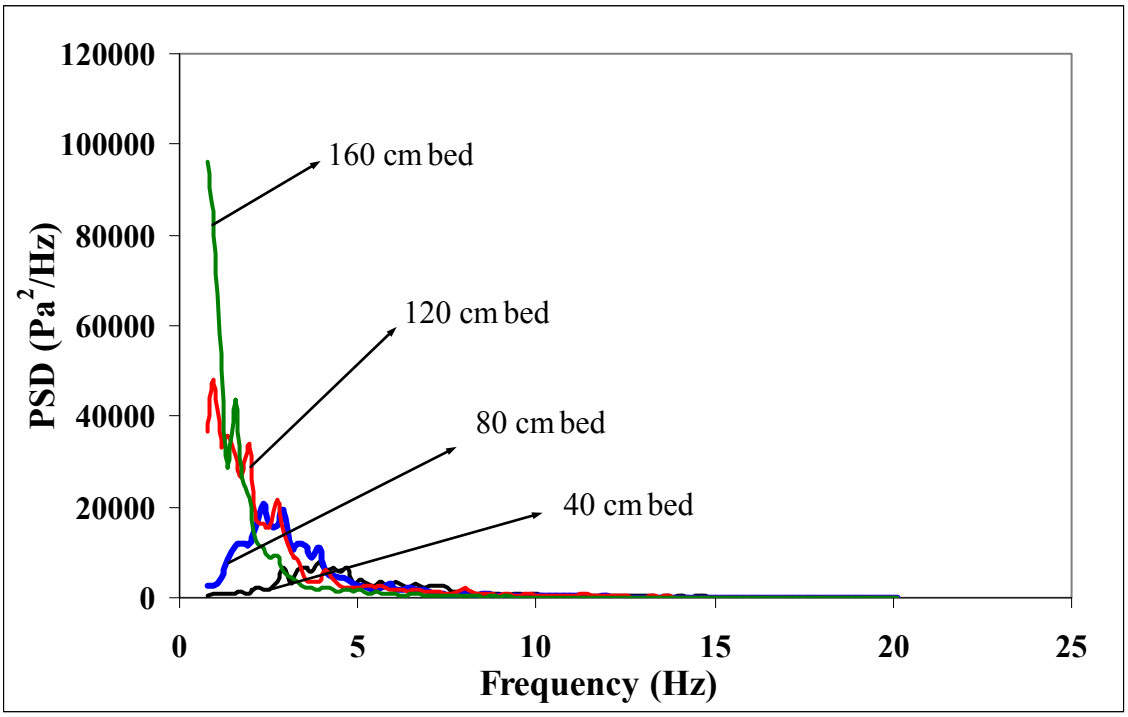

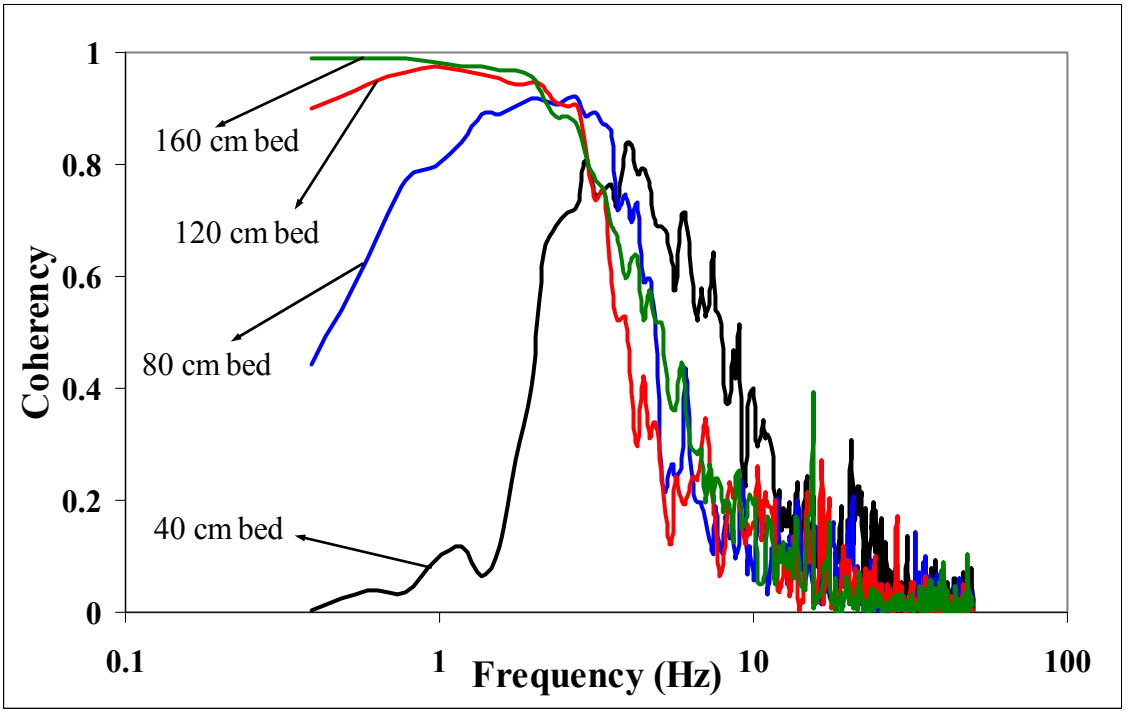

Figure 2.4. (c) PSD and (d) Coherency of pressure fluctuations for different bed depths, coarse FCC (3% fines content), HPD distributor, U_0=35 U_{mf}. Pressure fluctuations correspond to an axial position of 30 cm above the distributor plate.

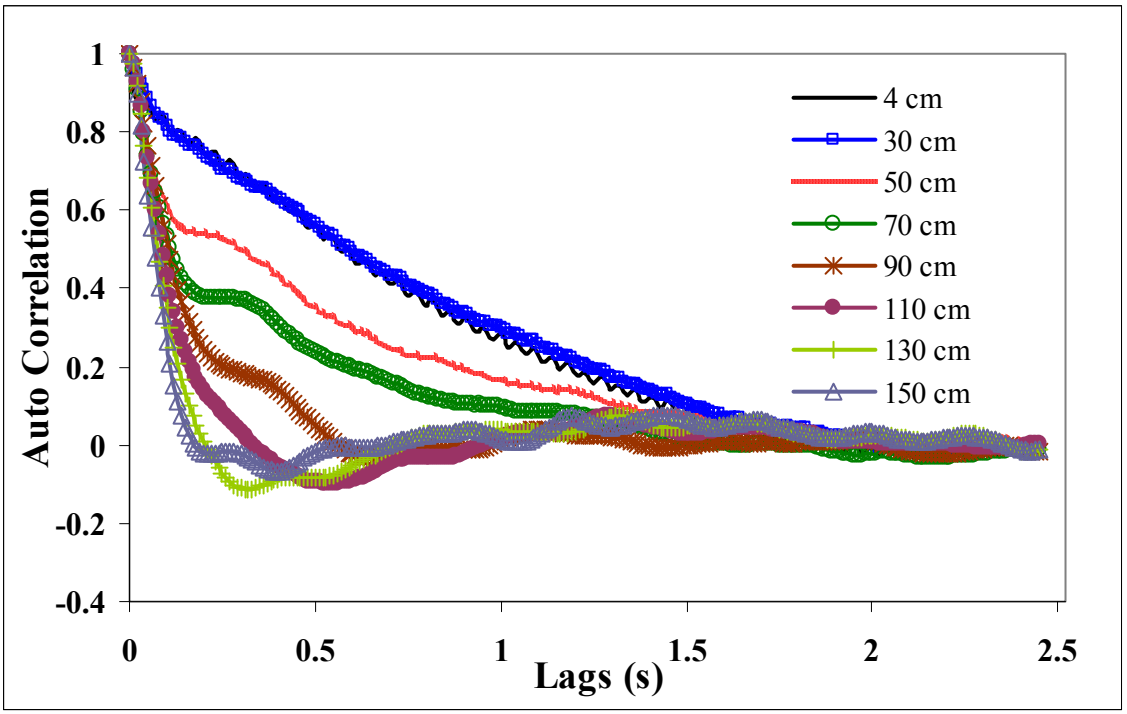

Figure 2.5. The autocorrelation coefficient at different axial positions above the gas distributor for the case of coarse FCC (3% fines content), HPD distributor, H=160 cm, and U_0=10 U_{mf}

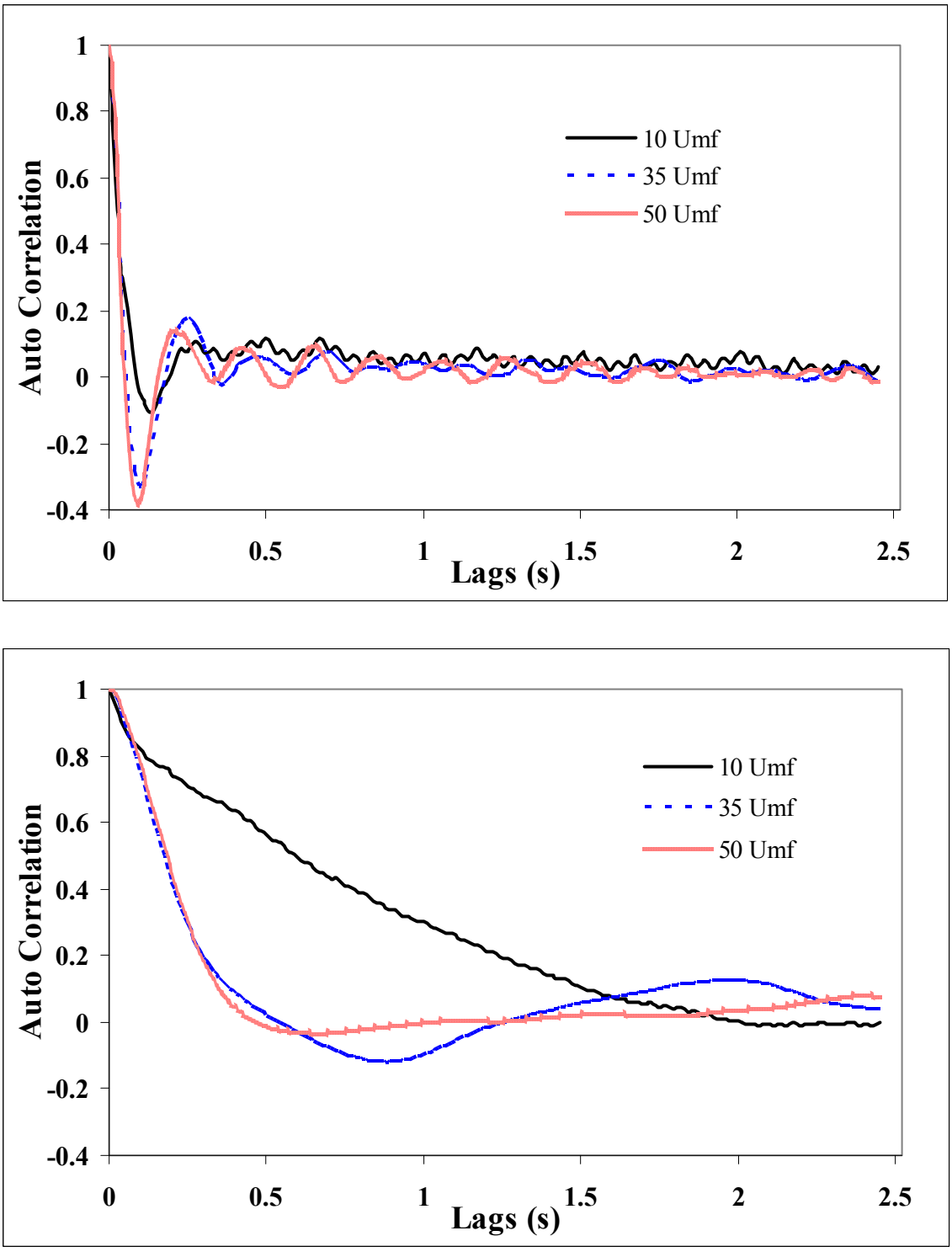

Figure 2.6. The autocorrelation coefficient of pressure fluctuations for different gas velocities, coarse FCC (3% fines content), HPD distributor, a) *H*=40 cm, b) *H*=160 cm. Pressure fluctuations correspond to an axial position of 30 cm above the distributor plate.

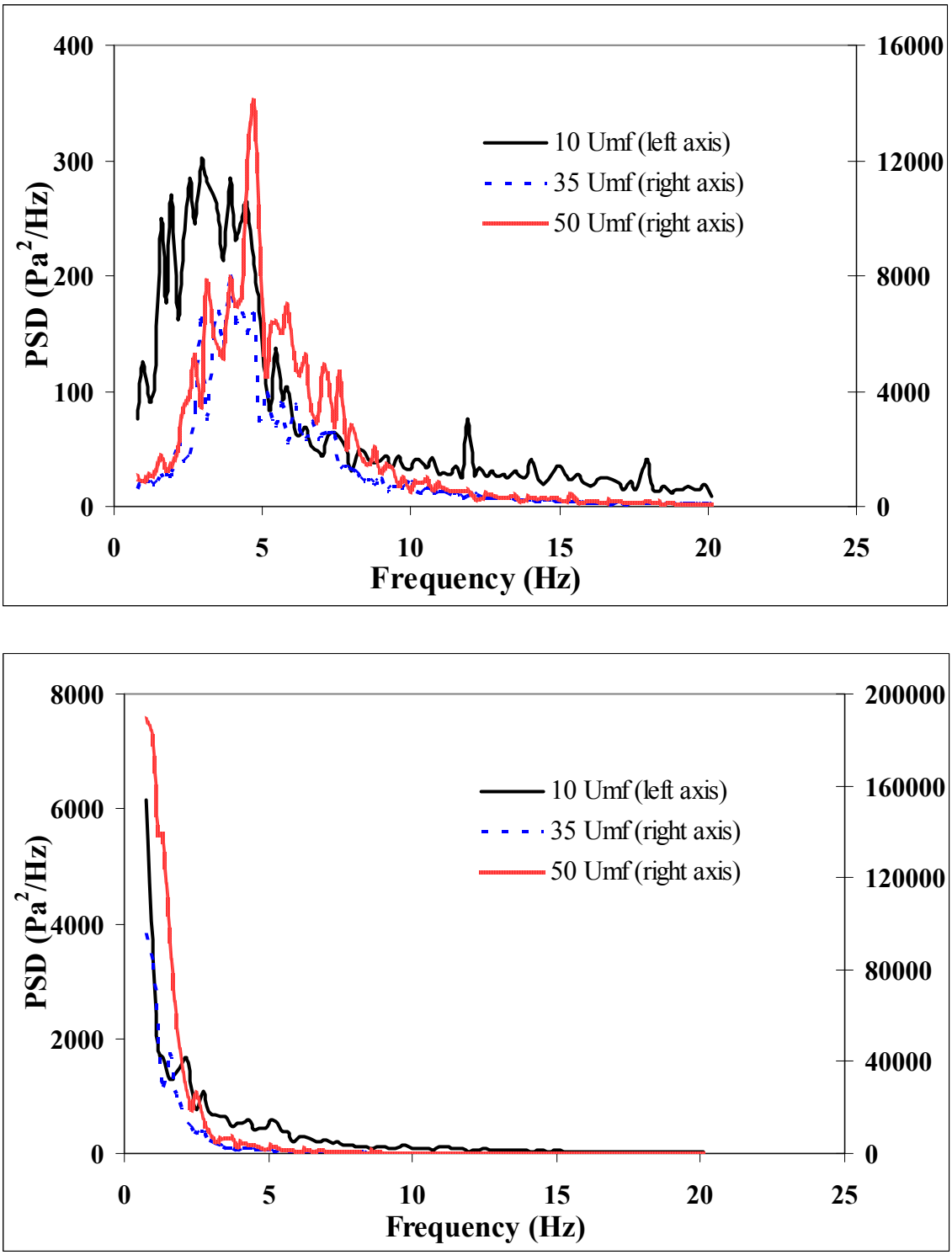

Figure 2.7. The PSD of pressure fluctuations for different gas velocities, coarse FCC (3% fines content), HPD distributor, a) *H*=40 cm, b) *H*=160 cm. Pressure fluctuations correspond to an axial position of 30 cm above the distributor plate.

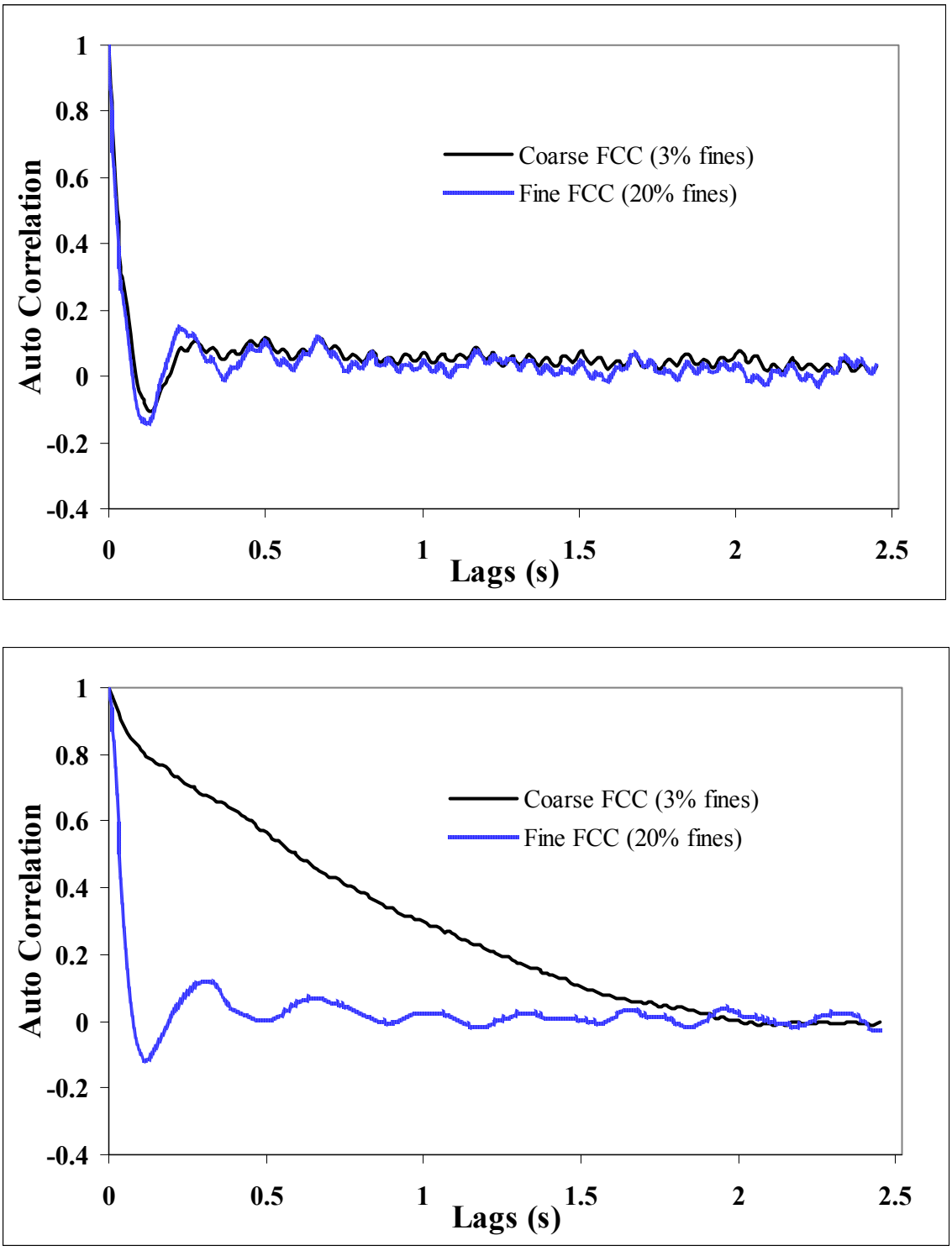

Figure 2.8. The autocorrelation of pressure fluctuations for different particle sizes, U_0=10 U_{mf}, HPD distributor, a) H=40 cm, b) H=160 cm. Pressure fluctuations correspond to an axial position of 30 cm above the distributor plate.

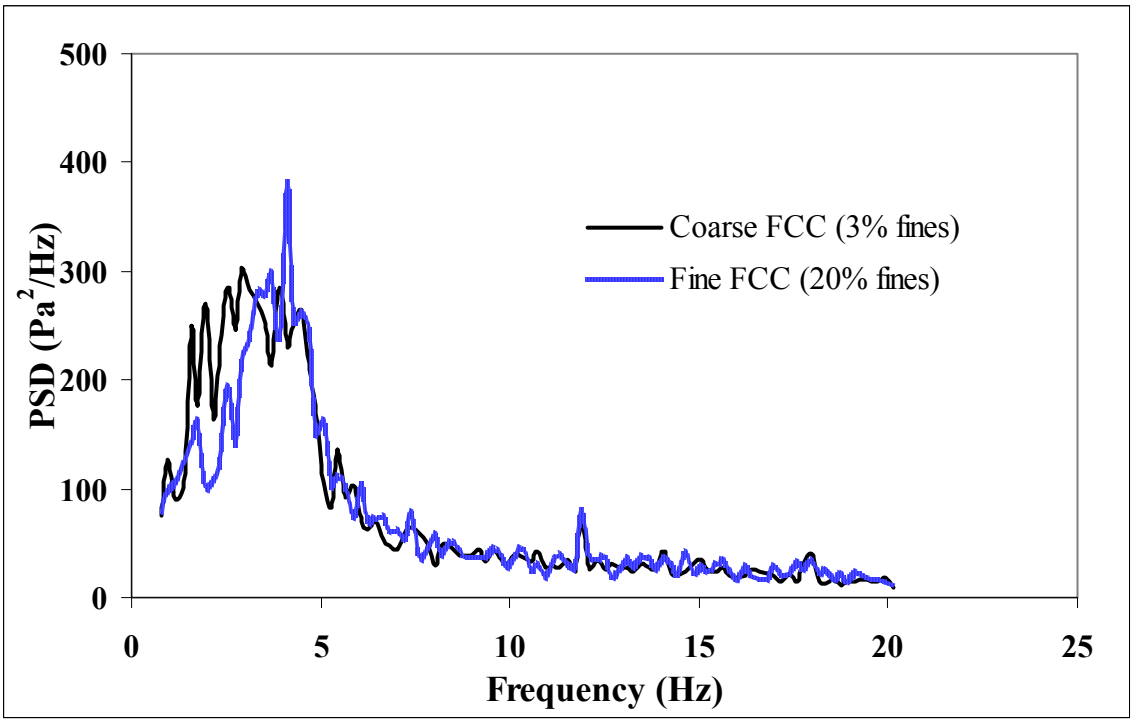

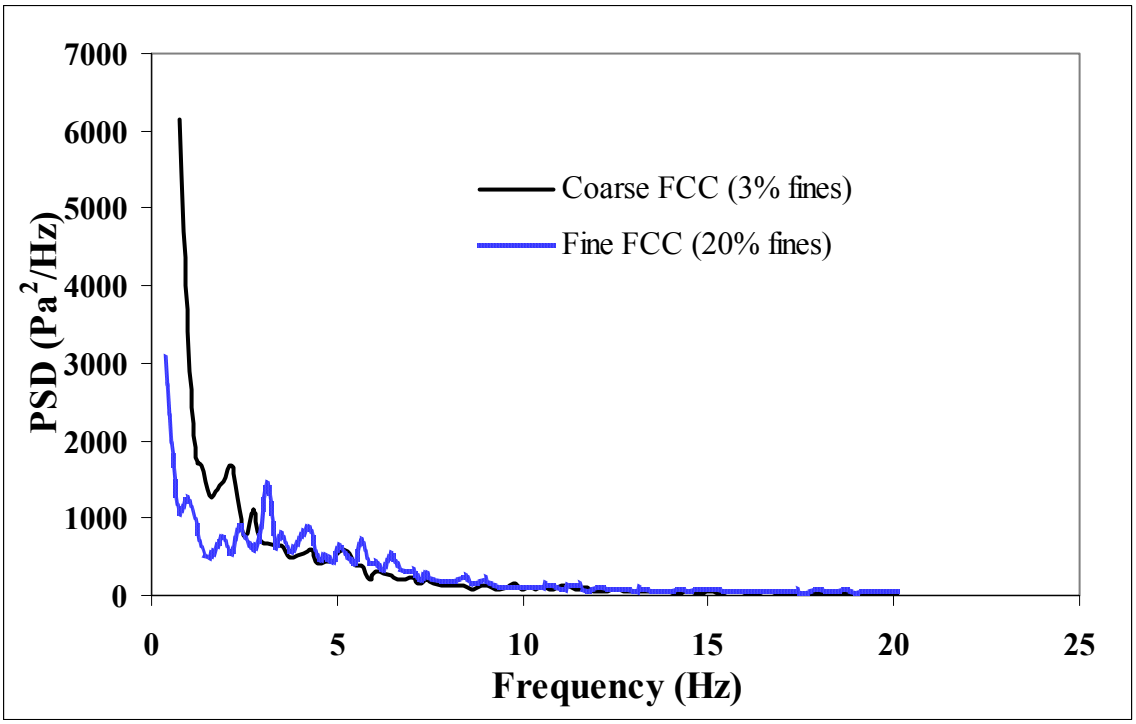

Figure 2.9. The PSD coefficient of pressure fluctuations for different particle sizes, U_0=10 U_{mf}, HPD distributor, a) H=40 cm, b) H=160 cm. Pressure fluctuations correspond to an axial position of 30 cm above the distributor plate.

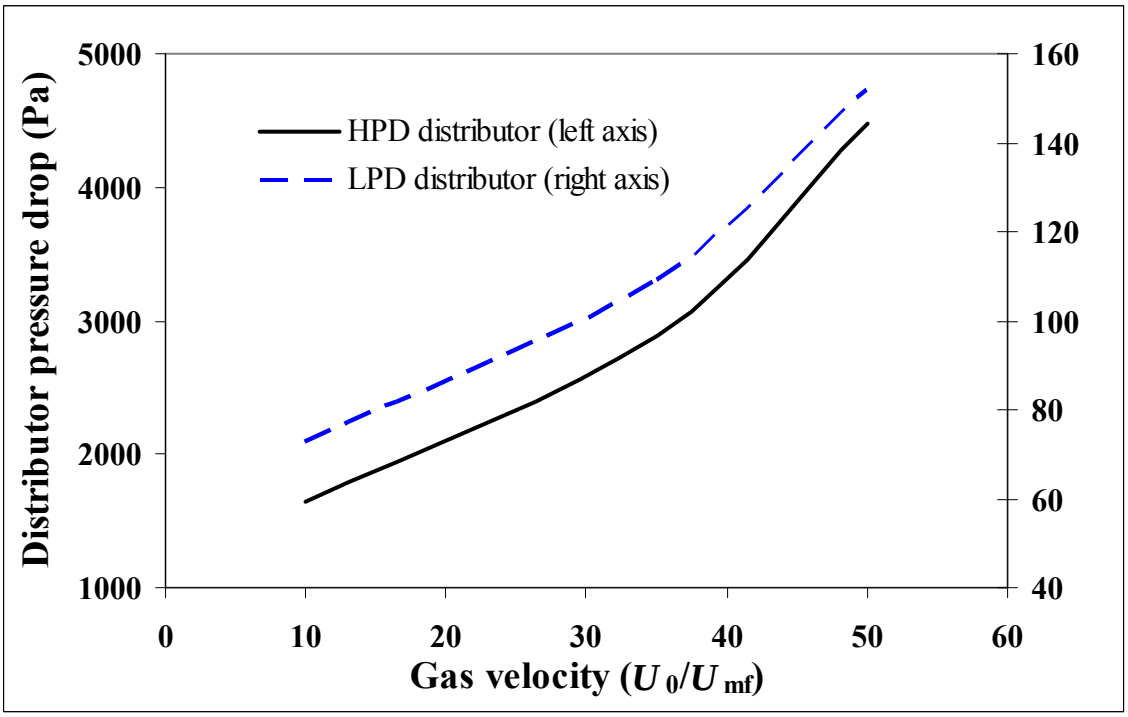

Figure 2.10. The pressure drops of the HPD and LPD distributors as a function of gas velocity.

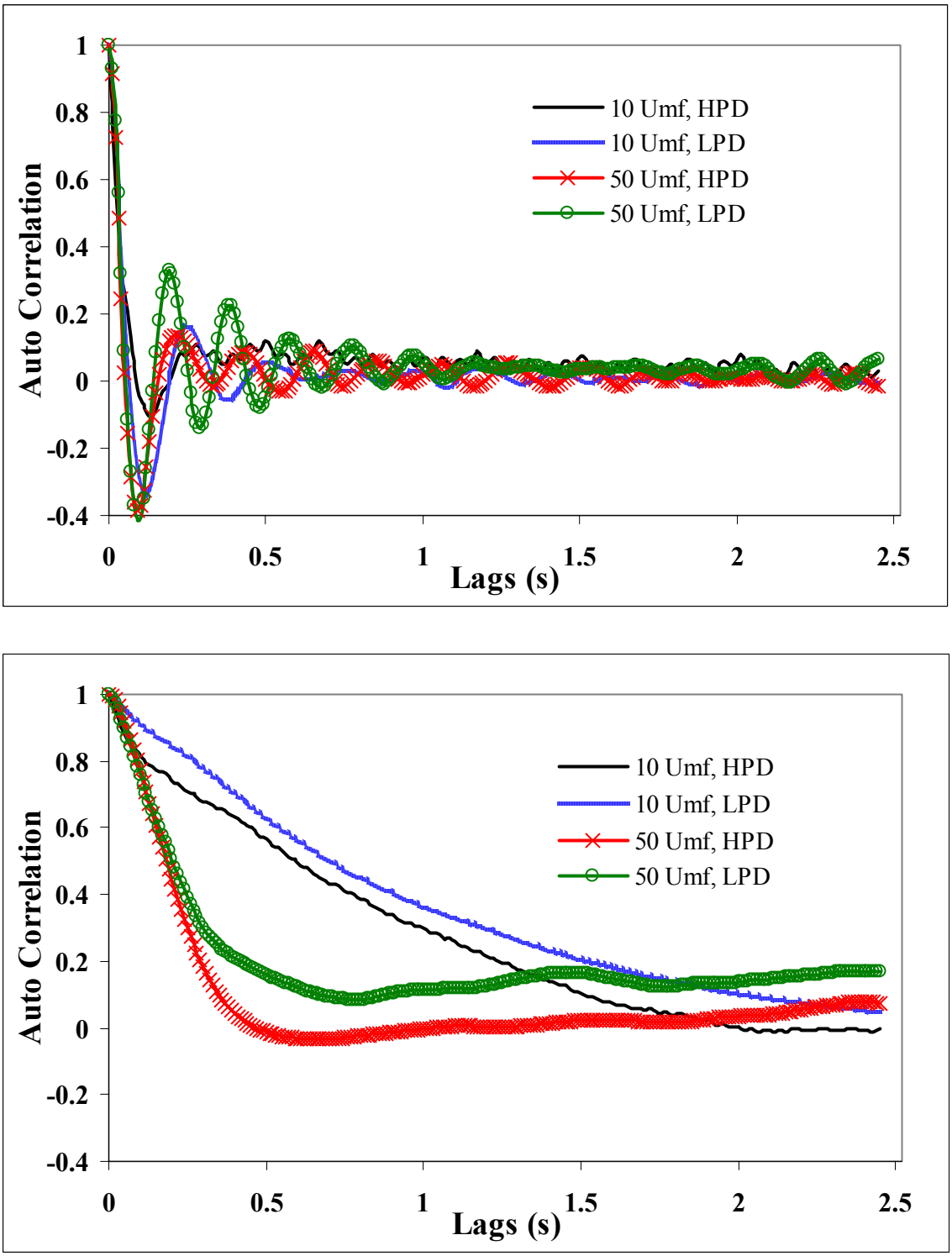

Figure 2.11. The autocorrelation of pressure fluctuations for coarse FCC (3% fines content) with different distributors, a) *H*=40 cm, b) *H*=160 cm. Pressure fluctuations correspond to an axial position of 30 cm above the distributor plate.

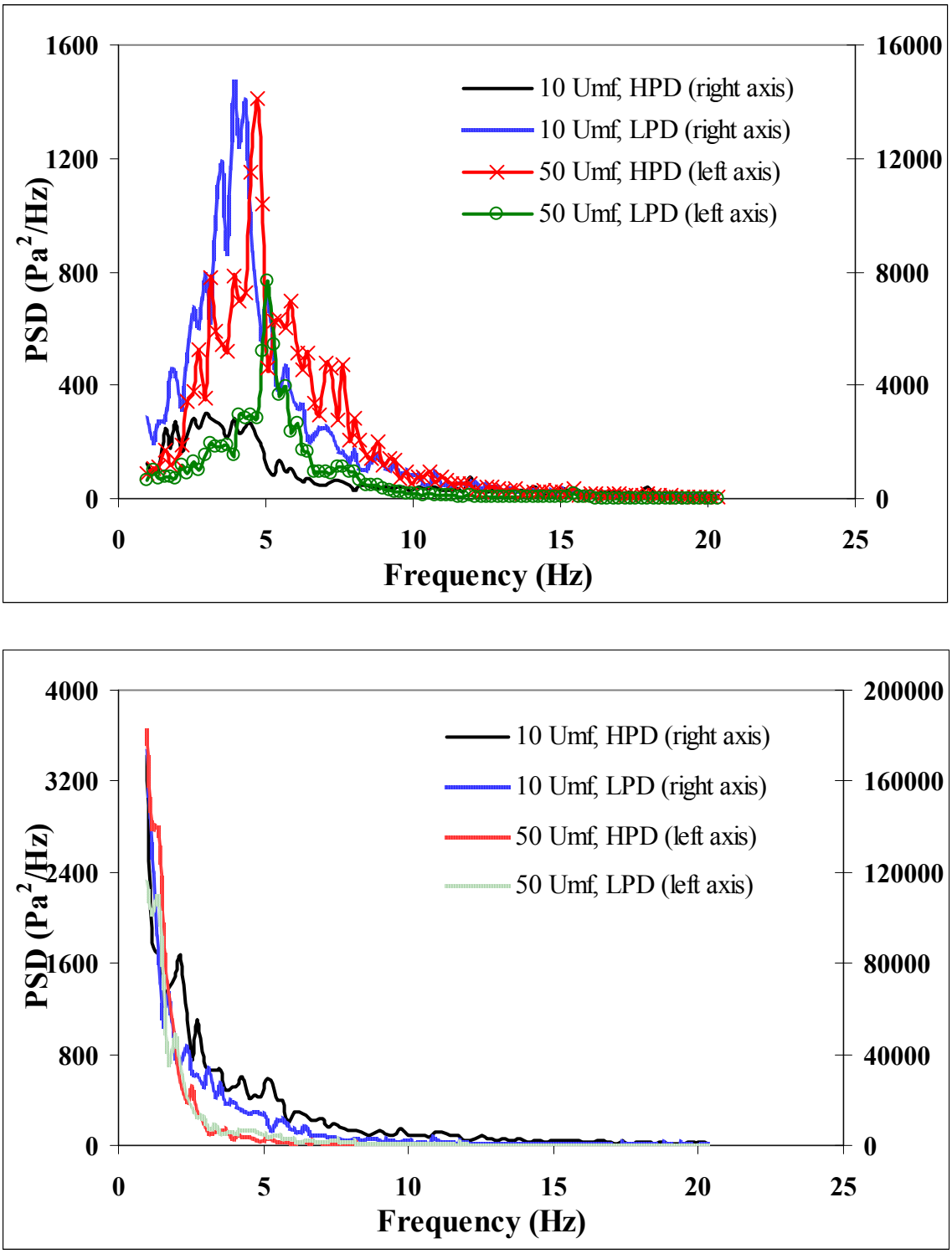

Figure 2.12. The PSD of pressure fluctuations for coarse FCC (3% fines content) with different distributors, a) *H*=40 cm, b) *H*=160 cm. Pressure fluctuations correspond to an axial position of 30 cm above the distributor plate.

CHAPTER 3 - Experimental Study of the Nature of Gas Streaming in Deep Fluidized Beds of Geldart A Particles

The contents of this chapter have been submitted to the ***Chemical Engineering journal***. It has been submitted in a version similar to what appears in this chapter.

Citation

S. Karimipour, T. Pugsley, Experimental study of the nature of gas streaming in deep fluidized beds of Geldart A particles, Chemical Engineering journal, March 2010 (Ref. No. CEJ-S-10-00526).

Contribution of Ph.D. Candidate

The experiments performed for the purpose of this work were planned and performed by Shayan Karimipour. Todd Pugsley provided consultation regarding the experimental program. The programs for all of the data analysis were developed by Shayan Karimipour. All of the writing of the submitted manuscript was done by Shayan

Karimipour with Todd Pugsley providing editorial guidance regarding the style and technical content of the manuscript.

Contribution of this Paper to the Overall Study

The objective of the present work is to execute a more fundamental investigation of the streaming flow using a comparative analysis of the streaming with some well-defined phenomena (Jet flows and imposed streams) in order to further improve the understanding of the streaming flow gained in the previous work and establish some theories about the origin of streaming flow. Time series analysis and wavelet decomposition of the pressure fluctuations time series will be used.

3.1 Abstract

The characteristics of gas streaming in a deep fluidized bed containing Geldart's Group A powder has been investigated in a 30-cm ID cold flow unit. Four different experimental configurations including forced streaming flow, high and low-velocity jetting flows and natural streaming flow in deep beds were designed and conducted for bed depths and gas velocities ranging from 0.4 to 1.6 m and 0.04 to 0.20 m/s, respectively. The effect of fines content was also studied using two particle size distributions with Sauter mean diameters of 48 μm and 84 μm, corresponding to 20% and 3% fines content, respectively. Results indicated that the natural streaming closely resembles the forced streaming flow at the wall in which flow of gas is also present in the remaining regions of the distributor. The configurations of jet flows without primary gas from the distributor resemble the severe streaming that might happen in very deep beds with possible formation of completely

non-fluidized regions. Application of supporting jets in addition to the primary gas flow enhanced the fluidization quality to some extent, but was not sufficient to provide normal fluidization. Increasing the primary gas velocity from 10 to 50 U_{mf} was found to reduce the effect of supporting jets. It was also found that higher fine content improved fluidization. Wavelet analysis of pressure fluctuations showed that in deep fluidized beds, bubbling activity with the typical dominant frequency coexist with the streaming flow, with a minor contribution. Wavelet findings suggested that the streaming flow can be considered to form by increasing the relative importance of one of the available streams of bubbles with increasing bed depth.

3.2. Introduction

Fluidized bed technology is applied in a range of industrial sectors, including oil refining, coal gasification and combustion, and pharmaceutical manufacture. In certain applications, it is necessary to operate with very deep fluidized beds to control solids and/or gas residence time to achieve reactor performance targets. Recently, it has been revealed that in a sufficiently deep bed of Geldart's Group A particles (Geldart, 1973), gas bypassing may occur when the flow rate of the fluidizing gas is increased beyond the minimum fluidization velocity (Wells, 2001; Karri et al., 2004; Issangya et al., 2007; Karimipour and Pugsley, 2010) [2-5]. When this phenomenon occurs, the fluidizing gas bypasses the bed in the form of streams of gas, leaving a large fraction of the bed unfluidized or poorly fluidized. Since many industrial fluidized bed processes might work with deep beds, gas streaming is a potential problem that can decrease the efficiency of these chemical and physical fluidized bed processes.

The concept of gas streaming was first reported in the literature by Wells (2001). He studied the effects of fines content (particles smaller than 44 μm), distributor design, anti-static agents, baffles, and bed depth in large scale units with up to 2.5 m diameter and 5 m bed depth. He reported no influence of the various parameters, with the exception of bed depth and baffles. The streaming phenomenon was attributed to gas compression caused by the pressure head of the deep bed over the distributor. The onset of streaming corresponded to an increase in the emulsion suspension density above that at minimum fluidization. The bed then defluidized and gas streaming occurred. Karri et al. (2004) investigated the formation of streaming flow in a column of 0.3 m inner diameter and 4.9 m height. They found that the standard deviation of pressure drop in a bed exhibiting streaming was much greater than a uniformly fluidized bed. Karri et al. (2004) also evaluated the use of baffles and found that two baffles separated vertically by a distance of 0.76 cm eliminated the streaming flow. Issangya et al. (2007) performed another study in a 0.9-m-diameter and 6.1 m tall test unit. They attributed the larger differential pressure fluctuations measured by certain transducers to the passage of streams closer to that transducer. Issangya et al. (2007) also concluded that the maximum in the plot of standard deviation of the pressure fluctuation measured across the entire bed *versus* gas velocity, which has been shown in the literature to be an indication of the transition between the bubbling and turbulent fluidization regimes, is not present for deep beds that are subject to streaming.

Recently, Karimipour and Pugsley (2010) have done a systematic study on the streaming flow in a 30-cm ID cold flow unit of FCC particles with two different distributor designs. They discussed the characteristics of the streaming flow based on analysis of the pressure fluctuations time series measured in the fluidized bed at 8 locations from 4 to 150 cm above the gas distributor for bed depths and gas velocities ranging from 0.4 to 1.6 m and 0.04 to 0.20 m/s, respectively. They also studied the effect of fines content on gas streaming using two particle size distributions with Sauter mean diameters of 48 μm and 84 μm for each bed depth and gas velocity. They concluded that streaming flow emerges gradually in beds with greater than 1 m depth. Increasing gas velocity and fines content was found to delay the onset of streaming, but were not completely eliminate it over the range of velocities examined. They showed that two different distributor designs with much different pressure drops had no measurable effect on the streaming flow.

Wavelet transform is valuable analysis tool for understanding the detail of the intrinsic features of fluidized beds. One of the first direct applications of wavelets in fluidized bed research was by He et al. (1997). They used wavelet analysis to decompose the pressure fluctuations time series measured in a fluidized bed with 30 cm diameter and 60 cm bed depth. They argued that the gas jetting at the distributor and formation of small bubbles near the distributor are important sources of Gaussian random noise in the pressure fluctuations. These effects are transmitted upward and reduced gradually by the increase in height and finally superimposed on the larger fluctuations caused by bubble growth and motion. Lu and Li (1999) obtained the average peak frequency of different scales of pressure fluctuation time series measured in a 3.3 cm fluidized bed using wavelet

decomposition. They found the peak frequency of the scale 4 detail of the wavelet analysis to be equivalent to the bubble frequency obtained from Darton's correlation (1977). Guo et al. (2003) decomposed the time series of pressure fluctuations obtained in a 8.2 cm bed with 11.5 cm bed depth operating at high temperatures. By comparison of the detail part of the decomposed signals to the power spectral density (PSD) of the original signal, they concluded that the frequency of peaks in the scale 6 decomposition of detail signal is equal to the major frequency obtained from the PSD plot, thus each peak represents a bubble passing through the pressure probe. Zhao and Yang (2003) used wavelets to decompose the pressure time series measured in a 30 cm bed with 46 cm bed depth into several components or "levels". They classified the different levels as micro, meso and macro-scales based on the Hurst exponent calculated at each level. Ellis et al. (2003, 2004) studied the effect of probe scale on the voidage data measured by optical probes using wavelets. They showed that the probe size affects the scale of the detected voidage fluctuations in a way that smaller probes reflect small-scale fluctuation, while a larger probe reveals meso-scale fluctuations caused mostly by bubble motion (2004). Sasic et al. (2006) extracted and analyzed the time series representing single bubbles, exploding bubbles and pressure waves from the original pressure fluctuations time series using wavelets. These phenomena were identified as distinct local maxima in the energy distribution over wavelet scales. Guenther and Breault (2007) studied the cluster size and count at various radial and axial positions in a large scale circulating fluidized bed using fiber optic probes. To remove high frequency noise from the voidage time series, they used wavelets to decompose and then reconstruct the time series excluding scales 1 and 2 of detail components. Their results showed that remarkable changes in the cluster size

and count occurred when flow conditions changed from one regime to another. They also found that cluster count generally decreased toward the wall and increased toward the center of the riser.

Although the general appearance of the streaming flow has been studied, a more detailed look at the nature and behavior of the streaming is still absent in the literature. The objective of the present work is to execute a more fundamental investigation of the streaming flow using a comparative analysis of the streaming with other well-defined phenomena in order to further improve the understanding of streaming gained in the previous works by our group and other researchers. Time series analysis and wavelet decomposition of the pressure fluctuations time series will be used. For this purpose, three well-defined configurations of forced streams and jetting have been designed in order to compare their dynamic behavior with that of normal streaming flow in deep fluidized beds. Pressure fluctuations have been measured and analyzed in all of these configurations for various combinations of bed depth, gas velocity and particle size.

3.3. Experimental

The fluidized bed unit used in this study was comprised of a cylindrical Plexiglas column with an inner diameter of 30 cm and height of 3.3 m. Details of the experimental setup, instrumentation and the bed particulate material have been reported in a previous work of our group (Karimipour and Pugsley, 2010) and provided in chapter 2. In order to fully understand the nature of the streaming flow in the deep bed (referred to here as "normal streaming"), three configurations for the addition of air to the bed were designed and

implemented. The first configuration was a double-jet nozzle made of a copper tube with 4 mm inside diameter and mounted vertically upward at a height of 19 cm above the distributor plate. The arrangement of the nozzle can be seen in Fig. 3.1. The distance between the two jets was equal to 8 cm. Compressed building air was used for gas flow to the nozzle and the flowrate was measured using a rotameter before entering the nozzle system. The jetting experiments were performed at two gas velocities of 60 (No. 1) and 31 m/s (No. 2) from each of the two jets in the nozzle. To force the creation of a stream flow at the wall of the fluidized bed column as apposed to "normal streaming", a lateral opening was cut in the distributor at a location near the pressure transducers. The opening area is supported by a flange from below in a way that gas can enter from the wind-box, but particles can not leak back into the wind-box. This area indeed provides a preferential alternative pass-way with lower pressure drop for gas that helps the stream to be stabilized in the desired region of the bed for the purpose of further analysis. A diagram of this modified distributor is shown in also Fig. 3.1. The primary fluidization air through the distributor for both natural and imposed streaming was supplied by a 50 hp Kaeser® positive displacement blower. The air flowrate was measured using an orifice plate with a colored water manometer. The ranges of the studied variables are summarized in Table 3.1.

3.4. Analysis Methods

In our previous study (Karimipour and Pugsley, 2010) the well established analysis methods of autocorrelation function, cross correlation function, power spectral density (PSD) and coherency were applied to the fluidized bed pressure fluctuations. In the

present study the wavelet decomposition technique has been utilized to decompose the pressure time series into its basic components and extract more detail information about the streaming phenomenon.

The present theoretical form of the wavelet concept was first proposed by Jean Morlet and the team working under Alex Grossmann in France (Hubbard, 1998). The theory of wavelet transformation first appeared in the literature with the work of Grossman and Morlet (1984) and was motivated by application to the analysis of seismic data. The main algorithm of wavelet analysis dates back to the work of Mallat (1988, 1989). Following these efforts in the context of multiresolution signal analysis, Daubechies (1988, 1992) introduced the first highly practical families of orthogonal wavelets.

The wavelet translation of a signal $x(t)$ is defined in term of projections of $x(t)$ onto a family of functions that are all normalized dilation and translation of a prototype wavelet function $\psi(t)$ such that

$$w\{x(t)\} = X_v^{\mu} = \int_{-\infty}^{\infty} x(t)\psi_v^{\mu}(t)dt \tag{3.1}$$

$$\psi_v^{\mu}(t) = |\mu|^{-1/2}\,\psi\left(\frac{t-v}{\mu}\right) \tag{3.2}$$

where w is the wavelet transform operator and ψ is the prototype wavelet. The prototype wavelet, ψ, also called the mother wavelet, possesses some basic properties which are discussed in the wavelet literature (1992). The family of orthogonal wavelets proposed by Daubechies (1988) has been broadly used for analysis of time series generated in the fluidized beds in the recent years (Guo et al., 2003; Zhao and Yang, 2003; Ellis et al.,

2003; Ellis et al., 2004; Sasic et al., 2006; Guenther and Breault, 2007). Daubechies (1988) originally provided nine sets of coefficients corresponding to wavelet numbers 2 to 10 ("db2-db10"). The regularity of wavelets increases with increasing their number. Indeed, the ragged edges and sharp changes become smoother by increasing the regularity. Decomposing the original time series using wavelets with increased regularity provides smoother time series (1992). Considering a trade-off between complexity and regularity, Daubechies number 5 wavelet ("db5") was chosen as the mother wavelet for this study. A plot of this wavelet is provided in Fig. 3.2a. According to the theory of multi-resolution analysis, an original signal can be decomposed into successive lower resolution components. Fig 3.2b demonstrates a schematic diagram of a four level decomposition process. Each level of decomposition contains information associated with a scale. The scale is inversely proportional to the frequency of the Fourier analysis. During the decomposition process, the main body of the signal, with lower frequencies, will be stored as the approximation part (A) and the fluctuating component of the time series as the detail part (D). Continuing the decomposition process makes the approximation part more and more depleted of the high frequency fluctuating components. Therefore, the first detail time series contain the fluctuations with the highest frequencies of the pressure time series.

3.5. Results and Discussions

3.5.1. Effect of Bed Depth

Plots of the autocorrelation function and PSD corresponding to a 40 cm bed depth and a gas velocity of 10 U_{mf} through the distributor are provided in Figs. 3.3a-b. Pressure

fluctuations were measured at 30 cm above the distributor. As Fig. 3.3.3a illustrates, all configurations but one exhibit similar periodic oscillations in the autocorrelation function with a rapid initial decrease, signifying extensive mixing in the systems. The correlation for the case of high-velocity jet (No. 1 jet) with no primary air flow through the distributor remains higher than other configurations after an initial decrease. This indicates that the gas jet with higher velocity is able to pass through the entire 40 cm bed with its basic structure remaining intact. Hence, the system exhibits a greater extent of predictability, as evidenced by a higher value of the autocorrelation function. It should be noted that the autocorrelation for this configuration also tends to zero at higher delay times of about 20 seconds.

The PSD of the various configurations, provided in Fig. 3.3b, shows that the PSD is spread over a wider frequency domain and the dominant frequency is less distinctive when gas flow is only available through the distributor. As can be seen, the presence of a more coherent gas flow in other configurations imposes a clear dominant frequency in the PSD graph. The dominant frequency is 3 to 4 Hz for all configurations, which is the typical frequency of bubbling beds. This result is not surprising, because there is no inherent difference between the bubbles that form at the jet nozzles and those form at the distributor nozzles. In fact, many people have used the latter case to study the characteristics of bubbles in the fluidized beds (Rowe and Everett, 1972a, 1972b, 1972c).

Plots of the autocorrelation function and PSD of the different configurations for a 160 cm bed depth and primary gas velocity of 10 U_{mf} are provided in Figs. 3.4a-b. Pressure

fluctuations were again measured at a location of 30 cm above the distributor. As can be seen, there are clear differences between these graphs and the previous graphs for the 40 cm bed depth. Especially, the periodic oscillations are absent in the autocorrelation function and the function decays much more slowly. Furthermore, there is a clear shift of dominant frequency towards lower frequencies in the PSD graphs of the fluidized bed with 160 cm bed depth. We have presented these phenomena previously (Karimipour and Pugsley, 2010) and consider them to be characteristic of non-uniform flow and streaming in deep beds. According to Fig. 3.4a, the configurations that resulted in similar fluidization for the shallow bed, create three different classes of behavior in the deep bed. These classes are: jets with primary gas flow; natural and imposed streams; and jets without primary gas flow. As can be seen, there is a gradual change in the autocorrelation function between these groups. The two jet flows without primary gas, show a gradual decrease plus no observable periodic behavior. Therefore, these configurations represent a clear departure from the normal fluidization in shallow beds discussed above. The two configurations of natural and imposed streaming produce very similar behavior, illustrating the similarity in hydrodynamic behavior between these configurations for the 160 cm bed fluidized bed. As can be seen in the figure, adding jet flow to the fluidized bed affects all characteristics of the autocorrelation graph, including a more rapid decrease of the autocorrelation and the return of periodic oscillation. This indicates an improvement of the fluidization quality when jets are implemented in the bed with fluidizing gas already entering through distributor. The PSDs of all configurations in the 160 cm bed (Fig. 3.4b) all exhibit a shift from 3-4 Hz frequency (frequency of bubbling activity) toward lower frequencies with no clear dominant frequency. The configuration

which includes both primary gas flow through the distributor and high-velocity jet again displays a tendency to have some local frequencies, although trivial compared to the general trend towards lower frequencies.

These results for the 160 cm bed depth suggest that the streaming flow most closely resembles a fluidized bed in which a maldistribution of gas on the distributor leads to bypassing of gas through the bed. However, due to the relatively larger size of streams compared to jets (stream cross section was at least 5 times the cross section of jet after formation at the nozzle) which allows the gas to diffuse into and fluidize other parts of the bed) and availability of the gas entering through the distributor, the fluidization quality is better in case of streaming compared to a pure jetting fluidized bed.

3.5.2. Effect of Gas Velocity

Figs. 3.5a-b provide the autocorrelation function and PSDs of the pressure fluctuations for the same conditions as Figs. 3.3a-b, but with a higher primary gas velocity of 50 U_{mf}. The two configurations of jets without primary gas flow (which are evidently not affected by the primary gas flow) are not shown in these figures. Comparing Figs. 3.3a and 5a illustrates that increasing the primary gas velocity has a minor effect on the fluidized bed behavior. Furthermore, a slight increase of dominant frequency by about 2 Hz with increasing gas velocity from 10 to 50 times the minimum fluidization velocity can also be observed by comparing Figs. 3.3b and 3.5b. This increase can be attributed to the formation of more, faster-rising bubbles with increasing gas velocity.

Figs. 3.6a-b provide the autocorrelation and PSD of the pressure fluctuations in the 160 cm bed at the primary gas velocity of 50 U_{mf}. In this case, a more prominent effect of gas velocity on the behavior of the fluidized bed can be seen by comparing Figs. 3.4a and 3.6a. As Fig. 3.6a illustrates, the rate of decrease of correlation and the amplitude of the periodicity are greater at 50 U_{mf}. This is indicative of improved mixing in the bed at the higher gas velocity. However, as the PSD graph of Fig. 3.6b shows, the frequency domain does not show a significant change compared to Fig. 3.4b. It can be concluded that although increasing the gas velocity leads to slight improvement in mixing, it is still not able to provide normal bubbling with bubble frequencies in the typical 3 to 4 Hz range for fluidized beds. Fig. 3.6b also signifies that at high primary gas velocities through distributor, the PSD graph of jetting and non-jetting configurations approach each other and the effect of jets for enhancing the fluidization becomes negligible.

3.5.3. Effect of Particle Size Distribution (Fines Content)

Figs. 3.7a-b provide the autocorrelation function of the pressure fluctuations corresponding to 20% fines content, a primary gas velocity of 10 U_{mf} and bed depths of 40 and 160 cm. The experiments of imposed stream were not performed for fine FCC fluidized beds. Comparison of Figs. 3.3a and 3.7a illustrates that fluidized beds with 3% and 20% fines content exhibit very similar behavior in the case of 40 cm bed depth. The rate of decline of autocorrelation is somewhat more for the case 20% fines content which can be related to the tendency to form channeling flow in fluidized beds of fine particles. A comparison between figures 3.4a and 3.7b reveals that particle size has a visible influence on the characteristics of different flow configurations studied here in the 160

cm deep bed. As can be seen the appearance of the graphs in Fig. 3.7b mostly resemble Figs. 3.3a and 3.7a of 40 cm bed depth, thus, showing the tendency of the system toward a normal bubbling fluidized bed. The two cases of jet flows without primary gas flow decline very slowly compared to Fig. 3.4a of FCC particles with 3% fines content. As mentioned above, this feature can be attributed to the intrinsic characteristics of fines particles to form channels and possible effect of jets to create these phenomena in the bed. The endurance of the pressure fluctuations they cause, and the statistical similarity of the events in the bed at different times might lead to these types of autocorrelation graphs.

3.5.4. Wavelet Decomposition and Analysis

The time series of the pressure fluctuations measured for the 3% fines content FCC has been used for wavelet analysis here. For this purpose, the time series is decomposed into 6 levels or scales. Then, the PSD of the resulting approximate and detail parts of the time series have been calculated. The PSD of the approximate and detail parts for 40 cm bed, 160 cm bed, imposed stream and high-velocity jet are provided in Figs. 3.8-3.11. As can be seen in Fig. 3.8a, the shape of the PSD graph and the dominant frequency of the approximate time series remain almost constant at around 3 Hz until scale 3 of the decomposition. This dominant frequency is equal to the dominant frequency of the original pressure fluctuation time series (Fig. 3.3b) and is related to the bubbling activity in the fluidized bed. Following scale 3, a decrease in the dominant frequency and power occurs. This indicates that by transferring from scale 3 to scale 4 decomposition, a change in the content of the time series occurs that removes the contribution of bubbling activity

from the main body of the time series. Studying Fig. 3.8b shows that the first two detail time series contain very high frequency fluctuations However, the power of these fluctuations is very low relative to the power of the next detail time series, which indicates their limited contributions in the main pressure time series. The PSD of scale 4 detail time series shows the higher power and a dominant frequency of less than 4 Hz, which is similar to the dominant frequency of the approximate time series of less than scale 3 decomposition. Hence, the contribution of the bubbling activity in the original time series transfers from scale 3 approximate to the scale 4 detail time series by continuing the decomposition. Thus, As the figure shows, scale 5 detail presents a dominant frequency of 2 Hz. Since the presence of several bubbling activities with different dominant frequencies has been reported in the previous literature (Falkowski and Brown, 2004), scale 5 detail may be presenting another bubbling activity. After decomposition of scale 4, the dominant frequency of the detail parts shifts towards lower frequencies with lower power in the PSD graph. Therefore, it can be concluded that the dominant frequency of 3 Hz, found for 40 cm fluidized bed, is a superposition of these two bubbling activities.

As Fig. 3.9a indicates, all the approximate times series for 160 cm bed depth provide similar PSD graphs. Only the contribution of the higher frequencies decreases in the PSD with continuing the decomposition, which is generally considered to be trivial. As Fig. 3.9b shows, scale 4 and 5 detail time series of the 160 cm bed exhibit dominant frequencies of 4 and 2 Hz, respectively, which is similar to the 40 cm bed depths. However, the relative power of the scale 5 component with 2 Hz frequency increases

compared to the scale 4 part with 4 Hz frequency. Furthermore, contrary to the 40 cm bed, the power of scale 6 part which possesses lower dominant frequency, increases compared to the previous scales. This signifies the appearance of other activities with greater influence on the overall fluidized bed hydrodynamics. This can be related to the emergence of streaming flow in the 160 cm fluidized bed. Therefore, it can be postulated that similar bubbling activity that exists in the 40 cm bed fluidized bed is present for 160 cm bed fluidized bed, however, its contribution is much less than the streaming flow that is present at the same time.

Figs. 3.10 and 3.11 illustrate the PSD of the approximate and detail parts of the pressure fluctuations for the imposed stream and high-velocity jet configuration in the 160 cm bed fluidized bed. As these figures demonstrate, the power of the higher scale decompositions with lower dominant frequencies gradually increases. The ratio of the power of scale 5 (beginning of streaming) detail to scale 4 detail (contains the activities related to bubbling) are calculated as 1, 2.3, 3.6 and 10, respectively, for normal bubbling in the 40 cm bed, natural streaming in the 160 cm bed, imposed stream in the 160 cm deep bed and high-velocity jet without primary air flow. These numbers reveal a gradual change of power ratio from a case of shallow fluidized bed containing normal bubbling activity with a uniform distribution of gas towards a packed bed with one internal jet. Therefore, streaming flow can be considered to form by increasing the relative importance of one available stream of bubble activity compared to other activities with increasing the bed depth and suppressing the uniform gas distribution. It should be noted that although fluidized beds with different bed depths apparently have PSD powers with different

orders, the calculated values, discussed above, are power ratios and thus, are not influenced by absolute values of power.

A thorough review of the literature reveals that these findings can be explained by the observations reported previously by other authors. Rowe and Yacono (1976) compared the bubbling fluidization of different particle sizes based on the concept of permeability. The permeability is defined as the ability of gas to diffuse into the bed of particles and is related to the bed voidage. It has been calculated using by the Kozeny-Carmen relation, Scheidegger (1960):

$$\kappa = \frac{1}{180}\frac{\varepsilon^3 d_p^2}{(1-\varepsilon)^2} \tag{3.3}$$

where κ is the permeability of the particle bed.

Rowe and Yacono (1976) found that the permeability decreases for deeper fluidized beds. The presence of preferred bubble tracks and channeling has also been reported in the literature by various researchers (Rowe and Yacono, 1976; Rowe, 1971; Glicksman et al., 1987). Furthermore, Matsuno and Rowe (1970) have argued that bubbles prefer to rise successively along the preferred paths and increasing the superficial gas velocity increases the number of bubbles, thus their frequency, in a specific path rather than generating new paths. It is probable that some adjacent streams of fast bubbles join each other to form streams of gas in the fluidized bed. Since permeability is expected to be much lower at the bottom of very deep beds, these bubble streams can be stabilized in the bed, especially at the bottom region. Other available bubble streams can gradually join this stream and provide a lower pressure drop passage for the gas flow. Therefore, the streaming would be directly related to lower permeability at the bottom of the deep bed

for fluidized beds of small particles. This is in conformity with visual observations reported in our previous work (Karimipour and Pugsley, 2010) and the findings of this work which indicates that streams form by the changing the relative importance of the activities present in the bed with increasing bed depth. Other, less important bubble streams that have not attached to the main stream can also be simultaneously present in the system. It is worth mentioning here that based on the findings of the previous chapter, increasing the fine content improves the fluidization behavior which is in contrary to the lower permeability expected for finer particles. Thus, the dominant effect of fine content in improving the fluidization quality should be related to the other effects of fines (Lockett and Harrison, 1967; Geldart, 1972; Rowe et al., 1978) as have been discussed in the previous chapter.

3.6. Conclusions

Study of natural streaming flow, forced streaming, and jetting flows revealed that there is no significant difference between the configurations for a fluidized bed with 40 cm bed depth. However, differences emerge by increasing the bed depth to 160 cm. It was found that the natural streaming in a deep fluidized bed closely resembles the case of forced stream in which the gas flow is also present in the remaining regions of the distributor. The jet flows without the primary gas flow could be considered as the cases of severe streaming that might happen in very deep beds with possible formation of completely non-fluidized regions. Application of supporting jets with primary gas flow could enhance the fluidization quality to some extent. Increasing the primary gas velocity from 10 to 50 U_{mf} was found to reduce the effect of supporting jets. It was also found that finer

FCC particles relatively represent better fluidization. Wavelet analysis showed that even in deep fluidized beds that are dominated by the streaming flow, bubbling activity with the same dominant frequency as the shallow bed coexists, although with a minor contribution. These findings suggested that the streaming flow can be considered to form by increasing the relative importance of available stream of bubbles compared to other activities as the bed depth increases.

3.7. References

Darton, R.C., La Naueza, R.D., Davidson, J.F., Harrison, D., 1977. Bubble growth due to coalescence in fluidized beds. Chemical Engineering Research and Design 55, 274-280.

Daubechies, I., 1992. Ten lectures on wavelets, Philadelphia, PA, SIAM.

Daubechies, I., 1988. Orthogonal bases of compactly supported wavelets. Communications of Pure Applied Mathematics 41, 909-996.

Ellis, N., Briens, L.A., Grace, J.R., Bi, H.T., Lim, C.J., 2003. Characterization of dynamic behaviour in gas-solid turbulent fluidized bed using chaos and wavelet analyses. Chemical Engineering Journal 96, 105-116.

Ellis, N., Bi, H.T., Lim, C. J., Grace, J.R., 2004. Influence of probe scale and analysis method on measured hydrodynamic properties of gas-fluidized beds. Chemical Engineering Science 59, 1841-1851.

Falkowski, D., Brown, R.C., 2004. Analysis of Pressure Fluctuations in Fluidized Beds, Industrial and Engineering Chemistry Research 43, 5721-5729.

Geldart, D., 1973. Types of gas fluidization. Powder Technology 7, 285-292.

Glicksman, L.R., Lord, W.K., Sakagami, M., 1987. Bubble properties in large-particle fluidized beds. Chemical Engineering Science 42, 479-491.

Grossman, A., Morlet, J., 1984. Decompositions of hardy functions into square integrable wavelets of constant shape, SIAM Journal of Mathematics 15, 723-736.

Guenther, C., Breault, R., 2007. Wavelet analysis to characterize cluster dynamics in a circulating fluidized bed. Powder Technology 173, 163-173.

Guo, Q., Yue, G., Suda, T., Sato, J., Flow characteristics in a bubbling fluidized bed at elevated temperature. Chemical Engineering and Processing 42, 439-447.

He, Z., Zhang, W., He, K., Chen, B., 1997. Modeling pressure fluctuations via correlation structure in a gas-solids fluidized bed. AIChE Journal 43, 1914-1920.

Hubbard, B.B., 1998. The world according to wavelets: The story of a mathematical technique in the making, 2nd edition, A.K. Peters, Natick, Massachusetts.

Issangya, A., Knowlton, T., Karri, S.B.R., 2007. Detection of gas bypassing due to jet streaming in deep fluidized beds of group A particles. In: Fluidization XII, Berruti, F., Bi, X., Pugsley, T. (Eds.), Vancouver, British Columbia, Canada, May 13-17.

Karri, S.B.R., Issangya, A.S., Knowlton, M., 2004. Gas bypassing in deep fluidized beds. In: Fluidization XI, Arena, U., Chirone, R., Miccio, M., Salatino, P. (Eds.), Ischia (Naples), Italy, May 9-14.

Lu, X., Li, H., 1999. Wavelet analysis of pressure fluctuation signals in a bubbling fluidized bed. Chemical Engineering Journal 75, 113-119.

Mallat, S., 1989. Multiresolution approximations and wavelet orthogonal bases of $L^2(R)$. Transactions of American Mathematics Society 315, 69-87.

Mallat, S., 1988. Multiresolution representation and wavelets, Ph.D. Thesis, University of Pennsylvania, Philadelphia.

Matsuno, R., Rowe, P.N., 1970. The distribution of bubbles in a gas fluidised bed. Chemical Engineering Science 25, 1587-1593.

Rowe, P.N., Everett, D.F., 1972. Fluidised bed bubbles viewed by X-rays-Part I-Experimental details and the interaction of bubbles with solid surfaces, Chemical Engineering Research and Design 50, 42-48.

Rowe, P.N., Everett, D.F., 1972. Fluidised bed bubbles viewed by X-rays-Part II-The transition from two to three dimensions of undisturbed bubbles, Chemical Engineering Research and Design 50, 49-54.

Rowe, P.N., Everett, D.F., 1972. Fluidised bed bubbles viewed by X-rays-Part III-Bubble size and number when unrestrained three-dimensional growth occurs, Chemical Engineering Research and Design 50, 55-60.

Rowe, P.N., Yacono, C.X.R., 1976. The bubbling behaviour of fine powders when fluidised. Chemical Engineering Science 31, 1179-1192.

Rowe, P.N., 1971. Experimental properties of bubbles. In: Fluidization, Davidson, J.F., Harrison D. (Eds.), Academic Press.

Sasic, S., Leckner, B., Johnsson, F., 2006. Time-frequency investigation of different modes of bubble flow in a gas-solid fluidized bed. Chemical Engineering Journal 121, 27-35.

Scheidegger, A.E., 1960. The physics of flow through porous media. University of Toronto Press, Toronto, Canada.

Wells, J., 2001. Streaming flow in large scale fluidization. AIChE Annual Meeting, Particle Technology Forum, Reno, Nevada, USA.

Zhao, G., Yang, Y., 2003. Multiscale resolution of fluidized-bed pressure fluctuations. AIChE Journal 49, 869-882.

3.8. Nomenclature

A1-4 Approximate components of the pressure fluctuations time series

ACF autocorrelation function

d_p particle diameter (m)

D1-4 Detail components of the pressure fluctuations time series

t time (s)

U_0 superficial gas velocity (m/s)

w wavelet transform operator

x pressure fluctuations time series (Pa)

X wavelet transform

Greek Letters:

κ permeability (m^2)

ε voidage

ψ mother wavelet

μ dilation of the mother wavelet

υ translation of the mother wavelet

Table 3.1. The range of operating conditions studied in this work

Variable	**Range**
Bed depth (cm)	40, 160
U_0/U_{mf}	10, 50
Fines content	3%, 20%
Distributor	1 mm holes and 0.54% opening, 2 mm holes and 2.15% opening
Jet velocity (m/s)	31 (No. 2), 60 (No. 1)

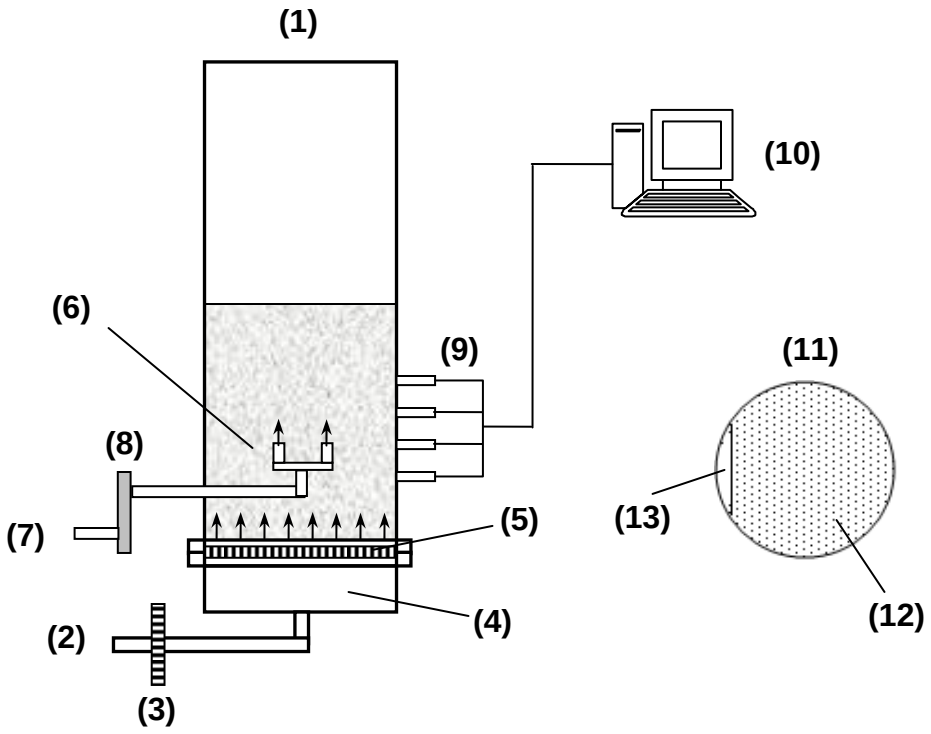

Figure 3.1. Schematic diagram of the experimental apparatus, showing the double-jet nozzle and the distributor modified to produce a force streaming flow in the bed: (1) Fluidized bed unit, (2) Primary air flow from blower, (3) Orifice plate, (4) Wind-box, (5) Distributor, (6) Double-jet nozzle with 8cm distance between two jets and 19 cm distance from distributor, (7) Jet air flow from building air, (8) Flow meter, (9) Pressure transducers, (10) PC and data acquisition system, (11) Modified distributor, (12) Perforated area, (13) Opening area. Arrows in the figure indicate the direction of the air flow.

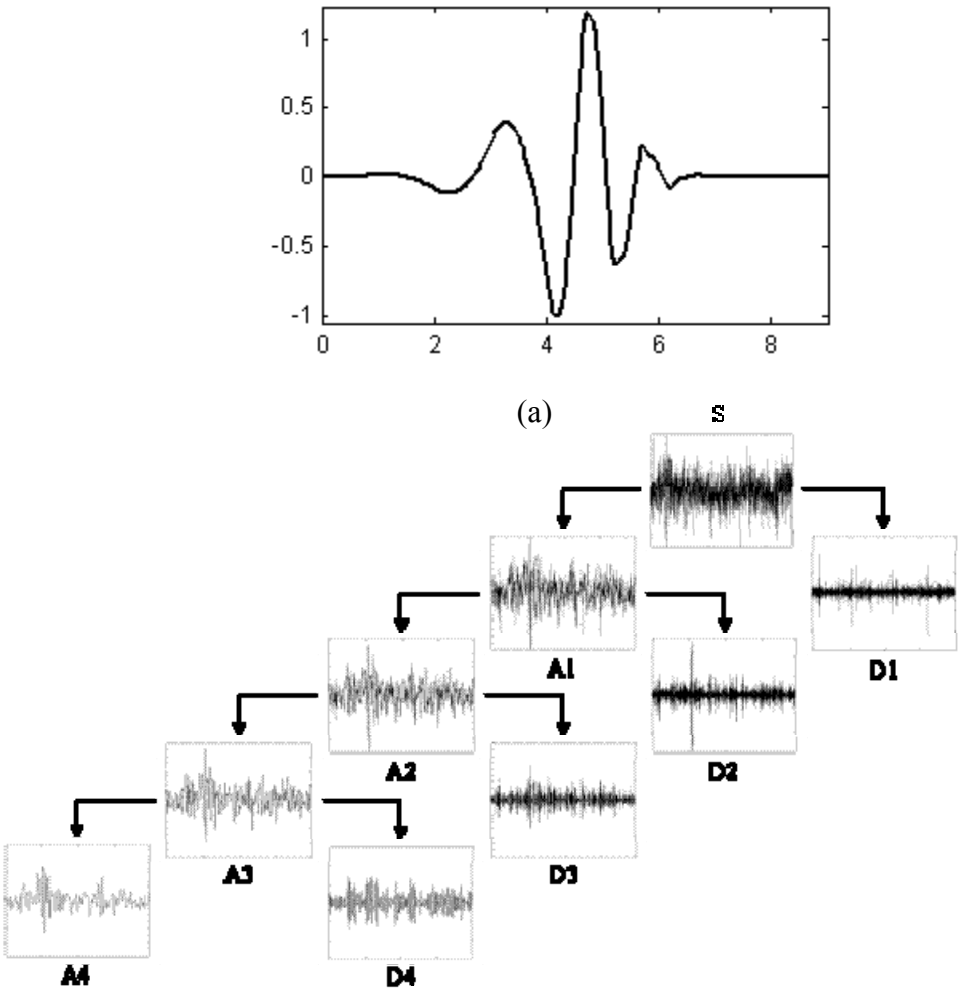

Figure 3.2. (a) Daubechies number 5 wavelet ("db5") which has been used in the present work as the mother wavelet, (b) Decomposition of a signal (S) into its components using Wavelet transform

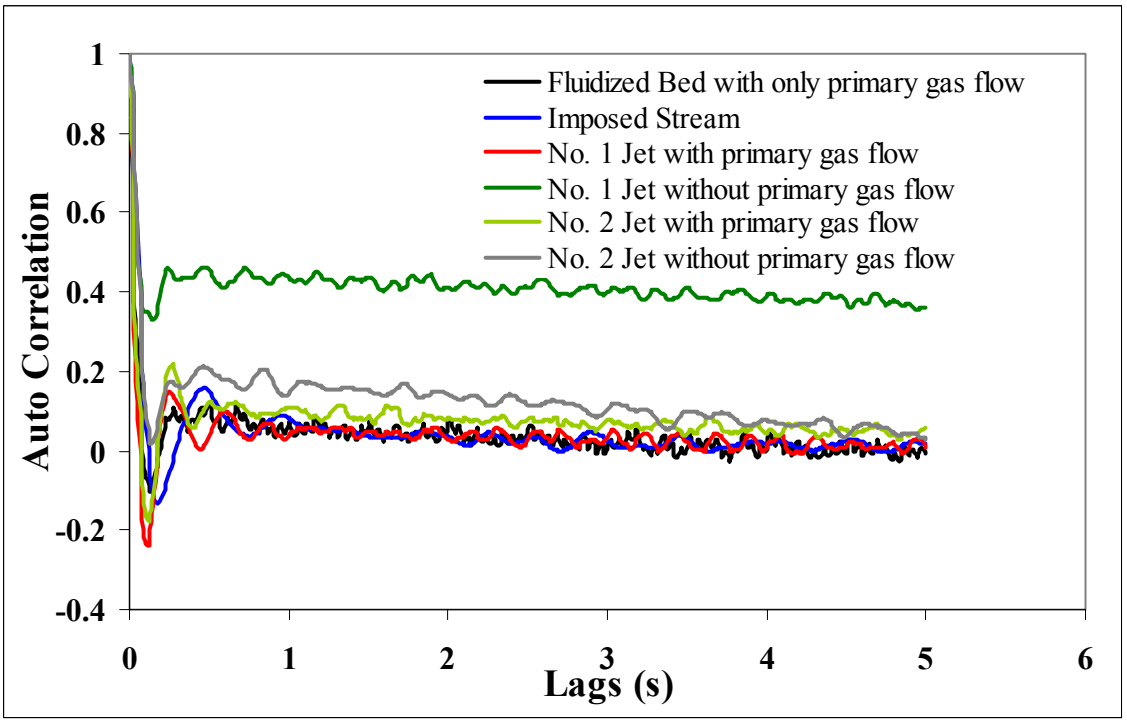

(a)

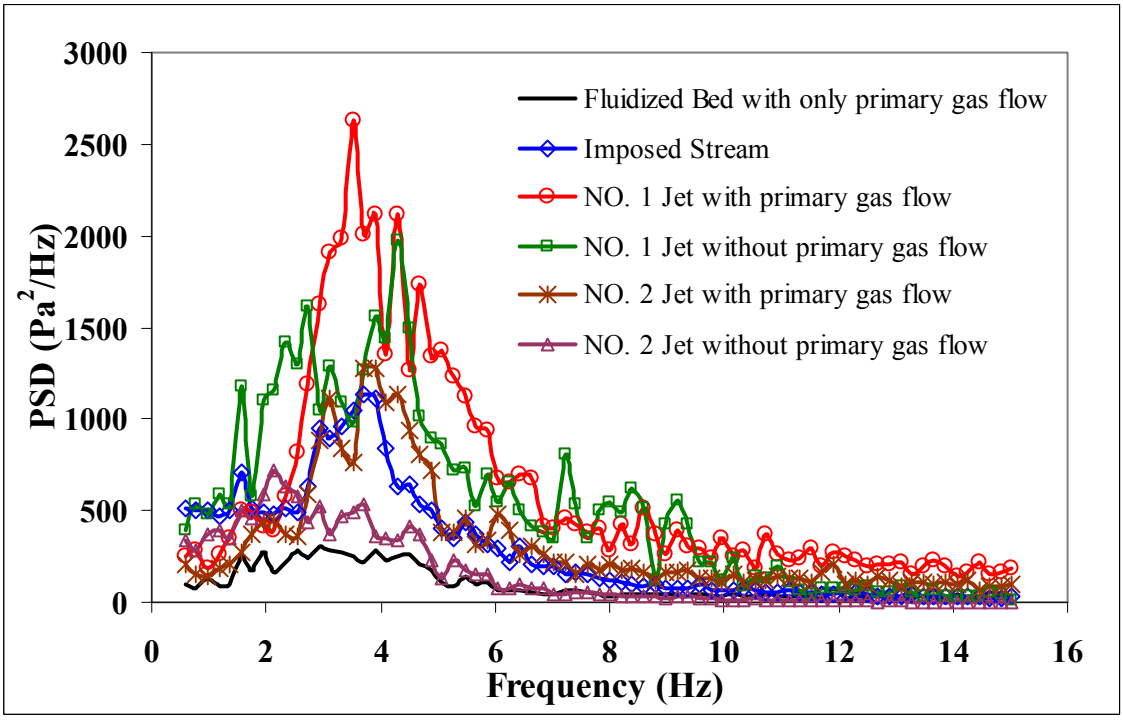

(b)

Figure 3.3. (a) Autocorrelation and (b) PSD of pressure fluctuations for the different test configurations, 40 cm bed depth, coarse FCC (3% fines content), U_0=10 U_{mf}

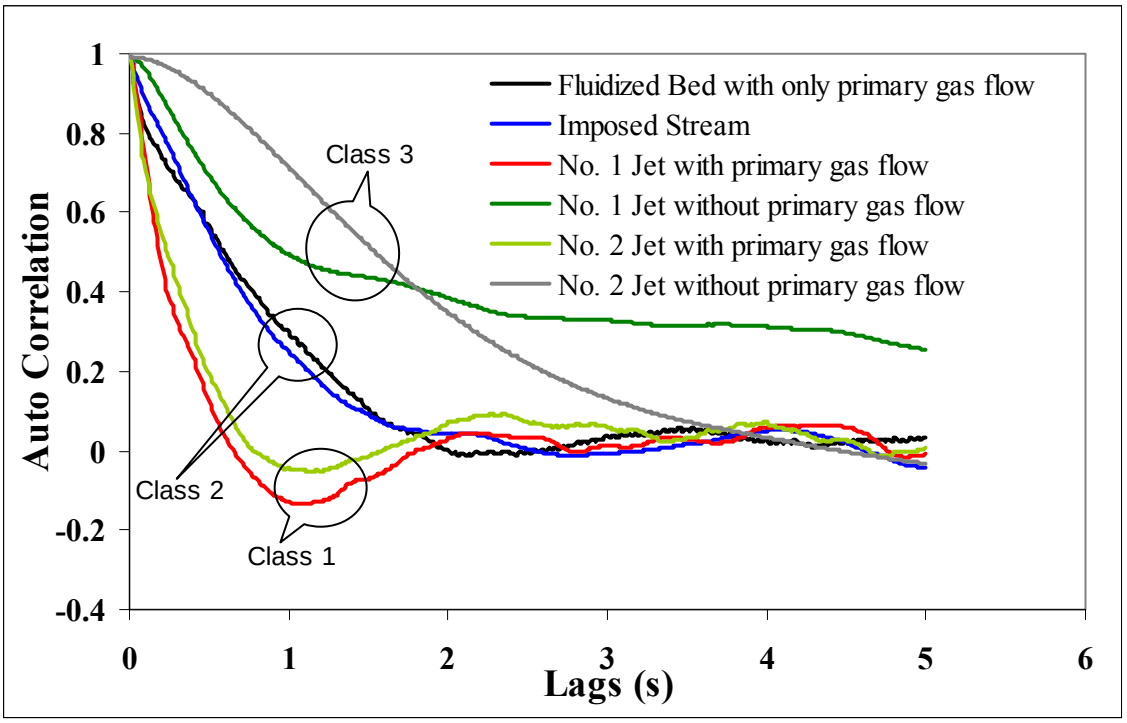

(a)

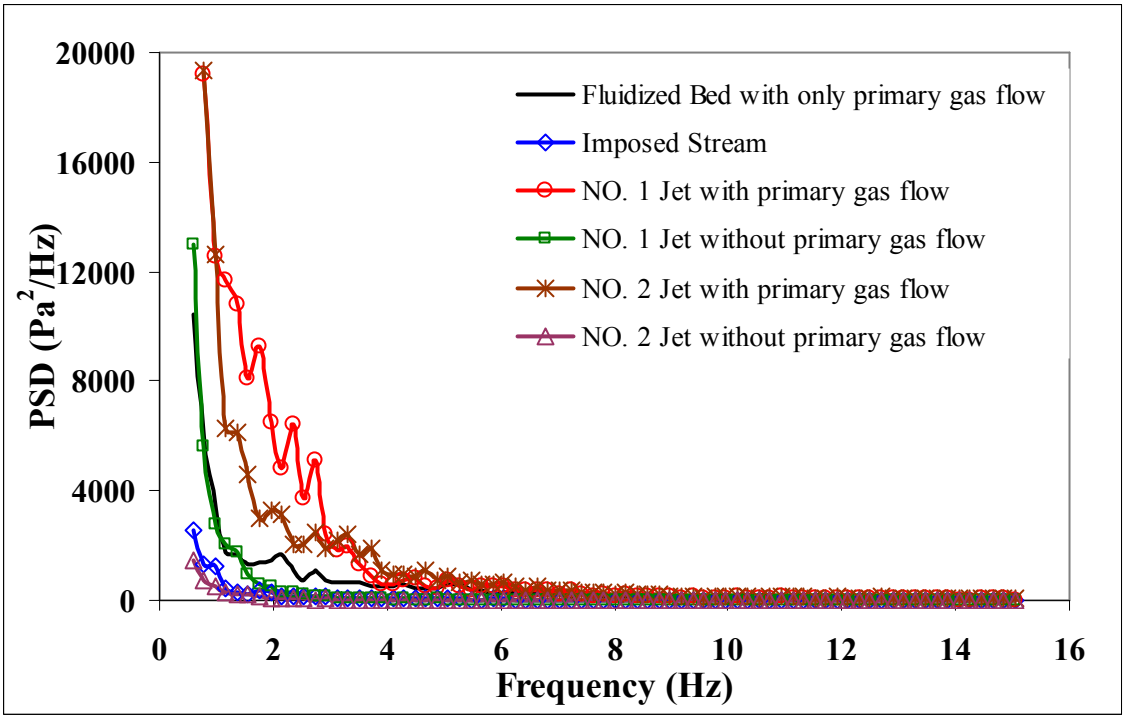

(b)

Figure 3.4. (a) Autocorrelation and (b) PSD of pressure fluctuations for the different test configurations, 160 cm bed depth, coarse FCC (3% fines content), U_0=10 U_{mf}

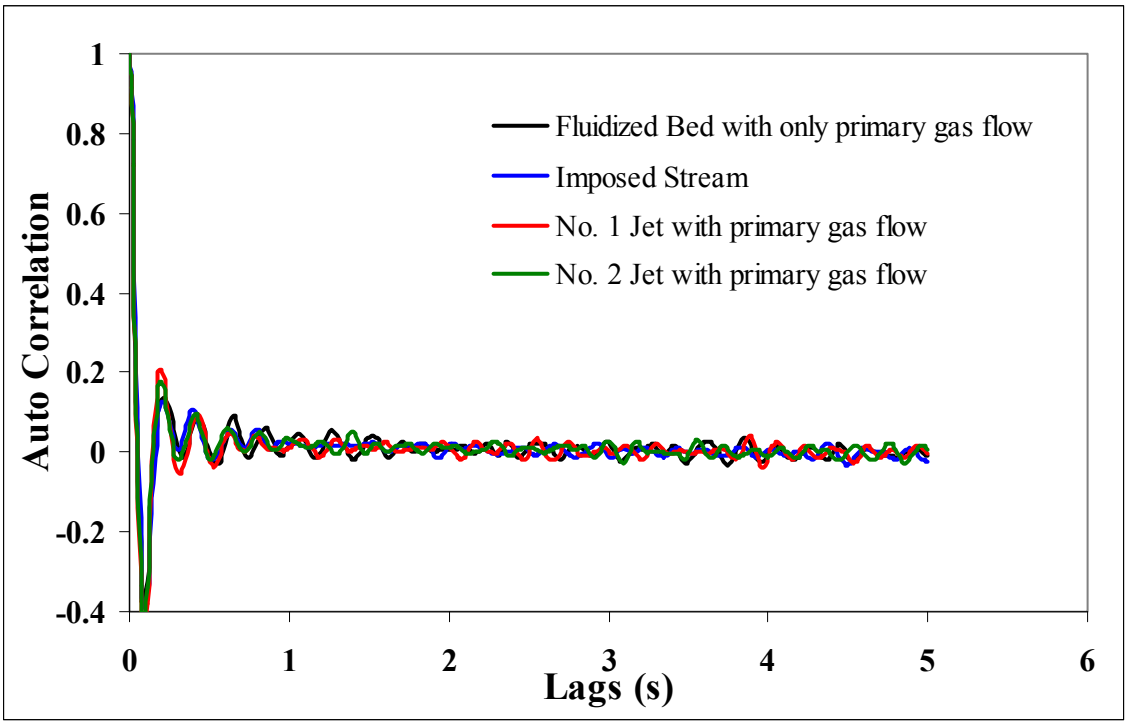

(a)

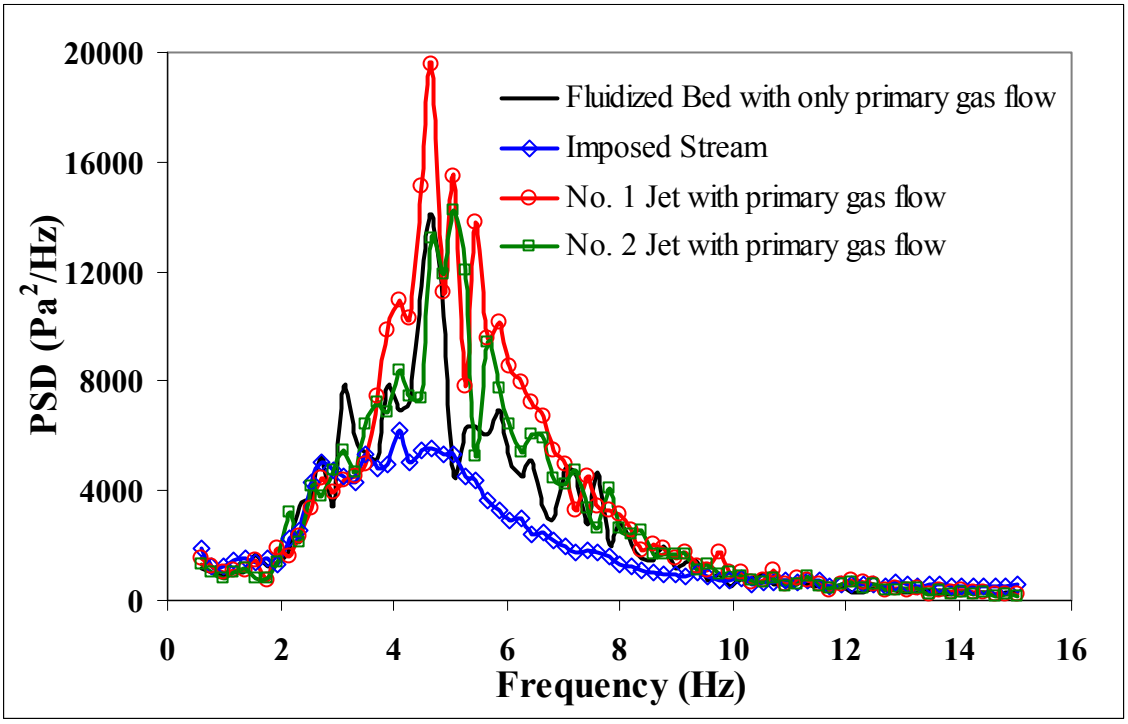

(b)

Figure 3.5. (a) Autocorrelation and (b) PSD of pressure fluctuations for the different test configurations, 40 cm bed depth, coarse FCC (3% fines content), U_0=50 U_{mf}

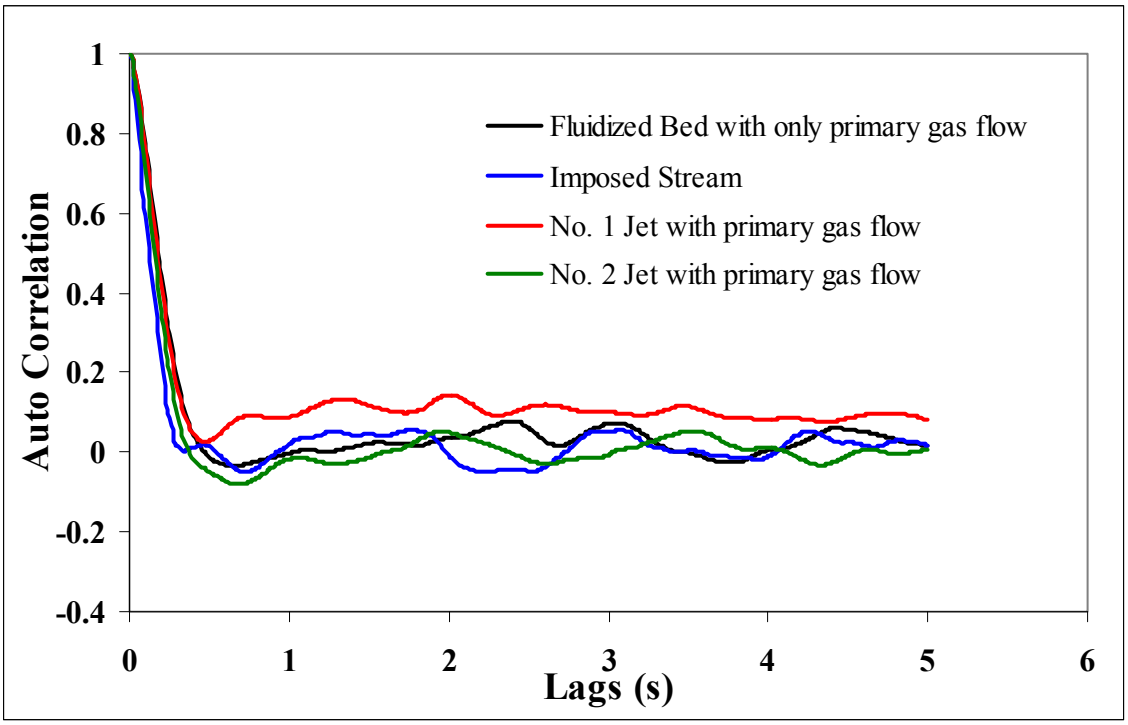

(a)

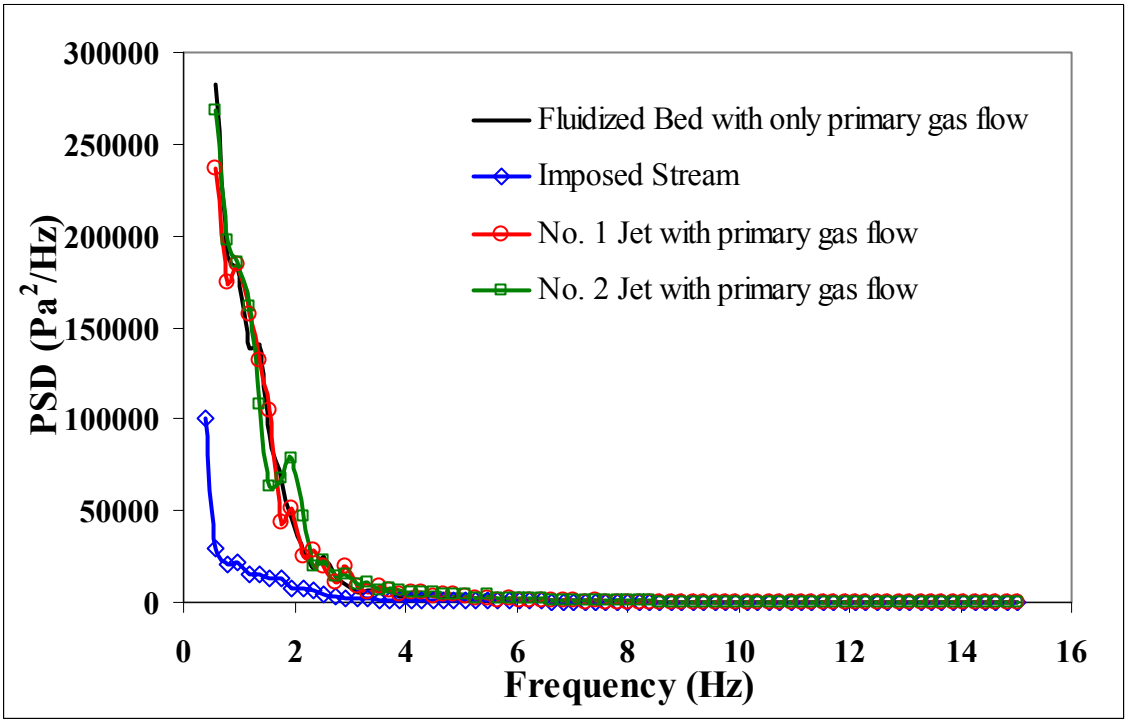

(b)

Figure 3.6. (a) Autocorrelation and (b) PSD of pressure fluctuations for the different test configurations, 160 cm bed depth, coarse FCC (3% fines content), U_0=50 U_{mf}

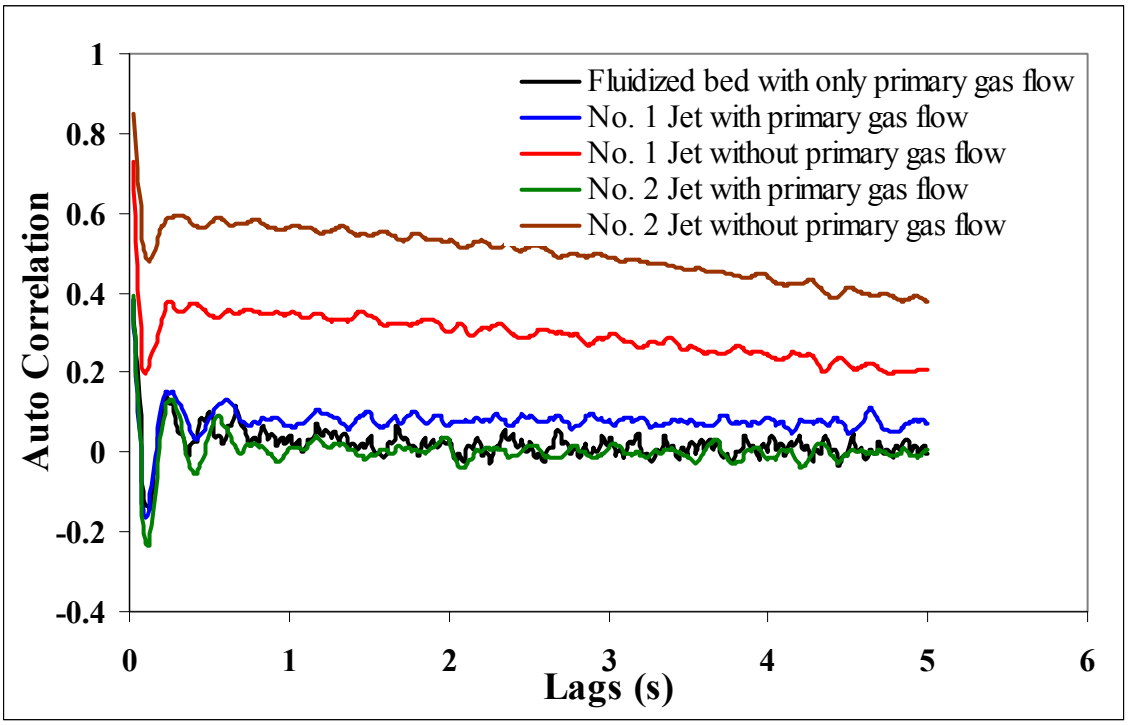

(a)

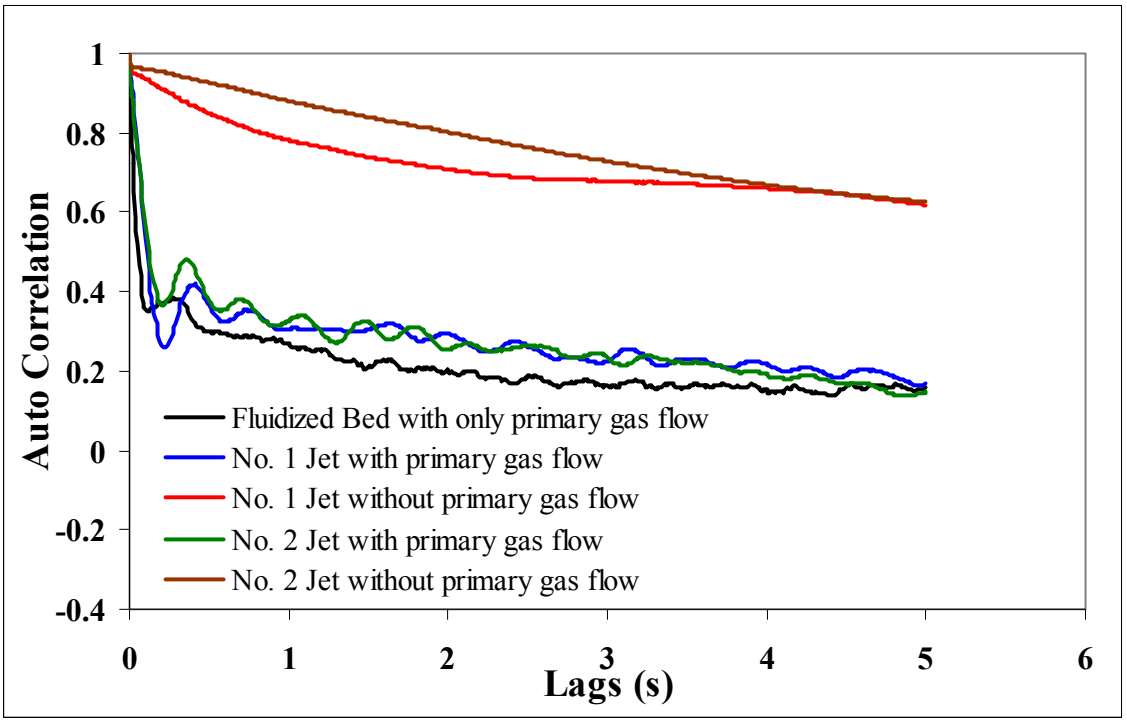

(b)

Figure 3.7. The autocorrelation function of pressure fluctuations for the different test configurations, fine FCC (20% fines content), U_0=10 U_{mf}, (a) 40 cm bed depth, (b) 160 cm bed depth

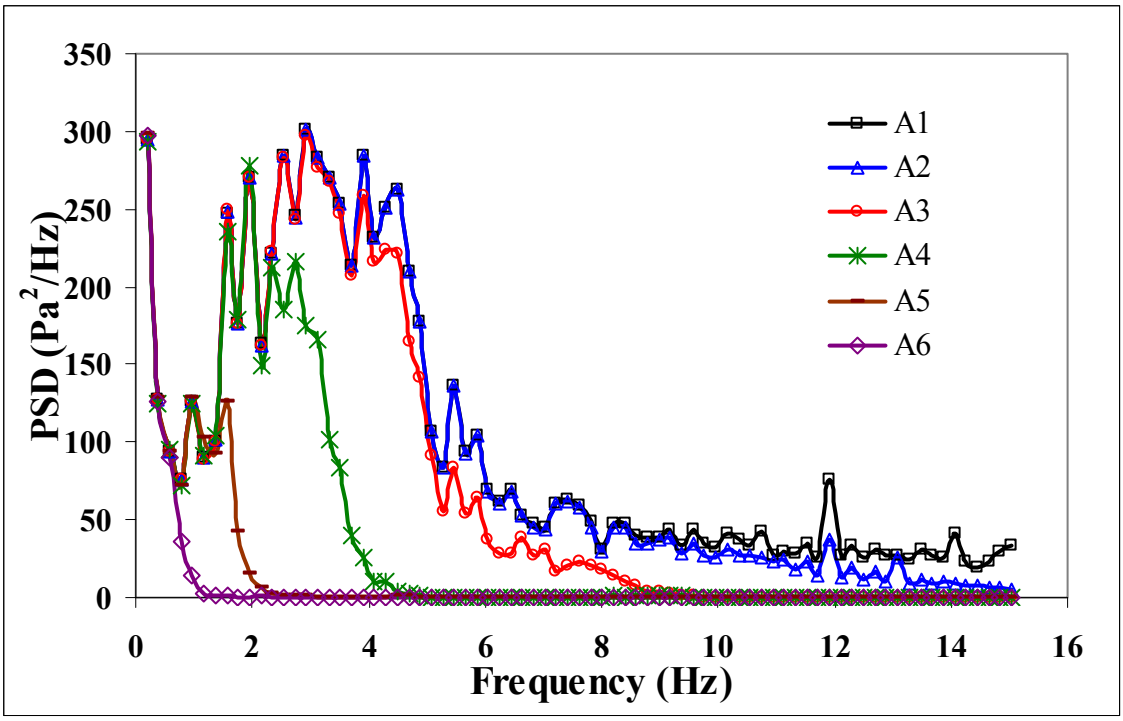

(a)

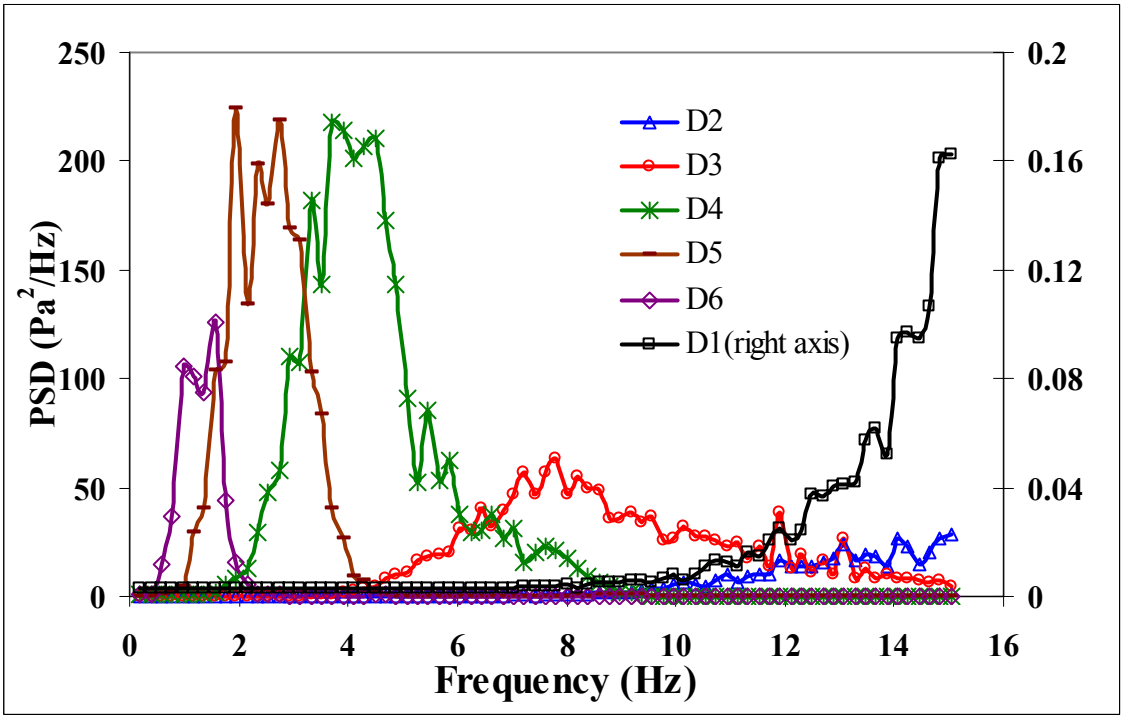

(b)

Figure 3.8. The PSD of the approximate and detail parts of the pressure fluctuations obtained by Wavelet decomposition, U_0=10 U_{mf}, coarse FCC (3% fines content) in 40 cm bed, (a) Approximate (A), (b) Detail (D)

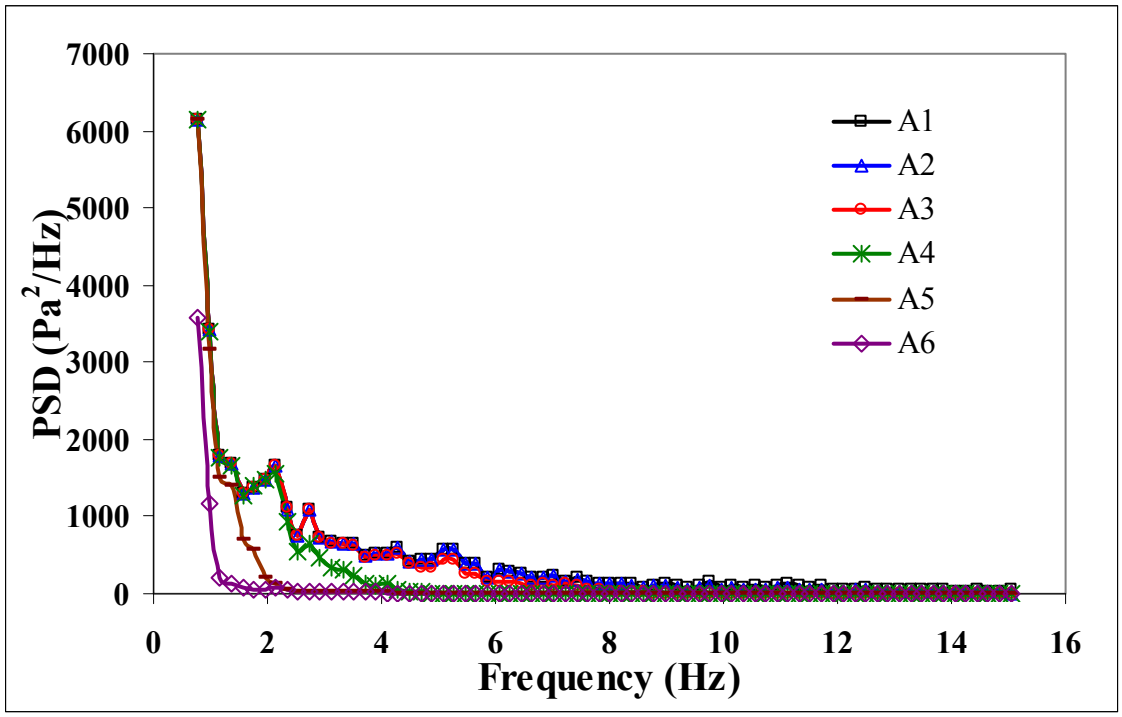

(a)

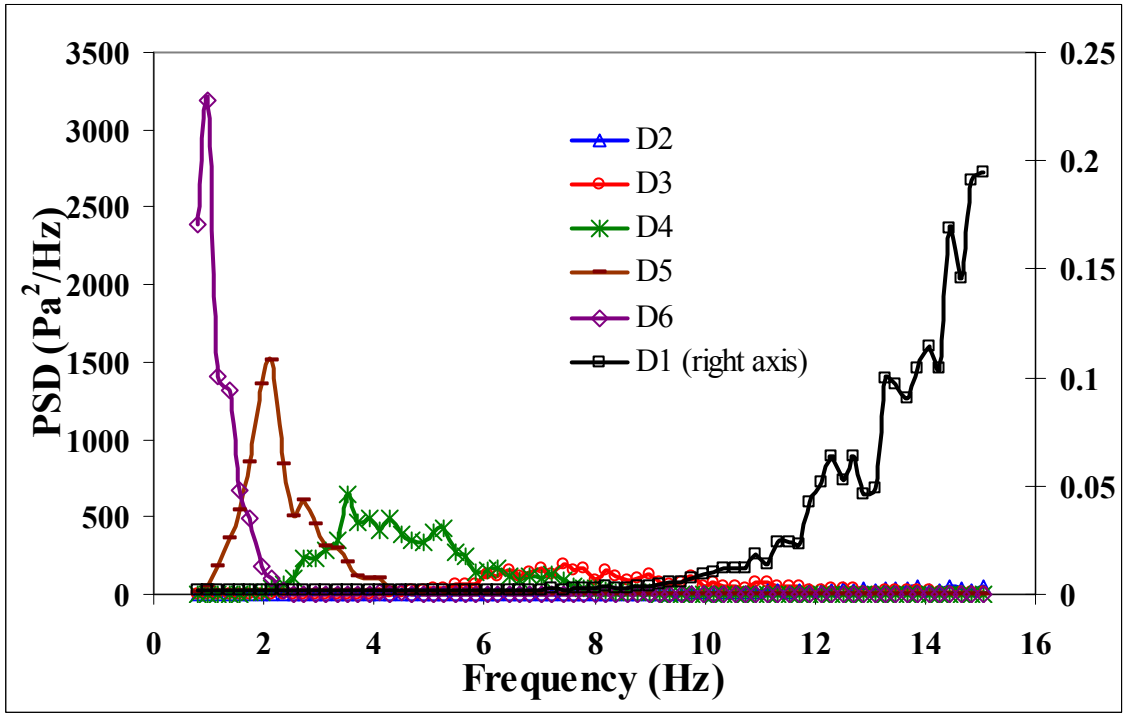

(b)

Figure 3.9. The PSD of the approximate and detail parts of the pressure fluctuations obtained by Wavelet decomposition, U_0=10 U_{mf} and coarse FCC (3% fines content) in 160 cm bed, (a) Approximate (A), (b) Detail (D)

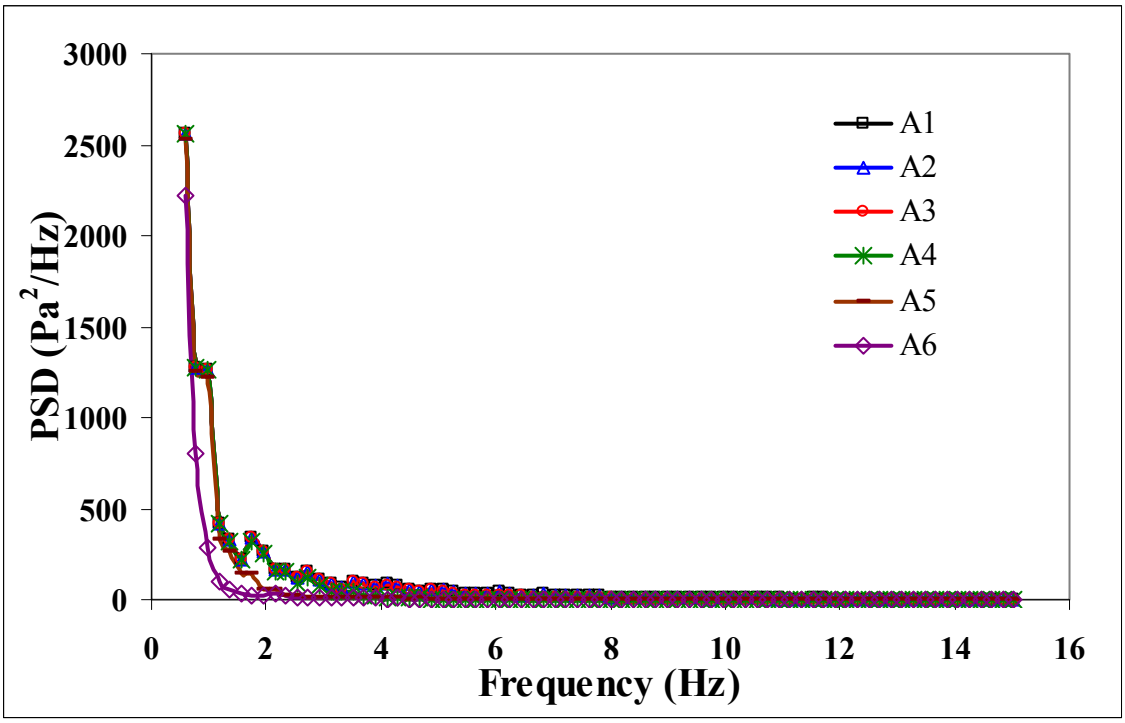

(a)

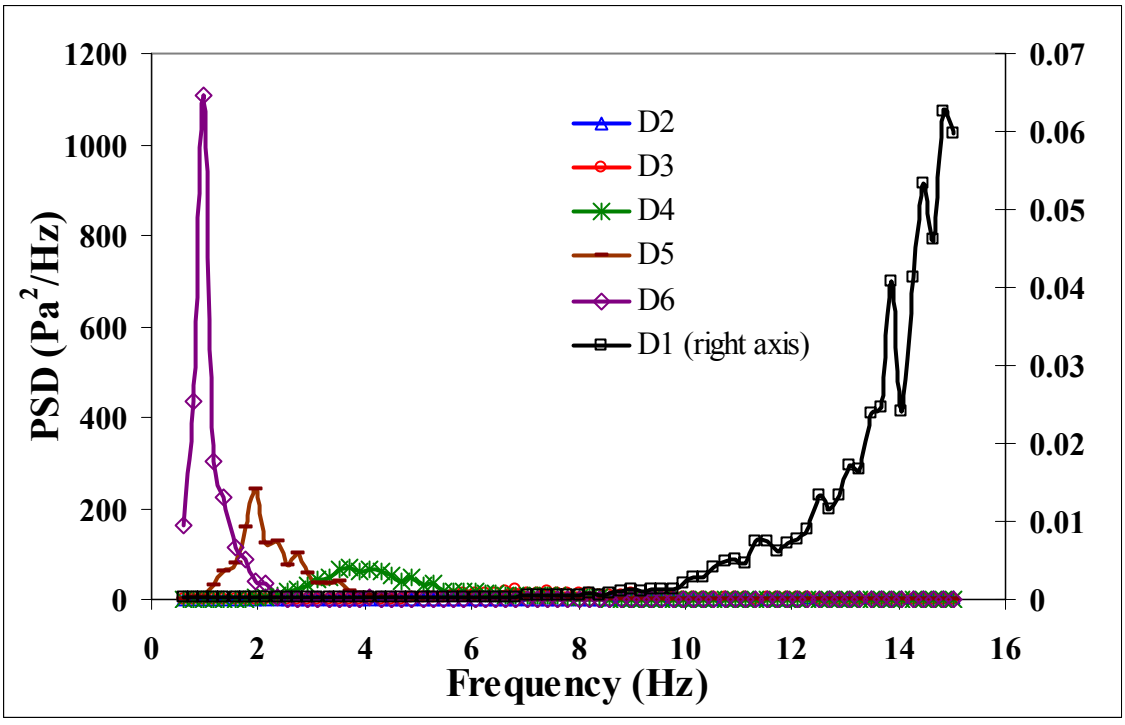

(b)

Figure 3.10. The PSD of the approximate and detail parts of the pressure fluctuations obtained by Wavelet decomposition, U_0=10 U_{mf} and coarse FCC (3% fines content) in 160 cm bed with imposed stream, (a) Approximate (A), (b) Detail (D)

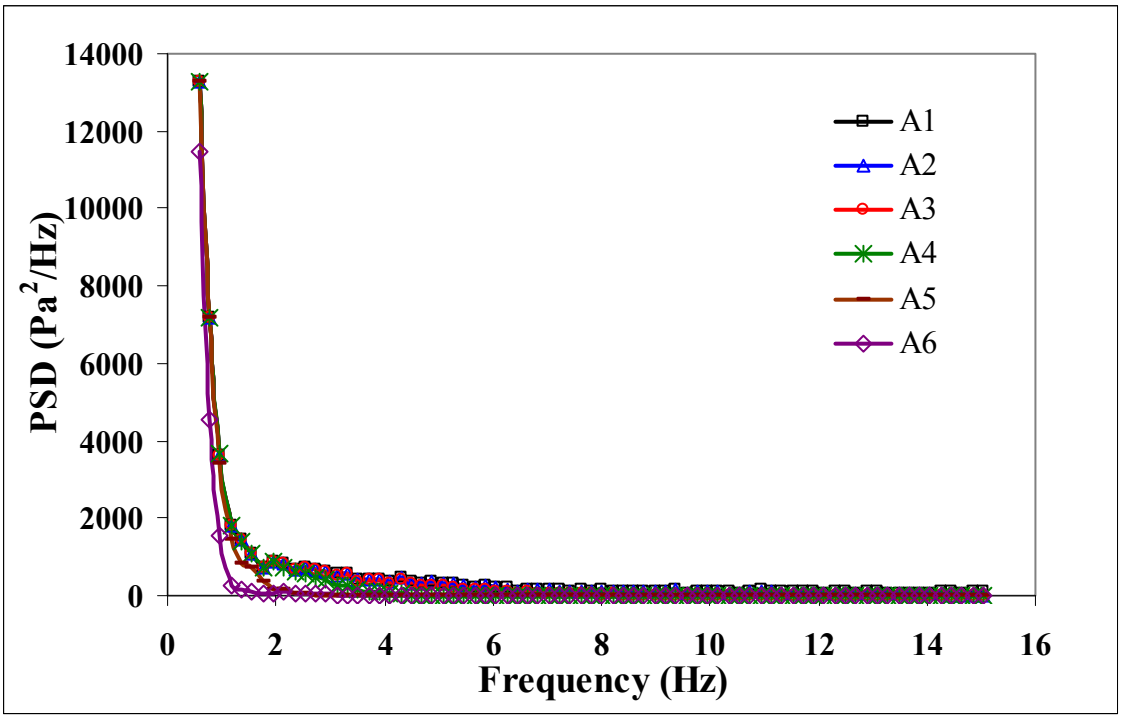

(a)

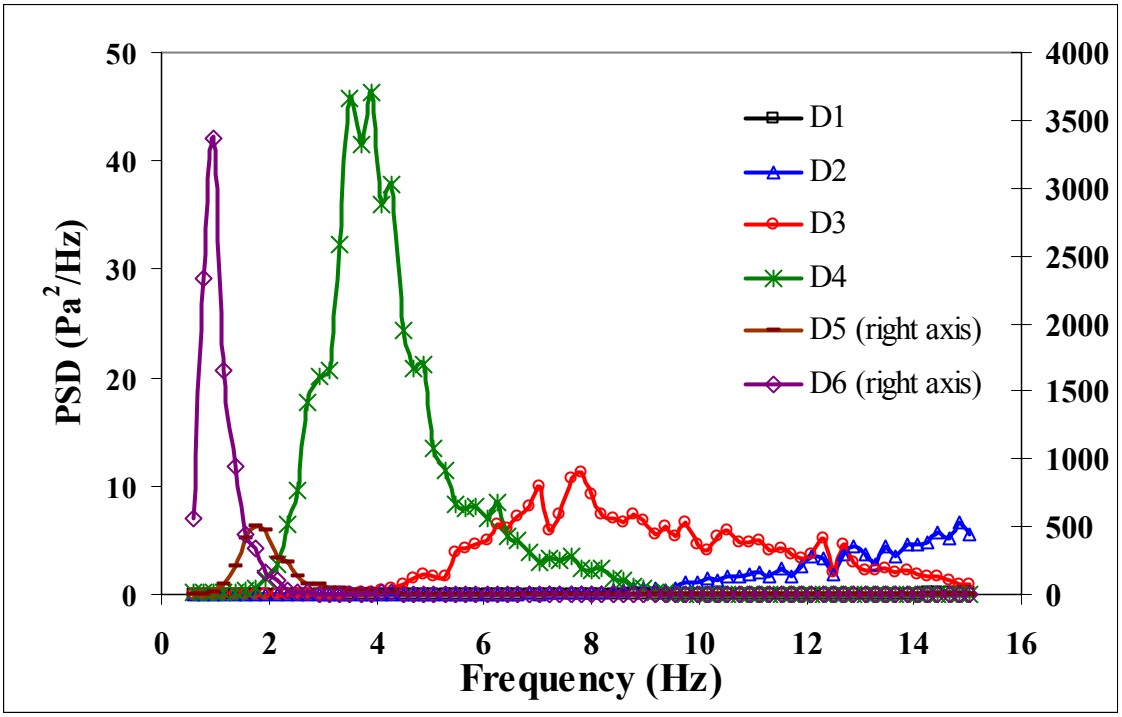

(b)

Figure 3.11. The PSD of the approximate and detail parts of the pressure fluctuations obtained by Wavelet decomposition, U_0=10 U_{mf} and coarse FCC (3% fines content) in 160 cm bed with No. 1 jet, (a) Approximate (A), (b) Detail (D)

CHAPTER 4 - CFD Simulation of a Bubbling Fluidized Bed of Geldart A Particles using the Multiphase Particle in Cell Approach

The contents of this chapter have been submitted to the ***AIChE Journal***. It has been submitted in a version similar to what appears in this chapter.

Citation

Sh. Karimipour, T. Pugsley, CFD Simulation of a Bubbling Fluidized Bed of Geldart A Particles using the Multiphase Particle in Cell Approach, AIChE Journal, February 2010 (Ref. No. AIChE-10-12468)

Contribution of Ph.D. Candidate

The CFD simulations performed for the purpose of this work and measuring pressure fluctuations in the fluidized bed were planned and performed by Shayan Karimipour. Todd Pugsley provided consultation regarding the design of simulation cases. The programs for all of the data analysis were developed by Shayan Karimipour. All of the

writing of the submitted manuscript was done by Shayan Karimipour with Todd Pugsley providing editorial guidance regarding the style and technical content of the manuscript.

Contribution of this Paper to the Overall Study

Since initial test of the commercial CFD codes FLUENT and MFIX did not show any sign of gas streaming in the deep fluidized bed, the CFD code BARRACUDA^{TM} that has been claimed by the developers to be appropriate for this purpose was tested. Due to the lack of data on the performance of this code, a simple case of modeling a freely bubbling fluidized bed of Geldart A particles in a 14 cm diameter column was attempted first. The results of this study are provided in this chapter. I should be noted that similar to the previous mentioned codes, this code also failed to capture the streaming flow when applied to a deep fluidized.

4.1 Abstract

The capability of the multiphase Particle in Cell (PIC) approach to resolve the characteristics of a bubbling fluidized bed of Geldart A particles has been investigated. Four different simulation cases, which include three different uniform grid sizes (0.5, 1, and 2 cm) and two drag models with a realistic particle size distribution have been designed and tested for this purpose. The simulated bubble size distribution, rise velocity, and bubble frequency as well as bed expansion and voidage distribution have been compared with commonly accepted correlations and experimental data provided in this work and from the literature. The dynamic characteristics of the different cases are also evaluated using the time series of pressure fluctuations generated by the simulations. The

results show a promising predictive capability of the multiphase PIC approach without the need to modify the drag model or other constitutive relations.

4.2. Introduction

The hydrodynamics of a gas-solid fluidized bed influence such bed characteristics as solid and gas mixing, heat and mass transfer between particles, gas, and immersed surfaces, and elutriation of particles from the bed. The hydrodynamics of fluidized beds operating in the bubbling regime are largely governed by the distribution of the size, velocity, and number of bubbles passing through the bed. Therefore, proper prediction of bubble properties by computational fluid dynamics (CFD) models is essential if these models are to provide a realistic picture of bed performance.

Although there have been numerous experimental studies of bubble characteristics from the early days of fluidization research, most of the modeling efforts of gas-solid fluidized beds in the literature have been limited to qualitative evaluations. This is due to the difficulty of extracting the bubble properties and the need for relatively high resolution simulations that are computationally costly. In some recent works, researchers have begun to quantitatively discuss the simulation cases by extracting the bubble size distribution and rise velocity from the simulation results (Wachem et al., 1999; Wachem et al., 2001; Cammarata et al, 2003; McKeen and Pugsley, 2003; Patil et al., 2005). However, most of these investigations have been based on coarser particles, belonging to the Geldart B or D classification of powders (Geldart, 1973) and Geldart A models are still scarce (McKeen and Pugsley, 2003).

Although mathematical models have been able to provide acceptable results for the modeling of coarser particles (Boemer and Renz, 1997; Goldschmidt et al., 2001; Taghipour et al., 2005), attempts at the simulation of finer Geldart A class of powders have encountered some significant challenges (McKeen and Pugsley, 2003; Makkawi et al., 2006). This difficulty arises due to the relative importance of interparticle cohesive forces compared with the gravitational forces when dealing with Geldart A powders (e.g. Massimilla and Donsi, 1976). According to Molerus (1982), cohesive forces can be neglected for the larger group B and D particles. Neglecting cohesive forces in CFD models of dense fluidized beds of Geldart A particles can lead to over-prediction of bed expansion by as much as 100% (McKeen and Pugsley, 2003; Makkawi et al., 2006). In fact, by neglecting these forces the underlying assumption is that mainly the collisional effects control individual particle-particle contacts, thus a large part of the remaining dynamic energy of the particles is consumed for propelling the particles towards the top of the bed.

McKeen and Pugsley (2003) were among the early researchers who reported this over-prediction of bed expansion. They argued that interparticle forces lead to the formation of particle clusters with a corresponding reduction in gas-solid drag. They found that by scaling the drag model of Gibilaro et al. (1985) with a fractional constant equal to 0.25, realistic bed expansion and bubble properties were predicted. Incorporation of equations for the interparticle cohesive forces was attempted by Kim and Arastoopour (2002), who extended the kinetic theory of granular flow to cohesive particles by modifying the solid distribution equation. However, the final expression for the particulate stress was

complex and difficult to incorporate into the current CFD models. Neither their model nor the model of McKeen and Pugsley (2003) considered the size distribution of particles in the fluidized bed.

As pointed out by Grace and Sun (1991), particle size distribution has a significant influence on the bed expansion. Therefore, considering the size distribution of the particles in the computational models might eliminate the problem of over-prediction of the bed expansion. However, the presence of different types and sizes of particles complicates the modeling process because separate continuity and momentum equations must be solved for each size and type (Risk, 1993; Gidaspow, 1994). As a result, these models have been only used for up to three solid phases in the literature, due to the computational limitations. The multiphase Particle in Cell (PIC) approach (Andrews and O'Rourke, 1996; Snider, 2001; Snider et al., 2001; Karimipour and Pugsley, 2009), which is essentially an Eulerian-Lagrangian model, provides a numerical scheme in which particles are grouped into computational parcels each containing a number of particles with identical density, volume and velocity, located at a specific position. The evolution of the particle phase is governed by solving a Liouville equation for the particle distribution.

In the present work, the capability of the multiphase PIC approach for simulating a bubbling fluidized bed of Geldart A particles will be investigated. The model predictions of bed expansion and bubble properties as well as radial and axial profiles of bed voidage will be validated by comparison with published correlations and experimental data. The

ability of the model to resolve the dynamic characteristics of the fluidized bed will also be evaluated using the time series of pressure fluctuations generated by the model.

4.3. Material and Experiments

A cylindrical Plexiglas vessel with an internal diameter of 14 cm and equipped with electrical capacitance tomography (ECT) sensors is used for conducting the bubbling fluidized bed experiments. Details of the ECT system can be found elsewhere (McKeen and Pugsley, 2003). Spent FCC catalyst powder with a Sauter mean diameter of 79 μm, low fines content (4% < 44 μm), and particle density of 1400 kg/m^3 was used as the bed material. The particle size distribution, provided in Fig. 4.1, was measured using a Microtrac particle size analyzer (Microtrac, Montgomeryville, USA).

Fluidized bed pressure fluctuations were measured using a series of Omega® pressure transducers mounted along the fluidized bed column. The transducers were flush-mounted to the internal wall of the fluidized bed with 15 cm long by 4.5 mm diameter stainless steel tubes covered by a 10 μm mesh at the tip to prevent fine particles from entering. The tube volume was less than 2500 mm^3 as recommended by Johnsson et al. (2000) to minimize the damping effect on the pressure fluctuations. The pressure measurements were performed at a sampling frequency of 100 Hz. This is far above the major frequency component of fluidized bed pressure fluctuations, which is normally below 10 Hz (Johnsson et al., 2000). The sampling time was 10 min. The data acquisition equipment was interfaced with a continuous data logging program built with LabVIEW® (National Instruments, Austin, USA).

4.4. Model Development

The governing equations of the multiphase PIC formulation are provided in Table 4.1. In the PIC model, the mass and momentum balance equations are solved for the continuous phase (fluid) and a Liouville-type equation is solved for the particle phase to find the distribution of particle positions with different velocities and sizes.

The Liouville equation is a differential equation which gives the future coordinates of the particle locations based on the current coordinates of the particles and the particle properties in the phase-space. It is assumed that the mass of each particle is constant through time (no mass transfer between particles or to the fluid), but particles can have a distribution of sizes and densities. Particles are grouped into computational parcels each containing N_p particles located at position, x_p. The particles in each parcel are considered to have identical density, volume and velocity. Parcels are smaller than the computational cells and thus each cell contains multiple parcels. These parcels move freely within the computational domain, similar to the movement of particles in the Lagrangian simulations. The Liouville equation conserves the particle numbers in parcel volumes, moving along dynamic trajectories in the particle phase-space. By using the Liouville equation for calculating the particle distribution function integrated over velocity, density and volume of all particles, the probable number of particles per unit volume at $\boldsymbol{x}$ and t that have the velocity, density and volume in the interval of ($\boldsymbol{u}_p$, $\boldsymbol{u}_p$+d$\boldsymbol{u}_p$), (ρ_p, ρ_p+dρ_p) and (V_p, V_p+dV_p) can be obtained. In this way, the size distribution of the particles will be applied in calculating the interphase momentum transfer. The particle phase is implicitly

coupled to the fluid phase through the interphase drag. The relations describing drag and solid stress are discussed in the next two sections.

4.4. 1. Drag Models

Ergun (1952) developed his correlation based primarily on the experimental data measured from the flow of gas through packed beds of coke particles with particle volume fractions ranging from 0.47 to 0.59. He extended the application range of his model using literature data measured for systems with particle volume fractions of up to 0.7. Wen and Yu (1966) conducted defluidization experiments in a liquid-solid system. They started at a fluidized state and gradually decreased the flow rate to reach the fixed bed condition. Their investigation covered the range of particle volume fractions between 0.28-0.61, but they also used literature data for particle volume fractions of as low as 0.01. Thus, the Ergun equation totally covers the range of particle volume fraction from 0.47-0.7 and the Wen and Yu (1966) equation covers the range of 0.01-0.61. However, the transition point used in the Gidaspow drag model (1994) occurs at a solid volume fraction of 0.2 which is not in the range of the overlapping between two models which is between 0.47-0.61. In order to prevent possible numerical problems due to the sharp transition or discontinuity in the Gidaspow drag model (1994), the application of a switching function has been recommended by some researchers.

As can bee seen in Table 2, a linear transition between two drag models as a function of the particle volume fraction at the close pack condition has been used in the present work. Assuming the close pack solid fraction as 0.6, the transition between two drag models

occurs between solid fractions of 0.51 and 0.45 which is in the overlapping range of two models.

The other drag models plotted in Fig. 4.2 are the original Gidaspow model (1994), the Syamlal and O' Brien (1989) model in which the coefficients of the model are modified based on the minimum fluidization velocity using the method proposed by the authors (Syamlal and O' Brien, 1989) and the drag model proposed by Gibilaro et al. (1985) and its scaled version used by McKeen and Pugsley (2003). As the figure shows, McKeen and Pugsley (2003) had to scale down the Gibilaro drag model by 75% (the *Modified Gibilaro* drag model in the figure) to be able to predict a realistic bed expansion, while the two drag models used in the current study (the Wen and Yu and the modified Gidaspow model) are in the range of the other drag models.

4.4. 2. Solid Stress Model

The particle normal stress model used in this study is the Lun et al. (1984) model which is developed based on the dense phase kinetic theory of gases. It is assumed in this model that the acceleration of an individual particle due to the solids stress is independent of size and velocity. The solids stress equation is comprised of two parts. The first part represents the kinetic contribution and the second part represents the collisional contribution. In a physical view, the kinetic part accounts for the momentum transferred by particles moving across imaginary shear layers in the system. The collisional part refers to the momentum transferred by direct particulate collisions.

The radial distribution function term provides a correction to the possible number of collisions in the kinetic theory of granular flow, due to the presence of other particles. In the case of slightly inelastic collisions, where the collisional anisotropy plays a negligible role, the radial distribution function depends only on the local particle volume fraction (Ye et al., 2005).

4.4.3. Solution Procedure

Each computational parcel contains n_p real particles with identical density, ρ_p, velocity, $\mathbf{u}_p$, volume, V_p, and position, $\mathbf{x}_p$. The particle positions are updated using the following implicit approximations:

$$\boldsymbol{x}_p^{n+1} = \boldsymbol{x}_p^{n} + \boldsymbol{u}_p^{n+1}\Delta t \tag{4.1}$$

The particle velocity is updated by integration of the particle acceleration equation:

$$\boldsymbol{u}_p^{n+1} = \frac{\boldsymbol{u}_p^{n} + \Delta t\left[D\ \boldsymbol{u}_p^{n+1} - \frac{1}{\rho_p}\nabla p_p^{n+1} - \frac{1}{\rho_p \theta_p}\nabla \tau_p^{n+1} + g \right]}{1 + \Delta t\ D} \tag{4.2}$$

where $\boldsymbol{u}_p^{n+1}$ is the interpolated implicit particle velocity at the particle location, p_p^{n+1} is the interpolated implicit pressure gradient at the particle location, τ_p^{n+1} is the interpolated solids stress gradient at the particle location, g is gravity acceleration and D is the drag force. The particle velocity given by Eq. (4.2) can be solved directly at each time step using fluid properties updated from the current time step and old-time properties for the solids stress. Following the particle velocity calculation, the particle positions are updated. The final grid volume fraction is calculated using Eq. (4.3) by mapping the particle volumes to the grid:

$$\theta_{i,j,k} = \frac{1}{V_{i,j,k}} \sum_{m=1}^{Np} n_{p,m} V_{p,m} S_{i,j,k,m} \tag{4.3}$$

n_p is the number of particles in a parcel (a cloud of particles all with the same properties), N_p is the number of parcels, and the grid cell volume is $V_{i,j,k}$. This volume fraction will be used for the solution of gas continuity and momentum equations in the next time step. The new-time fluid volume fraction can be calculated by knowing the total solid fraction.

Generally, the multiphase PIC approach possesses some major differences with the usual multiphase flow formulations (Andrews and O'Rourke, 1996). Firstly, the interphase momentum transfer function is more detailed than in continuum models. The momentum transfer rate in continuum models is considered to be proportional to the difference between the mass-averaged velocities of the phases (Gidaspow, 1986; Risk, 1993; Gidaspow, 1994). However in the PIC method, the particle distribution function is solved. Thus, the detailed interphase momentum transfer can be computed by summing the contributions from particles of different velocities and sizes. Secondly, the equation of acceleration for the particle phase has some differences compared to the Lagrangian methods. In PIC, particles are grouped into parcels that contain a fixed number of identical particles, while individual particles are tracked in the Lagrangian approach. Furthermore, collisions between particles are not resolved explicitly. Instead, the effect of particle collisions is accounted for in an average manner using a continuum model for the solid-phase stress.

4.5. Model Set up and Parameters

4.5. 1. Fluidized Bed and Flow Conditions

A 14-cm ID fluidized bed containing FCC catalyst filled to a static bed depth of 50 cm was defined for all simulation cases. The FCC particles had a Sauter mean diameter of 79 μm and the particle size distribution provided in Fig. 4.1. All simulations were three-dimensional with uniform grid sizes of 0.5, 1, and 2 cm. The simulations in this work were carried out with the commercial CFD code BARRACUDA (CPFD-Software Technology, Albuquerque, USA).

4.5. 2. Boundary and Initial Conditions

A Dirichlet boundary condition is defined for the gas phase at the bottom of the fluidized bed in which the superficial gas velocity is specified; the wind box is not part of the simulation. A constant pressure boundary condition was employed at the top of the vessel, which was set to a reference value of atmospheric pressure. A uniform pressure equal to the atmospheric pressure and uniform gas velocity equal to the gas superficial velocity at minimum fluidization were defined over the entire vessel as the initial conditions. The initial solid fraction of the bed was considered to be equal to the solid fraction at minimum fluidization conditions which was assumed to be 0.55. Details of these boundary and initial conditions and other input parameters are provided in Table 4.3.

4.6. Extraction of Bubble Properties from the Simulation Results

Three different bubble diameters (chord length, bubble equivalent diameter, and bubble cross sectional diameter) were extracted from the simulation results. In order to extract

the two-dimensional bubble properties of chord length and bubble equivalent diameter from the three-dimensional simulations, two orthogonal vertical planes intersecting at the centre of the axis of the bed were defined. Both planes were divided into 6-cm segments in the axial direction of the bed (Fig. 4.3a). Bubble characteristics extracted from these vertical planes are analogous to measurements made with capacitance or fibre optic probes and X-ray fluoroscopy. In addition, a horizontal plane of circular cross-section was defined at an axial position 30 cm above the gas distributor (also depicted in Fig. 4.3a). The images of the bubble cross sectional diameter extracted from this plane are analogous to those captured with an ECT system (McKeen and Pugsley, 2003).

An example of the two-dimensional images extracted from the vertical planes for different grid sizes is provided in Fig. 4.3b. The bubble sizes were calculated based on a time average of bubble sizes in both planes at a given axial position taken between 12 s and 25 s. The first 12 s of the simulation were discarded in the time-averaging to avoid the influence of initial transients in the model output. To perform the quantitative analysis of bubble size and velocity, these gray-style images were converted to binary images using a global thresholding method. The threshold is a normalized darkness intensity value that lies in the range of [0, 1]. Pixels darker than the threshold are considered to be totally black and brighter pixels are assigned as white pixels. Otsu's method (Otsu, 1979) is used to find this threshold for each image. This method finds the proper threshold to minimize the variance of the black and white pixels in the images. By applying this method, the bubbles become visible objects in the images. The binary version of the previous images based on Otsu's method (Otsu, 1979), are provided in Fig. 4.3c. To

verify the relevance of the threshold value calculated by Otsu method, the binary images were produced with several other values around the value calculated by Otsu's method (Otsu, 1979). It was found that the Otsu's method provides the most proper threshold value, because with higher values of the threshold close bubbles could not be differentiated. To discard very deformed objects, the eccentricity of the detected objects was defined to be greater than 0.98. The eccentricity is the ratio of the distance between the foci of the ellipse-shape object and its major axis length. The value ranges between 0 (for a circle) and 1 (for a line segment). The value of 0.98 was found by visual checking of several objects with different shapes in the images.

After detecting the bubbles based on the procedure discussed above, the center of the bubbles is found. As it was mentioned before, each image is divided to several regions. The bubbles are assigned to a specific region when their center of mass is located in that region. Then the displacement of the center of mass of a specific bubble between subsequent images is calculated. Since the time delay between subsequent images is known, the velocity of bubble can be calculated the values of delay time and displacement. In order to increase the possibility of tracking the same bubble between images, a limit of 5 cm for the displacement between two successive images was defined. It was also checked that the bubbles were present in the same radial section in successive images.

The radial profile of bubble size and the bubble number were similarly determined by dividing the cross sectional images into 7 radial slices (Fig. 4.3a). While a bubble, as a

3D object, is passing the cross section, objects with different diameters are continuously produced. The objects in each part of the cross section were separately tracked and the equivalent diameters of these objects were determined simultaneously. In this way, a vector of sizes is provided for each section. The diameter associated to the points of maximum diameter in these vectors which are produced by the passage of the equator of the bubbles was taken as the bubble diameter.

According to Harlow and Amsden (1975), bubbles should be detected in the context of the local voidage, hence for calculating the average bubble voidage, local voidage gradients have been considered here for detecting the bubble boundaries in the cross sectional voidage data. Based on these voidage gradients, the boundary of a bubble is considered to correspond to the average of the voidage at the center of the bubble and the voidage of the emulsion around the bubbles. For example, if a bubble has a voidage of one at the center and its surrounding emulsion has a voidage of 0.5, the boundary of bubbles happen at the voidage of 0.75.

The bubble frequency can be obtained from the vectors obtained previously for calculating the bubble diameter from cross sectional images. The number of peaks in a vector of bubble diameters (which represents the passage of bubbles with time) corresponds to the number of bubbles passing through cross section during a specified time period. The bubble frequency can be defined as the number of these peaks divided by the sampling time.

4.7. Results and Discussions

In this section model predictions are compared with literature correlations for bubble properties and with experimental data. As seen in Fig. 4.3b, performing the simulation using a 2 cm grid is insufficient to resolve the bubbles. Hence, the bubble properties have not been calculated for this case. The simulations do not predict bubbling in the initial 10 cm of the bed, but rather shows that this region is dominated by pressure waves. This behavior has also been observed in simulations and experiments by previous authors (Burgess and Calderbank, 1975; Boemer et al., 1998). Time-averaged properties are based on the period between 12 to 25 s out of a total simulation time of 25 s, to eliminate the effect of the initial transient fluctuations.

4.7.1. Bed Expansion

Fig. 4.4 presents the cross-sectionally averaged axial profile of the solid fraction inside the fluidized bed. Except for the case of 2 cm grid, both of the drag models predict a uniform axial profile of solid fraction inside the dense bed, with the sudden sharp decrease corresponding to the interface between the upper surface of the dense bed and dilute freeboard. The percentage expansions from the static bed depth for all simulation cases are also reported in Fig. 4.4. These values show that the grid size has an important influence on the predicted bed expansion, while the effect of the drag model is negligible. The dependency of the bed expansion on the grid size was also reported earlier by Wang et al. (2009). They found that a sufficiently small grid size (of the order of three particle diameters for the case they studied) was required to be able to correctly predict the bed expansion using the two-fluid model (TFM) or Eulerian modeling approach. However,

employing grid sizes in the order of particles, as they proposed, makes the simulation very time consuming and decreases its functionality for larger scale simulations. As it was shown in Fig. 4.4, the PIC approach is able to correctly predict bed expansion with a practical grid size as well as an unmodified drag model.

4.7.2. Bubble Size

Fig. 4.5 presents the different bubble dimensions extracted from the simulation results at a superficial gas velocity of 0.1 m/s (0.5 cm grid and drag model 2). The figure illustrates that bubble shape varies with increasing distance above the gas distributor. Bubble width is greater than chord length along most of the fluidized bed except near the upper bed surface. At the top of the bed, the increased velocity of the bubbles, which will be discussed later, leads to a different distribution of forces throughout the bubble, making them more elongated in that region. The comparison between equivalent bubble diameter and bubble width and chord length in the figure shows that the bubble equivalent diameter is less than both other dimensions near the upper bed surface. This is probably due to deformation of the bubble arising from the vigorous mixing patterns and the influence of the bed surface fluctuations. Since the various bubble dimensions of Fig. 4.5 are similar, in the ensuing comparison with published literature correlations only the bubble equivalent diameter is used.

Fig. 4.6 compares the bubble equivalent diameter predicted by our model with the literature correlations as a function of height above the distributor. Six different correlations, including two more elaborate correlations proposed by Horio and Nonako

(1987) and Choi et al. (1998) that account for bubble coalescence and splitting have been used here. As the figure illustrates, the model results fall within the range of predictions of the correlations and close to the data of Werther (1976), which was obtained at experimental conditions similar to those defined in our model. As can be seen, the model predicts that bubble size increases with increasing height above the distributor, which is consistent with the experimental evidence on the topic. It is also interesting to note that the trends of the model predictions suggest a leveling-off of bubble growth as the upper surface of the bed is reached. This notion of a maximum bubble size for Geldart A powders has been extensively discussed in the literature. However, this trend is not consistent with two correlations of Agarwal (Agarwal, 1985; Agarwal, 1987) and Werthers's correlation (Werther, 1976). Most of the available data used by the authors to develop their correlations are based on Geldart B and larger particles. For For example, Agarwal used 268 μm glass particles in developing both of his correlations for bubble size (Agarwal, 1985; Agarwal, 1987) and Werther used sand particles of 100 μm diameter to develop his bubble size correlation (Werther, 1976). Since bubbles are larger for these types of particles, the correlations may not be completely appropriate for predicting the smaller bubble sizes that appear in the fluidization of Geldart A particles. Between the correlations of Horio and Nonako (1987) and Choi et al. (1998) which are expected to be more relevant for this case, one overpredicts and the other underpredicts the model and the experimental data. Owing to the differences between the predictions of the various bubble correlations and the range of data used in their development, a precise assessment of our model based on comparison with these correlations can not be made. However, it can be stated that these correlations have been used for both fluidized bed

design and analysis of experiments since they were introduced into the fluidization literature. In this regard, our model performs well and is consistent with these published correlations.

When bubbles form above the distributor and move upward, bubble coalescence takes place, leading to fewer bubbles of larger size. The probability distribution of the number of bubbles at different axial positions above the distributor for two grid sizes and two drag models is plotted in Fig. 4.7. The decreasing trend of bubble number is properly captured in the case of 0.5 cm grid and drag model 2. The case with drag model 1 and 0.5 cm grid also predicts the decreasing trend of bubble number, however the decrease begins at a higher elevation compared to the previous case. The case with 1 cm grid and drag model 2 predicts an increasing number of bubbles, which is against the actual trend. This behavior points to the likelihood of the 1 cm grid being too coarse to obtain satisfactory results.

4.7.3. Bubble Rise Velocity

Fig. 4.8 provides a comparison between the average bubble velocity predicted by our model with literature correlations for bubble velocity, as a function of height above the distributor. As the figure shows, the different simulation cases provide nearly similar values for bubble velocity along the fluidized bed. The correlations of bubble velocity require the rise velocity of a single bubble. The correlation proposed by Wallis (1969) that accounts for the effect of system geometry on the bubble rise velocity has been used for this purpose. As Fig. 4.8 demonstrates, the correlations of Davidson and Harrison

(1963) and Kunii and Levenspiel (1991), provide predictions that are closer to our model results. The basis of both the correlations of Werther (1978) and Hilligardt and Werther (1986) is the correlation proposed by Davidson and Harrison (1963). They added empirical coefficients to the original equation to improve the correlation for their experimental observations.

4.7.4. Bubble Solid Fraction

Fig. 4.9a is a cross sectional mesh plot of the solid fraction at an axial position of 30 cm above the gas distributor. The horizontal axes indicate x and y directions and vertical axis shows the solid fraction. The gradient of solid fraction is also represented using different colors and the color bar provided at the side of the figure. As can be seen bubbles are visible as three holes in the graph. The presence of a distribution of the solids fraction inside the bubbles is clearly observable. An example of this distribution for the case of 0.5 cm grid and drag model 2 is provided in Fig. 4.9b. As can be seen, only a small region at the center of bubble with a typical diameter of 1 cm seems to be free of particles, i.e. a so-called "pure bubble" as described by Cui et al. (2000). The profile of solid fraction inside the bubble generally has an "S" shape with a slow rate of increase. Yates et al. (1994) found similar trends for Geldart B particles. However, the variation of the solid fraction seems to be sharper for Geldart B particles, compared to Geldart A particles investigated here. Therefore, bubble boundaries are more clearly discernible for larger particles. According to the correlations proposed by Cui et al. (2000), the ratio of the average solid fraction of bubble to emulsion for Geldart A and B particles are 0.57 and 0.41, respectively. This confirms the existence of more solid-laden bubbles in case of

Geldart A particles which is also in conformity with the findings reported by Grace and Sun (1991). This suggests that considering a distribution of the solid fraction is necessary when modeling fluidized bed reactors in order to properly capture the extent of reaction occurring inside the bubbles.

The axial profiles of bubble and bed voidages are shown in Fig. 4.10. As can be seen, the average bed voidage increases slowly and then levels-off at about 20 cm above the distributor with a voidage of 0.55. The bubble voidage increases faster and levels-off at about 27 cm and with a voidage of 0.8. This decreasing trend of bubble voidage has also been reported previously (Rowe et al., 1978; Yue et al., 1986). It indicates that the ability of bubbles to entrain the particles decreases and the bubbles become more and more depleted of particles as they approach the bed surface. Therefore, although the bubble fraction in bed is increasing due to the presence of larger bubbles, the role of bubble in the overall conversion may decrease (for gas-solid reactions or reactions with solid catalysts) due to carrying much lower fractions of particles. Fig. 4.10 also shows that average voidage in a large part of the fluidized bed is more than minimum fluidization. This is against the postulations of the simple two-phase theory and proves the notion of having higher amounts of interstitial gas flow (Rowe et al., 1978).

4.7.5. Dynamic Characteristics

An example of pressure fluctuations time series for the case of 0.5 cm grid and drag model 2, at a height of 30 cm above the gas distributor is compared to the experimental pressure fluctuations in Fig. 4.11. The standard deviation of the pressure fluctuations for

all cases is also given in the figure. As can be seen, the general appearance of the pressure fluctuations predicted by the simulation is similar to the experimental data. The standard deviation decreases as the grid size is increased. A possible reason is that the pressure fluctuations waves can not easily transfer between adjacent grids when the resolution is not sufficient. Also previous comparisons indicated that the coarse grid can not resolve bubbles, which have a large contribution in the pressure fluctuations. The standard deviation is also somewhat lower for the case of the 0.5 cm grid with drag model 1. This suggests that the choice of drag model also influences predictions of the bed dynamic behavior.

4.8. Conclusion

In the present work, the capability of the multiphase Particle in Cell (PIC) approach with a realistic particle size distribution for simulating the bubbling fluidized bed of Geldart A particles has been investigated. For this purpose, four cases with three different grid sizes and two drag models have been simulated using PIC approach. After simulating the bubbling fluidized bed, the bubble properties such as bubble size distribution, bubble rise velocity and bubble frequency as well as bed expansion and voidage profile have been calculated based on the simulation results. The results have been compared with commonly accepted correlations as well as experimental data provided in this work and from the literature. The results show a promising prediction capability of the multiphase PIC approach without any kind of modification in the drag model or other constituents of the model. The results indicate that although both grid size and drag model affect the

simulation results, the effect of drag model is negligible compared to the effect of the grid size.

4.9. References

Agarwal, P.K., 1985. Bubble characteristics in gas fluidized beds. Chemical Engineering Research and Design 63, 323-337.

Agarwal, P.K., 1987. Effect of bed diameter on bubble growth and incipient slugging in gas fluidised beds. Chemical Engineering Research and Design 65, 345-354.

Andrews M.J., O'Rourke P.J., 1996. The multiphase particle-in-cell (MP-PIC) method for dense particulate flows. International Journal of Multiphase Flow 22, 379-402.

Boemer, A., Qi, H., Renz, U., 1997. Eulerian simulation of bubble formation at a jet in a two-dimensional fluidized bed. International Journal of Multiphase Flow 23, 927-944.

Boemer, A., Qi H., Renz U., 1998. Verification of Eulerian simulation of spontaneous bubble formation in a fluidized bed. Chemical Engineering Science 53, 1835-1846.

Burgess. J.M., Calderbank P.H., 1975. The measurement of bubble properties in two phase dispersions-III Bubble properties in a freely bubbling fluidized bed. Chemical Engineering Science 30, 1511-1518.

Cammarata, L., Lettieri, P., Micale, G., Colman D., 2003. 2D and 3D CFD simulations of bubbling fluidized beds using Eulerian-Eulerian models. International Journal of Chemical Reaction Engineering 1, Article A48.

Chiba, T., Terashima, K., Kobayashi H., 1973. Bubble growth in gas fluidized beds. Journal of Chemical Engineering of Japan 6, 78-83.

Choi, J, Son J., Kim, S., 1998. Generalized model for bubble size and frequency in gas fluidized beds. Industrial and Engineering Chemistry Research 37, 2559-2564.

Cui, H., Mostoufi, N., Chaouki J., 2000. Characterization of dynamic gas-solid distribution in the fluidized beds. Chemical Engineering Journal 79, 135-143.

Davidson, J., Harrison, D., 1963. Fluidized Particles. Cambridge University Press, New York.

Ergun, S., 1952. Fluid flow through packed columns. Chemical Engineering Progress 48, 89-94.

Geldart, D., 1973. Types of gas fluidization. Powder Technology 7, 285-292.

Gibilaro, L., Di Felice, R., Waldram, S., 1985. Generalized friction factor and drag coefficient correlations for fluid-particle interactions. Chemical Engineering Science 40, 1817-1823.

Gidaspow, D., 1986. Hydrodynamics of fluidization and heat transfer: supercomputer modeling. Applied Mechanical Review 39, 1-22.

Gidaspow, D., 1994. Multiphase flow and fluidization: Continuum and kinetic theory description. 1st edition, Academic Press, Boston.

Goldschmidt, M., Kuipers, J., van Swaaij, W., 2001. Hydrodynamic modelling of dense gas-fluidised beds using the kinetic theory of granular flow: effect of coefficient of restitution on bed dynamics. Chemical Engineering Science 56, 571-578.

Grace, J., Sun, G., 1991. Influence of particle size distribution on the performance of fluidized bed reactors. Canadian Journal of Chemical Engineering 69, 1126-1134.

Harlow, F., Amsden, A., 1975. Numerical calculation of multiphase fluid flow. Journal of Computational Physics 17, 19-52.

Hilligardt, K., Werther, J., 1986. Local bubble gas hold-up and expansion of gas-solid fluidized beds. German Chemical Engineering 9, 215-221.

Horio, M., Nonaka A., 1987. A generalized bubble diameter correlation for gas-solid fluidized beds. AIChE Journal 33, 1865-1872.

Johnsson, F., Zijerveld, R., Schouten, J., van den Bleek C., Leckner B., 2000. Characterization of fluidization regimes by time-series analysis of pressure fluctuations. International Journal of Multiphase Flow 26, 663-715.

Karimipour, S., Pugsley, T., 2009. Application of the particle in cell approach for the simulation of bubbling fluidized beds of Geldart A particles, 7th Int. Conf. on CFD in Min and Proc. Industries. Melbourne, Australia, December 9-11.

Kim, H., Arastoopour, H., 2002. Extension of kinetic theory to cohesive particle flow. Powder Technology 122, 83-94.

Kunii, D., Levenspiel O., 1991. Fluidization Engineering, 2nd edition, Butterworth-Heinemann, Boston.

Lun, C., Savage S., Jeffrey, D., 1984. Kinetic theories for granular flow: inelastic particles in coquette flow and slightly inelastic particles in a general flow field. Journal of Fluid Mechanics 1409, 223-256.

Makkawi, Y., Wright, P., Ocone, R., 2006. The effect of friction and inter-particle cohesive forces on the hydrodynamics of gas-solid flow: A comparative analysis of theoretical predictions and experiments. Powder Technology 63, 69-79.

Massimilla, L., Donsi G., 1976. Cohesive forces between particles of fluid-bed catalysts. Powder Technology 15, 253-260.

McKeen, T., Pugsley, T., 2003. Simulation and experimental validation of freely bubbling bed of FCC catalyst. Powder Technology 129, 139-152.

Molerus, O., 1982. Interpretation of Geldart type A, B, C and D powders by taking into account interparticle forces. Powder Technology 33, 81-87.

Otsu, N., 1979, A threshold selection method from gray-level histograms, IEEE Transactions on Systems, Man and Cybernetics 9, 62-66.

Patil, D., van Sint Annaland, M., Kuipers, J., 2005. Critical comparison of hydrodynamic models for gas-solid fluidized beds-Part II: freely bubbling gas-solid fluidized beds. Chemical Engineering Science 60, 73-84.

Risk, M., 1993. Mathematical modeling of densely loaded, particle laden turbulent flows. Atomization Sprays 3, 1-27.

Rowe, P.N., Santoro, L., Yates, J.G., 1978. The division of gas between bubble and interstitial phases in fluidized beds of fine powders. Chemical Engineering Science 33, 133-140.

Schiller, L., Naumann, Z., 1935. A drag coefficient correlation, VDI Zeitung 77, 318-320.

Snider, D.M., O'Rourke P.J., Andrews M.J., 1998. Sediment flow in inclined vessels calculated using a multiphase particle-in-cell model for dense particle flows. International Journal of Multiphase Flow 24, 1359-1382.

Snider, D.M., 2001. An incompressible three-dimensional multiphase particle-in-cell model for dense particle flows. Journal of Computational Physics 170, 523-549.

Syamlal, M., O'Brien, T., 1989. Computer simulation of bubbles in a fluidized bed. AIChE Symposium Series 85, 22-31.

Taghipour, F., Ellis, N., Wong, C., 2005. Experimental and computational study of gas-solid fluidized bed hydrodynamics. Chemical Engineering Science 60, 6857-6867.

van Wachem, B., Schouten, J., Krishna, R., van den Bleek, C., 1999. Validation of the Eulerian simulated dynamic behaviour of gas-solid fluidised beds. Chemical Engineering Science 54, 2141-2149.

van Wachem, B., Schouten, J., van den Bleek, C., 2001. Comparative analysis of CFD models of dense gas-solid systems. AIChE Journal 47, 1035-1051.

Wallis, G.B., 1969. One dimensional two-phase flow, McGraw-Hill, New York.

Wang, J., van der Hoef, M., Kuipers, J.A.M., 2009. Why the two-fluid model fails to predict the bed expansion characteristics of Geldart A particles in gas-fluidized beds: A tentative answer. Chemical Engineering Science 64, 622-625.

Wen, C., Yu, Y., 1966, Mechanics of fluidization, Chemical Engineering Progress Symposium Series 62, 100-111.

Werther, J., 1976. Bubble growth in large diameter fluidized beds. In: Fluidization Technology, Keairns D.L. (Ed.), Hemisphere Publishing Co, Washington DC.

Werther, J., 1978. Effect of gas distributor on the hydrodynamics of gas fluidized beds. German Chemical Engineering 1, 166-174.

Yates, J., Cheesman, D., Sergeev, Y., 1994. Experimental observations of voidage distribution around bubbles in a fluidized bed. Chemical Engineering Science 49, 1885-1895.

Ye, M., van Der Hoef, M., Kuipers, J.A.M., 2005. From discrete particle model to a continuous model of Geldart A particles. Chemical Engineering Research and Design 83, 833-843.

Yue, P.L., Rizzuti, L., Augugliaro, V., 1986, Bubble phase voidage and dense phase voidage in thin two-dimensional fluidized beds. Chemical Engineering Science 41, 171-177.

4.10. Nomenclature

A particle acceleration (m/s^2)

C particle velocity fluctuations averaged over the velocity space (m/s)

C_D drag coefficient

D drag force (kg/m^3s)

D_1 drag force in drag model 1 (kg/m^3s)

D_2 drag force in drag model 2 (kg/m^3s)

d_p particle diameter (m)

$f(x, u_p, \rho_p, V_p, t)$ Liouville equation

F rate of momentum exchange per unit volume from the gas to the particle phase (N/m^3s)

g gravitational acceleration (m/s^2)

g_0 solid radial distribution function

n_p number of particles in a parcel

N_p total number of parcels or clouds

p gas pressure (kPa)

P_c gas density (gas mass per unit volume occupied by the gas)

P_s constant with units of pressure (kPa)

Re Reynolds number ($\rho\ \varepsilon\ d_p\ (u_p - u_g\ )/\mu_g$)

$S_{i,j,k}$ interpolation function for cell centered variables

STD standard deviation of pressure fluctuations

t time (s)

u_g gas velocity (m/s)

u_p particle velocity (m/s)

U_{mf} minimum fluidization velocity (m/s)

$V_{i,j,k}$ grid cell volume (m^3)

V_p particle volume (m^3)

x_p particle position (m)

Greek Letters

ε gas volume fraction

γ restitution coefficient

μ_g gas viscosity (kg/m s)

ρ_g gas density (kg/m^3)

ρ_p particle density (kg/m^3)

$\bar{\rho}_p$ average particle density (kg/m^3)

τ particle normal stress (N/m^2)

∇_{u_p} Divergence operator with respect to velocity

θ particle volume fraction

θ_{cp} particle-phase volume fraction at close packing

Θ granular temperature (m^2/s^2)

Table 4.1. Governing equations of the multiphase PIC model

Fluid phase continuity equation:

$$\frac{\partial(\varepsilon\rho_g)}{\partial t} + \nabla_x(\varepsilon\rho_g \boldsymbol{u}_g) = 0$$

Fluid phase momentum balance:

$$\frac{\partial(\varepsilon\rho_g \boldsymbol{u}_g)}{\partial t} + \nabla_x(\varepsilon\rho_g \boldsymbol{u}_g \boldsymbol{u}_g) = -\varepsilon\nabla_x p + \varepsilon\mu_g\nabla^2\boldsymbol{u}_g - \boldsymbol{F} + \varepsilon\rho_g g$$

Rate of momentum transfer between gas and solid phase per unit volume:

$$\boldsymbol{F} = \iiint f V_p \rho_p \left[D(\boldsymbol{u}_g - \boldsymbol{u}_p) - \frac{1}{\rho_p}\nabla p \right] dV_p d\rho d\boldsymbol{u}_p$$

Liouville equation for finding the particle positions:

$$\frac{\partial f}{\partial t} + \nabla_x(f\boldsymbol{u}_p) + \nabla_{\boldsymbol{u}_p}(fA) = 0$$

Particle acceleration balance:

$$A = \frac{1}{\rho_p} D(\boldsymbol{u}_g - \boldsymbol{u}_p) - \frac{1}{\rho_p}\nabla_x p + g - \frac{1}{\theta\rho_p}\nabla_x \tau$$

Particle normal stress (Lun et al., 1984):

$$\tau = \left[\theta\overline{\rho}_p + \theta^2\overline{\rho}_p(1+\gamma)g_0 \right]\Theta$$

Granular temperature (calculated with kinetic theory of granular flow equations):

$$\Theta = \frac{1}{3}\left\langle C^2 \right\rangle$$

Radial distribution function (Gidaspow, 1994):

$$g_0 = \frac{3}{5}\left[1 - \left(\frac{\theta}{\theta_{cp}} \right)^{1/3} \right]^{-1}$$

Solid fraction in each cell:

$$\theta = \iiint f V_p dV_p d\rho_p d\boldsymbol{u}_p$$

Table 4.2. Equations of drag models

Model 1	$C_D = \frac{24}{Re}$	$Re < 0.5$
	$C_D = \frac{24}{Re}\left(1 + 0.15Re^{0.687}\right)$	$0.5 \le Re < 1000$
	$C_D = 0.44$	$Re \ge 1000$
	$D = \frac{3}{4} C_D \rho_g \theta \frac{\left\|u_g - u_p\right\|}{d_p} \varepsilon^{-1.65}$	
	$Re = \frac{\rho_g \varepsilon d_p \left\|u_g - u_p\right\|}{\mu_g}$	
Model 2	$C_D = \frac{24}{Re}$	$Re < 0.5$
	$C_D = \frac{24}{Re}\left(1 + 0.15Re^{0.687}\right)$	$0.5 \le Re < 1000$
	$C_D = 0.44$	$Re \ge 1000$
	$D_1 = \frac{3}{4} C_D \rho_g \theta \frac{\left\|u_g - u_p\right\|}{d_p} \varepsilon^{-1.65}$	
	$D_2 = \left(\frac{180\theta}{Re} + 2\right) \frac{\left\|u_g - u_p\right\|}{d_p} \rho_g \theta$	
	$Re = \frac{\rho_g \varepsilon d_p \left\|u_g - u_p\right\|}{\mu_g}$	
	$D = D_1$	$\theta < 0.75\theta_{CP}$
	$D = \frac{\theta - 0.75\theta_{CP}}{0.85\theta_{CP} - 0.75\theta_{CP}}\left(D_2 - D_1\right) + D_1$	$0.75\theta_{CP} \le \theta \le 0.85\theta_{CP}$
	$D = D_2$	$\theta > 0.85\theta_{CP}$

Table 4.3. Input parameters used in the simulation

Geometry	Three-dimensional, Cartesian
Vessel dimension	0.14 m diameter and 1 m height
Grid	0.5×0.5×0.5, 1×1×1, 2×2×2 cm
Total number of particles	1.31472×10^{10}
Total number of clouds	3.8944×10^{6}
Granular viscosity model	Lun et al. (1984)
Drag models	No. 1: Wen and Yu (1966) No. 2: Modified Gidaspow (1994)
Flow type	Compressible with no gas-phase turbulence
Simulation time	25 seconds
Time step	0.0001 seconds
Pressure-Velocity coupling	SIMPLE
Solid fraction at maximum packing	0.55
Initial condition	Bed at minimum fluidization
Minimum fluidization velocity	0.004 m/s
Minimum fluidization voidage	0.45
Boundary conditions	Uniform flow from bottom Atmospheric pressure at the top
Gas superficial velocity	0.1 m/s
Bed depth	0.5 m
Restitution coefficient	0.4

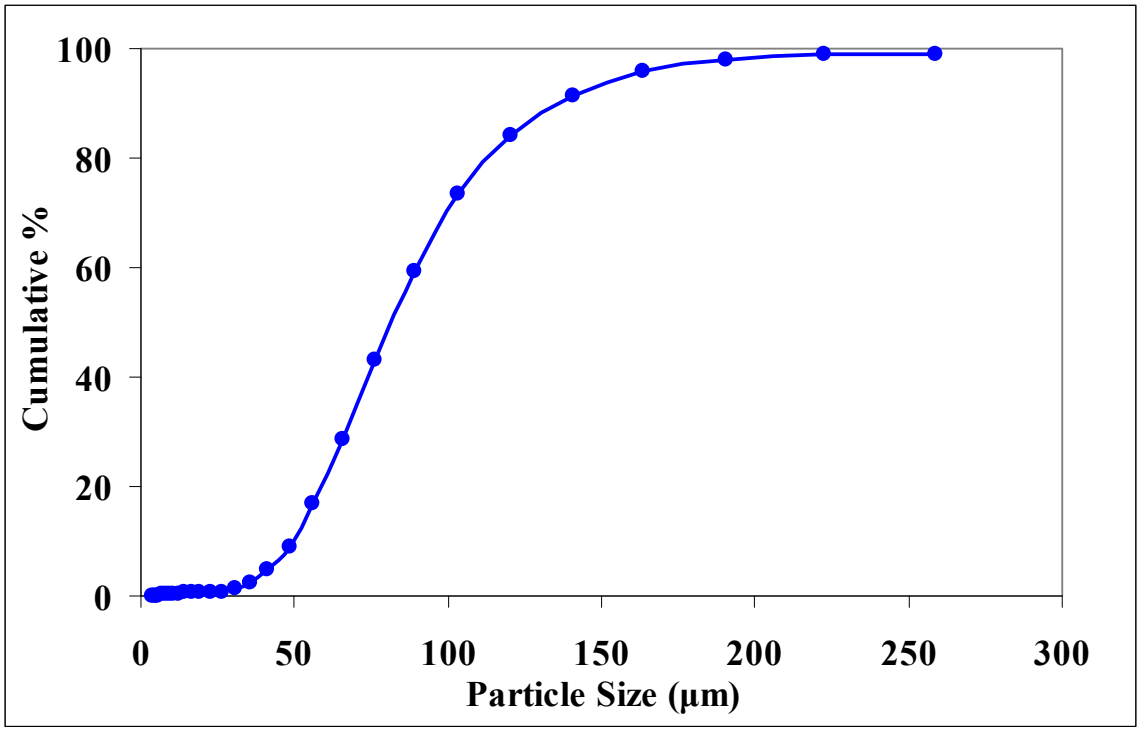

Figure 4.1. Particle size distribution of the FCC powders used in the experiments

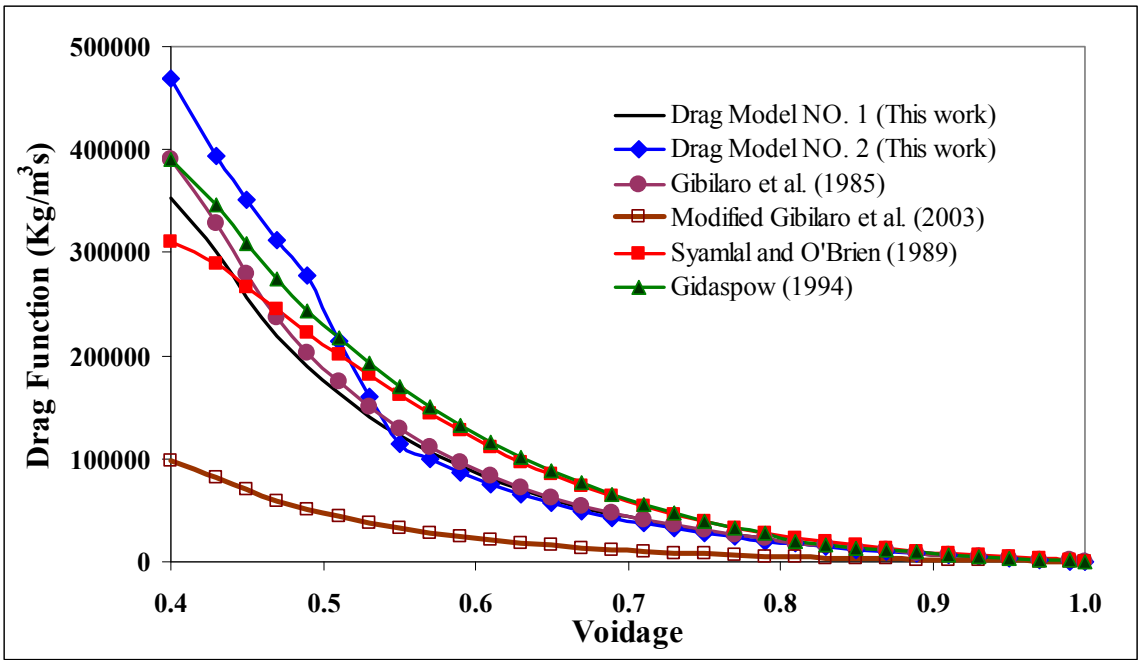

Figure 4.2. Comparison between different drag models used for CFD simulations in the literature

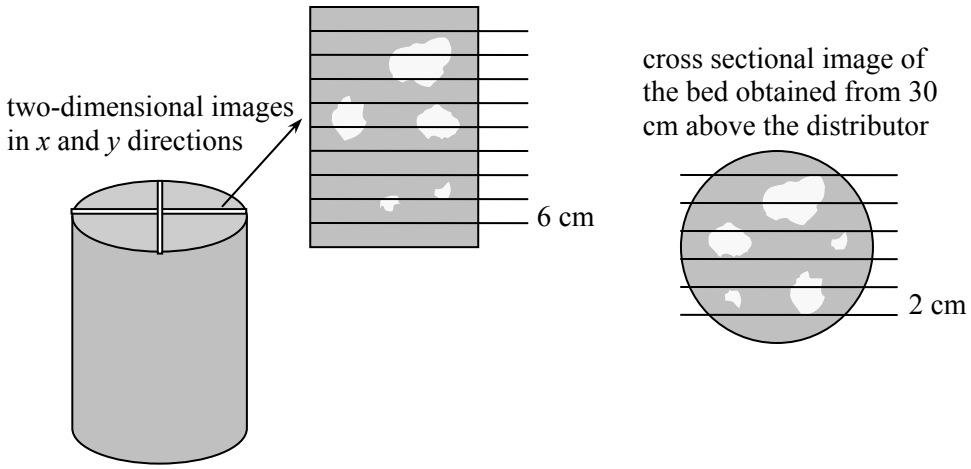

Figure 4.3a. The segmentation of the axial and cross sectional images for calculating the distribution of the bubble size

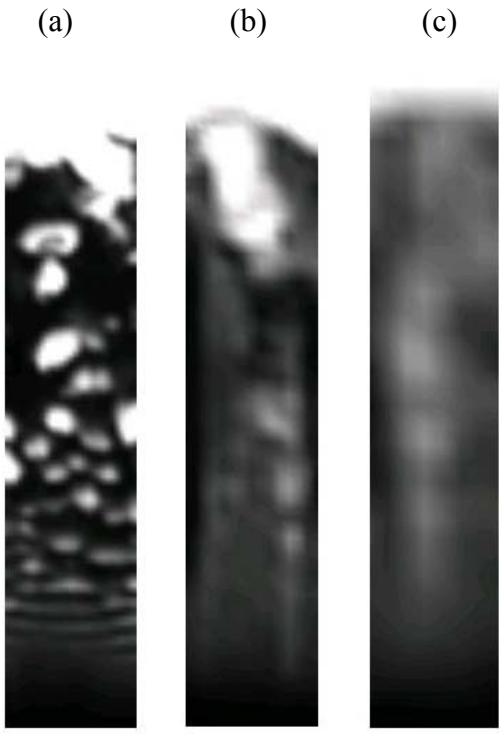

Figure 4.3b. Snapshots of the simulation cases with different grid size, a) 0.5 cm grid, b) 1 cm grid, c) 2 cm grid, the width of the images is 14 cm.

(a) (b) (c)

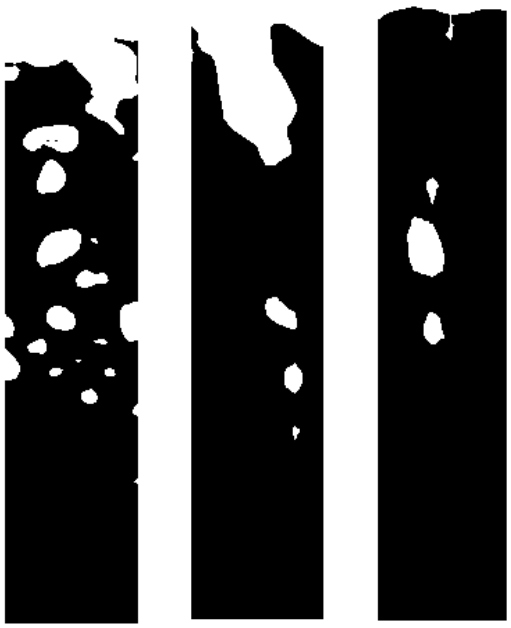

Figure 4.3c. Binary versions of the snapshots provided in Fig. 4.3b, a) 0.5 cm grid, b) 1 cm grid, c) 2 cm grid, the width of the images is 14 cm.

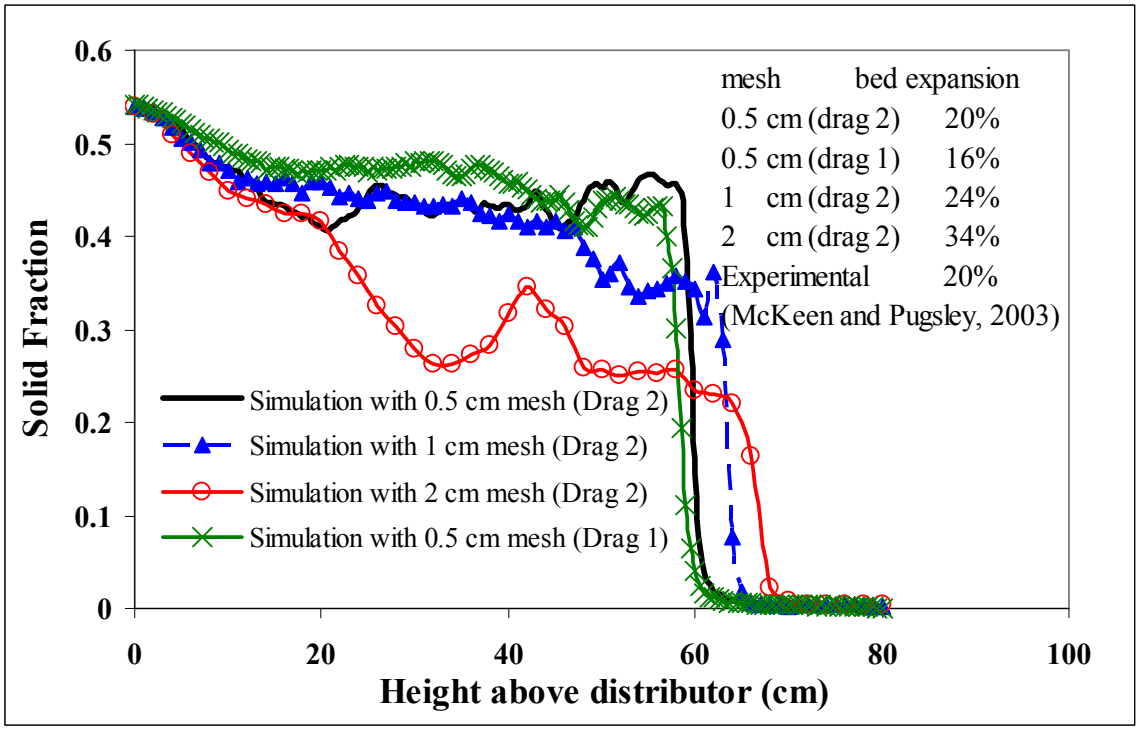

Figure 4.4. Axial profile of solid fraction inside the fluidized bed. U_0 = 0.1 m/s, time-averaged over the period 12-25 s.

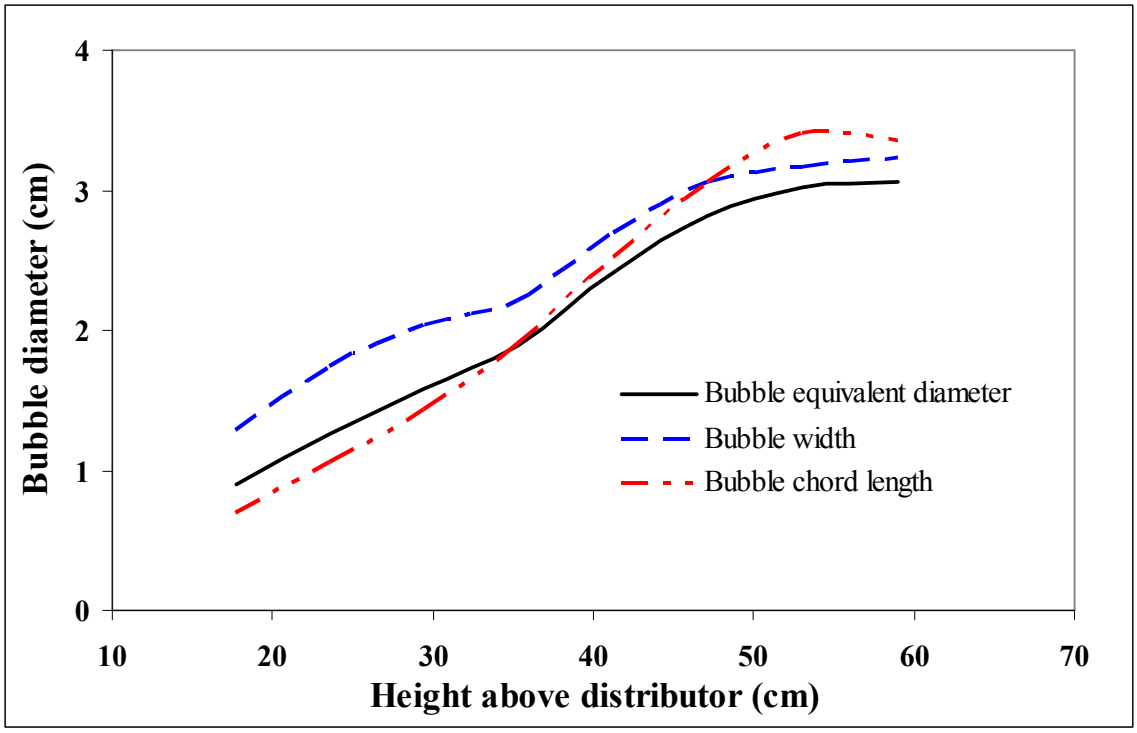

Figure 4.5. Axial profiles of bubble sizes extracted from the simulation results for the case of a 0.5 cm grid and drag model 2. U_0 = 0.1 m/s, time-averaged over the period 12-25 s.

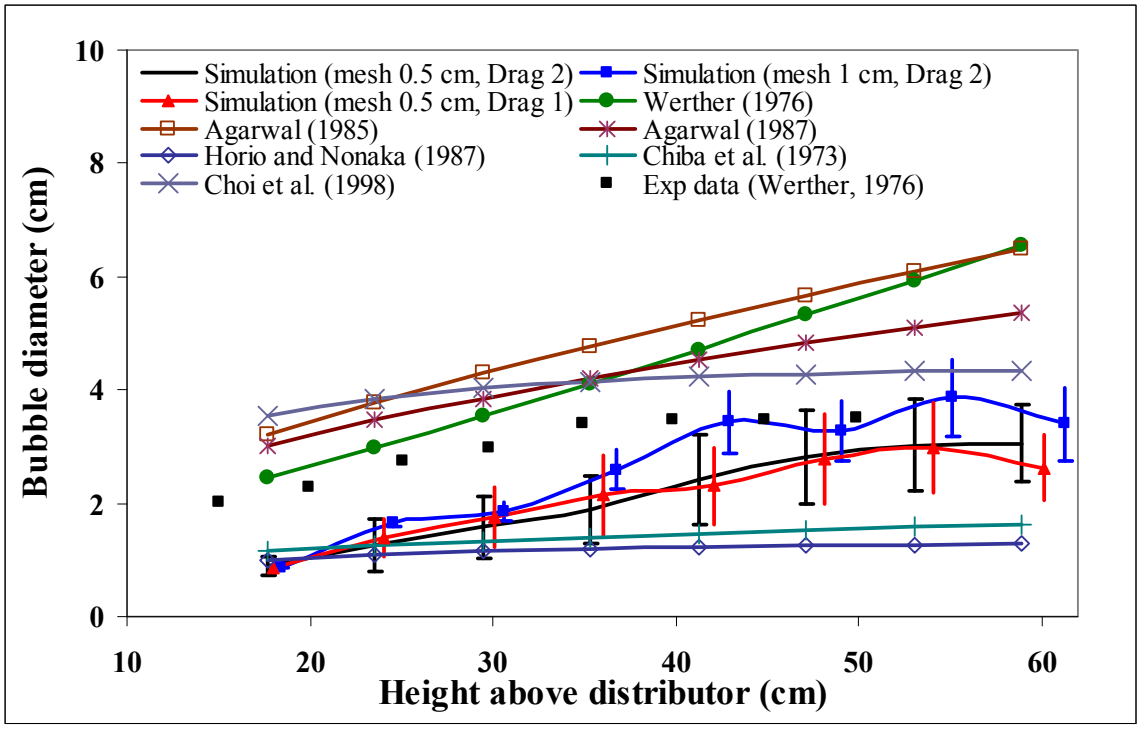

Figure 4.6. Comparison of model predictions of bubble average equivalent diameter as a function of height above the distributor with predictions of selected correlations and the experimental data of Werther (1976). U_0 = 0.1 m/s, time-averaged over the period 12-25 s.

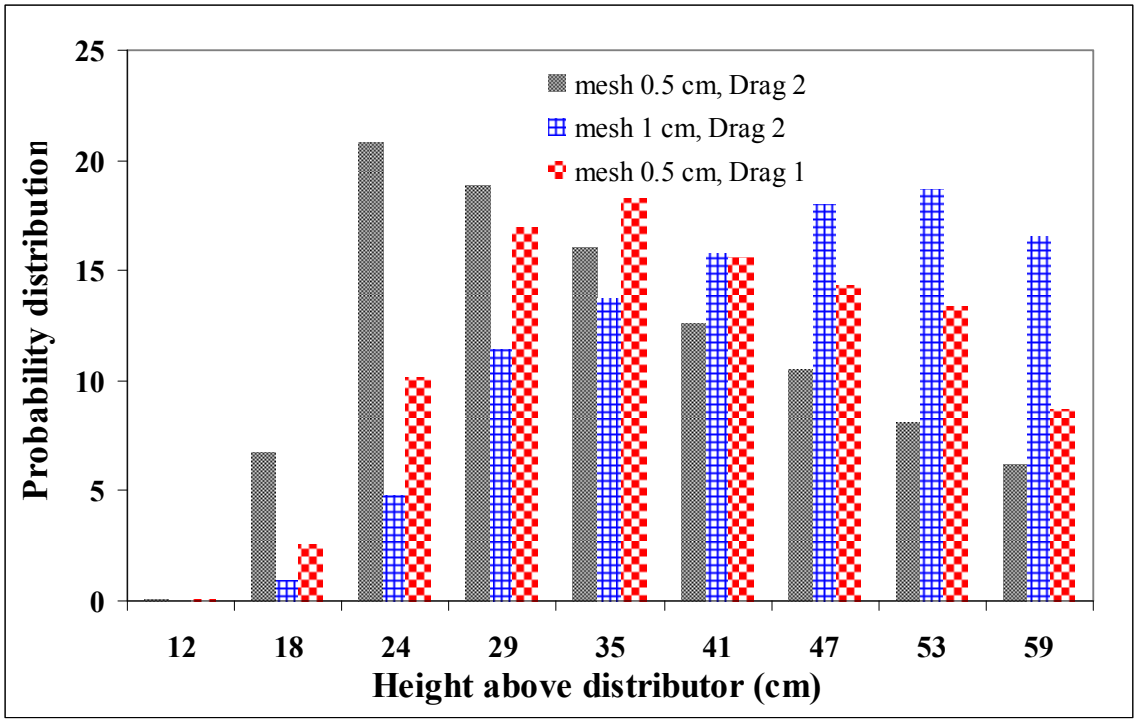

Figure 4.7. Model predictions of the probability distribution of the number of bubbles as a function of height above the distributor for differing mesh sizes and drag models. U_0 = 0.1 m/s, time-averaged over the period 12-25 s.

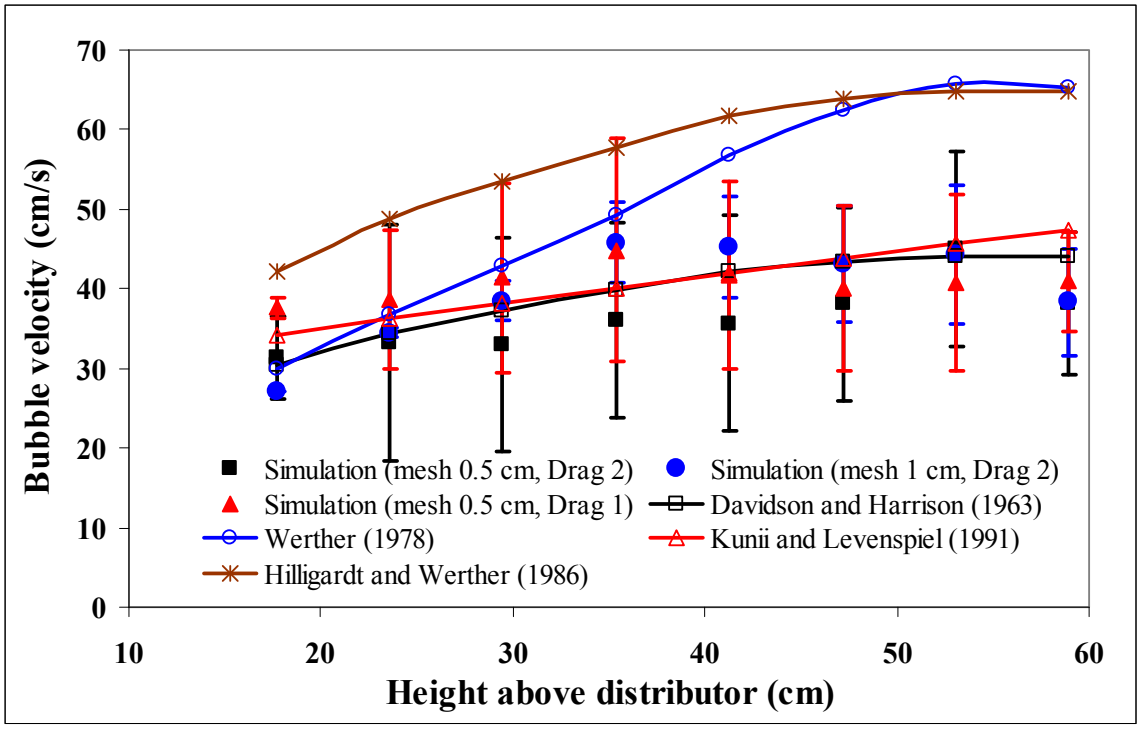

Figure 4.8. Comparison of model predictions of the bubble average velocity as a function of height above the distributor with the selected correlations from the literature. U_0 = 0.1 m/s, time-averaged over the period 12-25 s for the model predictions.

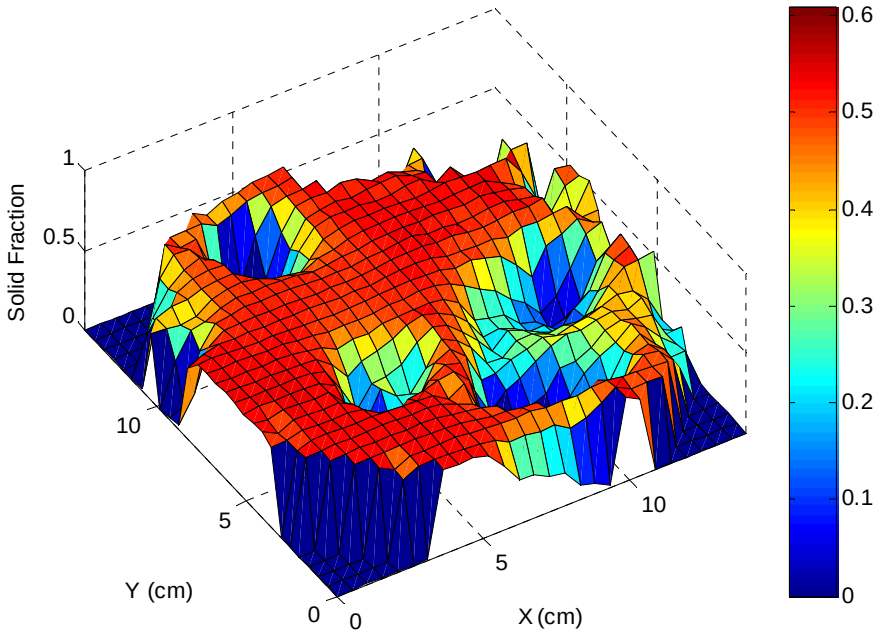

Figure 4.9a. Cross sectional mesh plot of the solid fraction in height of 30 cm of the fluidized bed; the color in the figure shows the distribution of solid fraction which is defined in the scaled color bar at the right. $U_0 = 0.1$ m/s, 0.5 cm grid size and drag model 2, time-averaged over the period 12-25 s.

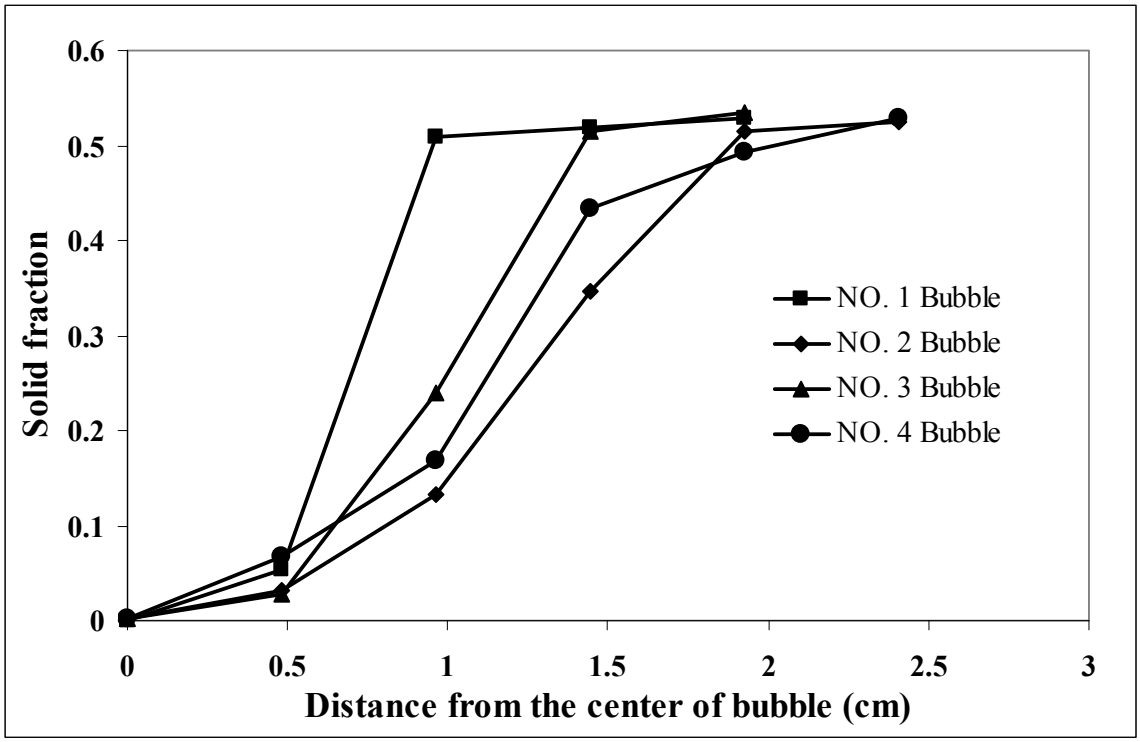

Figure 4.9b. Examples of the radial profile of the fraction of solids inside the bubbles. U_0 = 0.1 m/s, 0.5 cm grid size and drag model 2, time-averaged over the period 12-25 s.

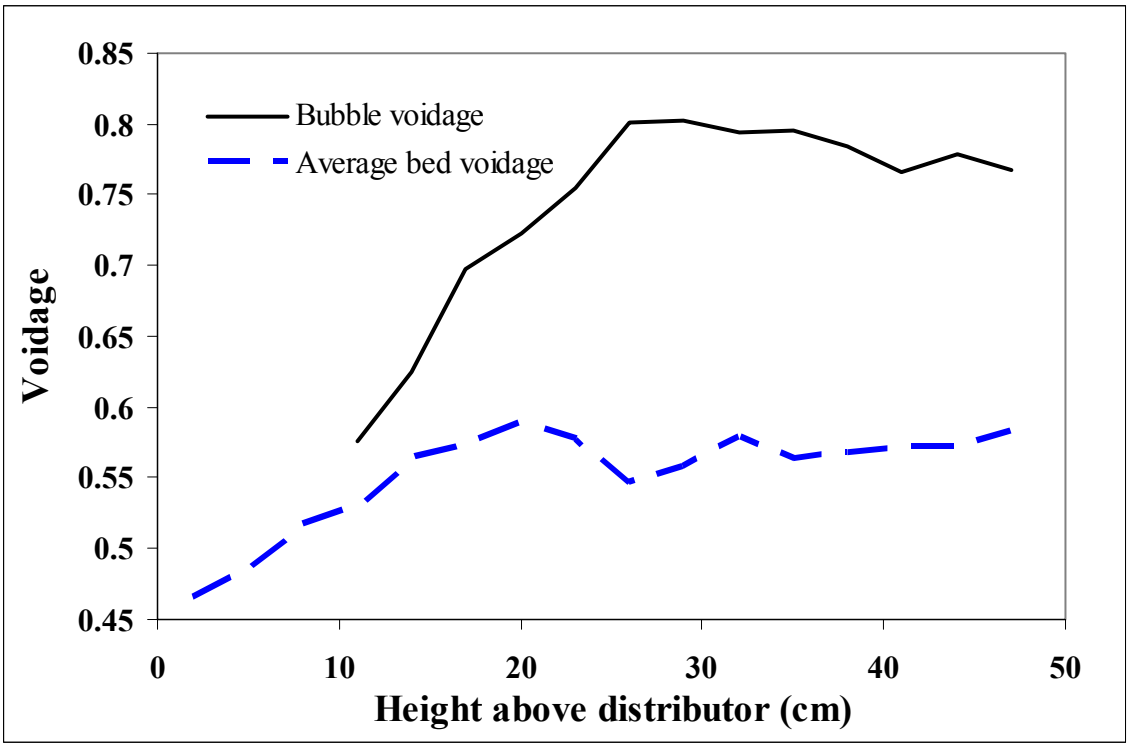

Figure 4.10. Axial profile of the average bubble voidage and the average bed voidage as a function of height above the gas distributor. U_0 = 0.1 m/s, 0.5 cm grid size and drag model 2, time-averaged over the period 12-25 s.

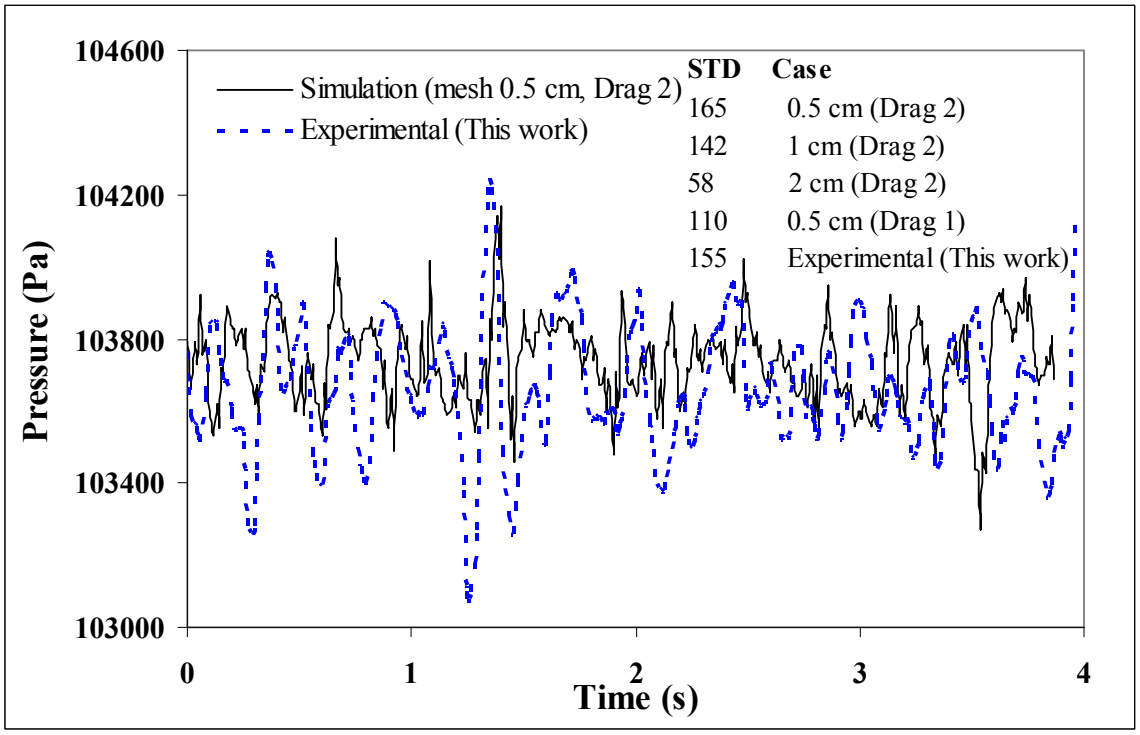

Figure 4.11. Comparison between simulated and experimental gage pressure fluctuations in the fluidized bed at the height of 30 cm above the gas distributor. U_0 = 0.1 m/s, 0.5 cm grid size and drag model 2, time-averaged over the period 12-25 s.

CHAPTER 5 - Modeling Study of Gas Streaming in a Deep Fluidized Bed of Geldart A Particles

The contents of this chapter have been submitted to the ***CFB10 -- International Conference on Circulating Fluidized Beds and Fluidized Bed Technology.*** It has been submitted in a version similar to what appears in this chapter.

Citation

S. Karimipour, T. Pugsley, Modeling study of gas streaming in a deep fluidized bed of Geldart A particles, CFB10 - International Conference on Circulating Fluidized Beds and Fluidized Bed Technology, Sun River, Oregon, USA, May 1-6, 2011

Contribution of Ph.D. Candidate

The CFD simulations performed for the purpose of this work were planned and performed by Shayan Karimipour. Todd Pugsley provided consultation regarding the design of simulation cases. The programs for all of the data analysis were developed by

Shayan Karimipour. All of the writing of the submitted manuscript was done by Shayan Karimipour with Todd Pugsley providing editorial guidance regarding the style and technical content of the manuscript.

Contribution of this Paper to the Overall Study

The objective of the present work is to develop a phenomenological model for the streaming flow. The model will then be used to evaluate the effect of bed depth, gas velocity, and particle size on the streaming flow and discuss possible causes of the appearance of this phenomenon by increasing the bed depth in fluidized bed.

5.1 Abstract

Gas streaming has been modeled in a deep fluidized bed of 5 m depth and 0.3 m inside diameter. The cross section of the bed is divided into two zones: stream and non-stream. The pressure drop in the stream zone is modeled based on a force balance over a single particle and the pressure drop of non-stream zone is considered to be equal to the head of the particle bed. The model results suggest that the lower pressure drop of the stream zone compared to the remainder of the bed is the reason for the formation and stability of the streaming flow. The effects of different parameters such as bed depth, gas velocity and particle size on the severity of the streaming flow are also evaluated with the model. The model results show that increasing the bed depth favors the streaming flow, while increasing the gas velocity increases the uniformity of the bed and decreases the streaming severity. Streaming flow was found to be less severe for larger particle sizes.

All of these findings are in conformity with experimental investigations reported previously in the literature.

5.2. Introduction

Several studies in the past decade have demonstrated that in sufficiently deep fluidized beds of Geldart A particles (Geldart, 1973), gas bypassing may occur by increasing the superficial gas velocity beyond minimum fluidization. When this phenomenon occurs, the fluidizing gas bypasses the bed in the form of streams of gas, leaving a large fraction of the bed unfluidized or poorly fluidized (Wells, 2001; Karri et al., 2004; Issangya et al., 2007; Karimipour and Pugsley, 2010). The concept of gas streaming was first reported in the literature by Wells (2001). He performed several experiments in large scale units with up to 2.5 m diameter and 5 m bed depth and observed streaming flow under conditions that were expected to lead to operation in the bubbling regime. He attributed the streaming phenomenon to gas compression, caused by the pressure head of the deep solids bed over the distributor.

Karri et al. (2004) investigated the formation of streaming flow in a column of 0.3 m inner diameter and 4.9 m height. They found that the standard deviation of pressure drop in a bed exhibiting streaming was much greater than a uniformly fluidized bed. They also reported that for all combinations of operating conditions investigated, the addition of a sufficient amount of fines to the bed of Geldart A particles was able to delay the streaming, even in deep beds. In another work, Issangya et al. (2007) used several pressure transducers mounted at various radial positions to detect the presence of

streaming flow. They concluded that the maximum in the plot of standard deviation of the pressure fluctuation *versus* gas velocity, which has been shown in the literature to be an indication of the transition between the bubbling to turbulent fluidization regimes, is not present for deep beds that are subject to streaming.

Recently, Karimipour and Pugsley (2010) have done a systematic study on the streaming flow in deep beds of FCC particles. They discussed the signs of streaming flow in the pressure fluctuations time series measured in the fluidized bed for different combinations of bed depth, gas velocity, particle size and distributor. They concluded that streaming flow does not appear suddenly, but emerges gradually in the bed by increasing the bed depth. They found that although changing some parameters can influence the severity of the streaming flow, streaming is the dominant phase for deep fluidized beds operating in normal conditions.

Although several experimental works have been performed to study the general characteristics of the streaming flow, mathematical representation and evaluation of the streaming flow is still absent in the literature. The only mathematical work presented by Wells (2001) to detect the onset of streaming flow does not include a functional dependency on conditions such as bed depth and gas velocity and seems not to be able to predict the correct situation for various cases. The objective of the present work is to develop a phenomenological model for the streaming flow and to use the model to evaluate the effect of bed depth, gas velocity, and particle size.

5.3. Model Development

Based on the visual observations made during a separate experimental campaign, the deep fluidized bed was divided into two adjacent regions in which the smaller region was occupied with the stream flow and the other region was assumed to be at minimum fluidization conditions. The stream is assumed to form near the wall and occupy one fourth of the bed diameter. The diameter of the stream is assumed to remain constant along the fluidized bed. A small zone above the distributor is reported to be better fluidized and gas and particles from other parts of the distributor find their way towards the stream and move upward through the stream. As such, particles can be assumed to move upward only in the stream and after discharging at the surface of the bed slowly return to the bottom through the non-streaming region. Similar to the acceleration zone of a circulating fluidized bed (Pugsley and Berruti, 1996; Karimipour et al., 2006), the stream can be modeled by a force balance over a single particle inside the stream. Three forces that act on a particle moving upward in a swarm of other particles are gravitational, buoyancy and gas-solid drag. The axial pressure drop along the stream can then be extracted from the force balance equation. Assuming the particles as spheres of constant diameter, the force balance equation can be written as follows:

$$\rho_p V_p \frac{d\upsilon_p}{dt} = \frac{1}{2}\rho_g \left(\frac{u_{st}}{\varepsilon_g} - \upsilon_p \right)^2 A_p C_D - (\rho_p - \rho_g) V_p g \tag{5.1}$$

Substituting V_p and A_p in Eq. 5.1 by the subsequent relations

$$V_p = \frac{\pi}{6} d_p^3 \tag{5.2}$$

$$A_p = \frac{\pi}{4} d_p^2 \tag{5.3}$$

and considering the following equality from the derivative theory

$$\frac{d\upsilon_p}{dt} = \upsilon_p \frac{d\upsilon_p}{dz} \tag{5.4}$$

Eq. 5.1 can be rearranged as

$$\frac{d\upsilon_p}{dz} = \frac{3\rho_g C_D}{4 d_p \rho_p \upsilon_p}\left(\frac{u_{st}}{\varepsilon_g} - \upsilon_p\right)^2 - \frac{g}{\rho_p \upsilon_p}(\rho_p - \rho_g) \tag{5.5}$$

The drag coefficient, C_D, in Eq. 5.5 can be estimated from one of the abundant correlations of the drag coefficient in the literature. The correlation of Mostoufi and Chaouki (1999) which has been developed for FCC particles, used in the experimental works in chapters 2 and 3, has been employed here. The porosity in these equations is calculated from the solids mass balance equation as follows:

$$G_p = \rho_p (1 - \varepsilon_g)\upsilon_p \tag{5.6}$$

The initial value of the particle velocity at the bottom of the stream is obtained from the solids mass balance. Thus, Eq. 5.5 will be solved subject to the following initial condition:

$$\upsilon_p\big|_{z=0} = \frac{G_p}{\rho_p (1 - \varepsilon_{mf})} \tag{5.7}$$

Once the axial profile of particle velocity in the stream is determined from Eq. 5.5, the corresponding solids holdup can be calculated from

$$\varepsilon_p = 1 - \varepsilon_g \tag{5.8}$$

The axial profile of the pressure drop along the stream can be determined from the momentum balance over the stream. The momentum balance could be expressed as follows:

$$\frac{dp}{dz}=\left(\frac{dp}{dz}\right)_{head}+\left(\frac{dp}{dz}\right)_{acceleration}+\left(\frac{dp}{dz}\right)_{friction} \tag{5.9}$$

where

$$\left(\frac{dp}{dz}\right)_{head}=\rho_p\varepsilon_p g+\rho_g\varepsilon_g g \tag{5.10}$$

$$\left(\frac{dp}{dz}\right)_{acceleration}=\rho_p\varepsilon_p\upsilon_p\frac{d\upsilon_p}{dz}+\rho_g\varepsilon_g\frac{u_{st}}{\varepsilon_g}\frac{d}{dz}\left(\frac{u_{st}}{\varepsilon_g}\right) \tag{5.11}$$

The pressure drop caused by friction includes two sources, i.e., gas-wall and particle-wall frictions:

$$\left(\frac{dp}{dz}\right)_{friction}=\left(\frac{dp}{dz}\right)_{gas-wall}+\left(\frac{dp}{dz}\right)_{particl-wall} \tag{5.12}$$

These pressure losses are defined by the Fanning equation as

$$\left(\frac{dp}{dz}\right)_{gas-wall}=f_g\frac{1}{2d_{st}}\rho_g\frac{u_{st}^2}{\varepsilon_g} \tag{5.13}$$

$$\left(\frac{dp}{dz}\right)_{particle-wall}=f_p\frac{1}{2d_{st}}\rho_p\varepsilon_p\upsilon_p^2 \tag{5.14}$$

Since gas-wall and particle-wall frictions form a minor portion of the overall pressure drop, type of the friction factor does not have a major effect on the results. Here, the gas-wall friction factor, f_g, has been calculated from the Blasius formula (Fox et al., 2003):

$$f_p=\frac{0.316}{Re_g^{0.25}},\qquad Re_g\le 10^5 \tag{5.15}$$

and the particle-wall friction factor has been estimated using the correlation of Kanno and Saito (1969):

$$f_p=\frac{0.057}{2\upsilon_p}\left(gd_{st}\right)^{1/2} \tag{5.16}$$

In order to solve these equations, the solid circulation rate (G_p) is needed as an input. Since the system is not a real circulating fluidized bed, a pseudo-circulating rate may be calculated from the correlations proposed for the internally circulating fluidized bed. An internally circulating fluidized bed resembles the current case in that both of the systems involve flow of gas and solids between a fluidized bed at minimum fluidization conditions and a dilute bed (a riser in an internally circulating fluidized bed and a stream in the current case). The net rate of the particle exchange between two zones along the fluidized bed is considered to be trivial. The correlation of Jeon et al. (2008) has been used for this purpose:

$$\Delta P_{or} = 5.327 \times 10^3 \left(\frac{U_0}{U_{mf}} \right)^{0.520} \left(\frac{u_{st}}{U_{mf}} \right)^{0.795} \left(\frac{d_p}{d_{or}} \right)^{0.728} \tag{5.17}$$

$$G_p = C_{dis} \frac{S_{or}}{S_{st}} \sqrt{2\rho_p (1-\varepsilon_{mf}) \Delta P_{or}} \tag{5.18}$$

In the above equations, the orifice refers to the point at the bottom of the bed that allows for the exchange of gas and particles between the stream and non-stream zone. Since there is no experimental data for S_{or}, this parameter has been considered as a tuning factor.

For the pressure drop through the none-streaming zone which is considered to be at minimum fluidization conditions, the pressure drop is assumed to be due to the mass of the particle bed:

$$\frac{dp}{dz} = \rho_p g (1-\varepsilon_g) \tag{5.19}$$

5.4. Results and Discussions

The model predictions of pressure drop along the fluidized bed for a bed depth of 5 m are provided in Fig. 5.1. As can be seen in the figure, the model predicts a lower pressure drop immediately above the distributor for the non-stream zone compared to the case of the stream zone. Therefore streams do not form in this region. However, the stream pressure drop decreases dramatically with increasing distance from the distributor, which makes the streams a preferable pathway for the gas. The higher pressure drop of the stream at right over distributor is due to the much higher flow of gas and particles in the stream compared to the non-stream zone. Similar trend of pressure drop has been reported for the bottom of FCC risers (Pugsley and Berruti, 1996). As illustrated in the figure, as the upper surface of the bed is approached, the difference between the pressure drop of the streaming and non-streaming zones decreases. The result of this would be that preferential flow of gas through the stream would be diminished, allowing gas to diffuse into other parts of the bed and provide more uniform fluidization at upper regions. This is consistent with visual observations from experiments, which showed improved fluidization at the upper regions of the bed.

5.4.1. Effect of Bed Depth

Fig. 5.2 illustrates the differences between the pressure drops of stream and non-stream pathways at the bottom of the fluidized bed for different bed depths. As can be seen, the difference in the pressure drops of the two zones, which is considered to be the motivation for the formation and stability of the streams, increases with increasing bed depth. Experimentally we found that the onset of streaming flow occurred gradually in

the fluidized bed as bed depth was increased. According to the model results, this can be attributed to the gradual increase of the difference in pressure drop between the streaming and non-streaming zones. This difference is probably low enough in shallow beds that the gas is able to fluidize all of the cross section and prevents the formation or permanence of streaming flow.

5.4.2. Effect of Gas Velocity

Fig. 5.3 provides the axial profile of the pressure drop in the fluidized bed for different superficial gas velocities. As model results provided in Fig. 5.3 illustrate, two changes occur in the fluidized bed by increasing the gas velocity. Firstly, the difference between the pressure drops of the streaming and non-streaming zones decreases and secondly, the region expands above the distributor where streaming is not preferred or present. The positive influence of increasing the gas velocity on diminishing the streaming flow has been emphasized in all of the previous experimental works in the literature (Wells, 2001; Karri et al., 2004; Issangya et al., 2007; Karimipour and Pugsley, 2010). As the figure indicates, at gas velocities higher than 1 m/s streaming flow is not preferred anywhere in the fluidized bed and uniform fluidization would be possible throughout the bed. It should be noted that these high velocities are usually higher than the bubbling-turbulent transition velocity for Geldart A particles at normal conditions. Therefore, although a uniform fluidization may be achieved by increasing gas velocity, the bubbling regime may be bypassed for deep fluidized beds.

5.4.3. Effect of Particle Size

Fig. 5.4 illustrates the axial profile of the pressure drop in the fluidized bed for different particle sizes and a constant particle density of 1400 kg/m^3. As can be seen, the pressure drop in the stream increases by increasing the particle size. Thus, its preference as an alternative pathway with lower pressure drop for gas decreases gradually. According to the literature, streaming flow has only been reported for Geldart A particles; it does not appear to exist for coarser Geldart B particles. The results show that the model is able to predict this directional effect of increasing particle size.

5.4.4. Effect of Solid Circulating Rate

The stream pressure drop increases by increasing the solid circulating rate. Therefore, increasing this parameter may delay the streaming flow by decreasing the preference of streams over the non-stream regions. At the other hand, a lower value of solid circulating rate increases the possibility of streaming. Fig. 5.5 shows the effect of 20% lower and higher than the calculated value of solid circulating rate on the model predictions. As can be seen, the trend of the results remains unchanged for different values of solid circulating rate. Therefore, application of the presented correlation for solid circulating rate seems to be sufficient for the qualitative analyses discussed here, until a correlation for the solid circulation rate of the streaming fluidized beds is provided.

5.5. Conclusions

In the present work, gas streaming flow has been modeled in a deep fluidized bed of 5 m bed depth and 0.3 m diameter. The model predictions have been qualitatively compared and validated with the experimental findings. According to the model results, the stream

represents a low pressure drop region compared to other parts of the bed, which is the most likely reason for the formation and stability of the streaming flow. The influence of different parameters on the severity of the streaming flow is also evaluated with the model. The model results show that increasing the bed depth favors the streaming flow, while increasing the gas velocity increases the uniformity of the bed and decreases the streaming severity. Streaming flow was found to be less severe for larger particle sizes. All of these findings are in conformity with experimental investigations reported previously in the literature.

5.6. References

Fox, R.W., McDonald, A.T., Pritchard, P.J., 2003. Introduction to fluid mechanics, 6th edition; Wiley, New York.

Geldart, D., 1973. Types of gas fluidization. Powder Technology 7, 285-292.

Issangya, A., Knowlton, T., Karri, S.B.R., 2007. Detection of gas bypassing due to jet streaming in deep fluidized beds of group A particles. In: Fluidization XII, Berruti, F., Bi, X., Pugsley, T. (Eds.), Vancouver, British Columbia, Canada, May 13-17.

Jeon, J.H., Kima, S.D., Kim, S.J., Kang, Y., 2008. Solid circulation and gas bypassing characteristics in a square internally circulating fluidized bed with draft tube. Chemical Engineering and Processing 47, 2351-2360.

Kanno, H., Saito, S., 1969. Pneumatic conveying of solid through straight pipes, Journal of Chemical Engineering of Japan 2, 211-217.

Karimipour, S., Pugsley, T., 2010. Study of gas streaming in a deep fluidized bed containing Geldart' Group A particles. Chemical Engineering Science 65, 3508-3517.

Karimipour, S., Mostoufi, N., Sotudeh-Gharebagh, R., 2006. Modeling the hydrodynamics of downers by cluster-based approach. Industrial and Engineering Chemistry Research 45, 7204-7209.

Karri, S.B.R., Issangya, A.S., Knowlton, M., 2004. Gas bypassing in deep fluidized beds. In: Fluidization XI, Arena, U., Chirone, R., Miccio, M., Salatino, P. (Eds.), Ischia (Naples), Italy, May 9-14.

Mostoufi, N. Chaouki, J., 1999. Prediction of effective drag coefficient in fluidized beds. Chemical Engineering Science 54, 851-858.

Pugsley, T.S., Berruti F., 1996. A predictive hydrodynamic model for circulating fluidized bed risers. Powder Technology 89, 57-69.

Wells, J., 2001. Streaming flow in large scale fluidization, Paper presented at the AIChE annual meeting, Particle Technology Forum, Reno, Nevada, USA.

5.7. Nomenclature

A_p cross-sectional area of particle (m^2)

C_{dis} gas discharge coefficient

C_D effective drag coefficient

d_p particle diameter (m)

d_{st} stream diameter (m)

D fluidized bed diameter (m)

f drag coefficient correction factor

f_p solid-wall friction factor

f_g gas-wall friction factor

g acceleration of gravity (m/s^2)

G_p solids flux (kg/m^2s)

p pressure (Pa)

ΔP_{or} orifice pressure drop (Pa)

Re_g gas Reynolds number ($D\ U_0\ \rho_g/\mu_g$)

S_{or} orifices cross sectional area (m^2)

S_{st} stream cross sectional area (m^2)

t time (s)

U_0 superficial gas velocity (m/s)

U_{mf} minimum fluidization velocity (m/s)

u_{st} gas velocity in stream (m/s)

v_p particle velocity (m/s)

V_p particle volume (m^3)

z fluidized bed height above distributor (m)

Greek Letters

ε_g gas voidage

ε_p gas voidage

ε_{mf} voidage at minimum fluidization

ρ_g gas density (kg/m^3)

ρ_p particle density (kg/m^3)

μ gas viscosity (

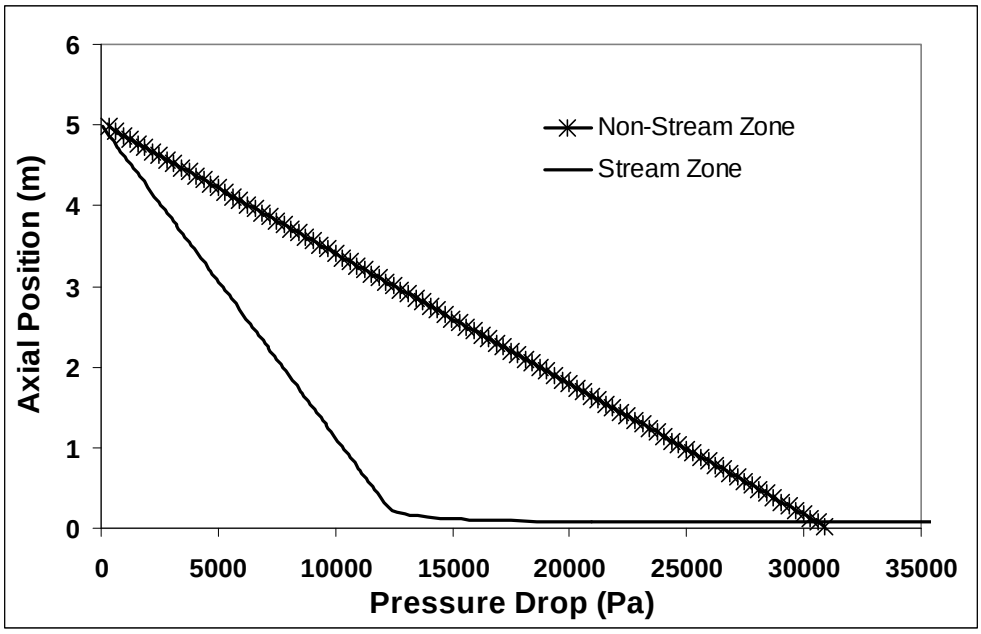

Figure 5.1. Axial profile of the pressure drop in the fluidized bed, Bed depth = 5 m, Superficial gas velocity = 0.2 m/s, Particle diameter = 84 microns

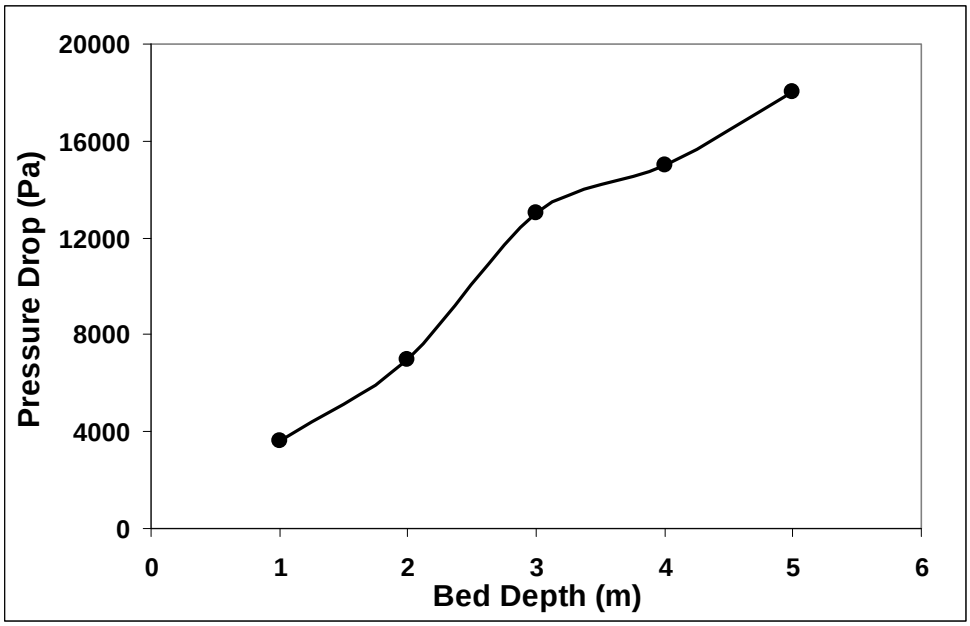

Figure 5.2. Difference between the pressure drop of Stream and Non-Stream pathways at the bottom of the fluidized bed for different bed depths, Superficial gas velocity = 0.2 m/s, Particle diameter = 84 microns

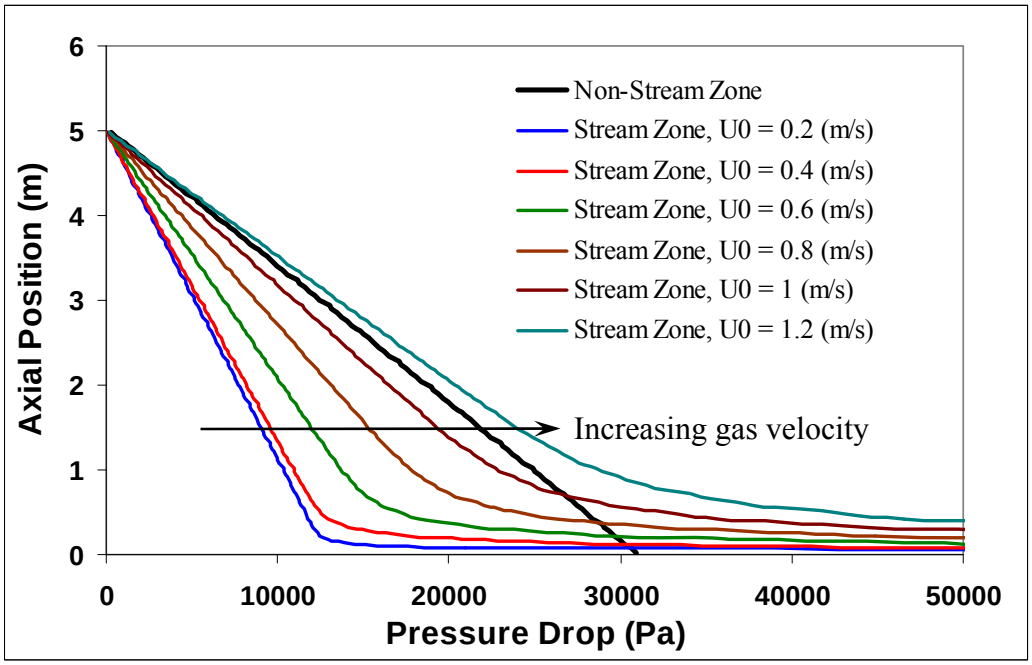

Figure 5.3. Axial profile of the pressure drop in the fluidized bed for different superficial gas velocities, Bed depth = 5 m, Particle diameter = 84 microns

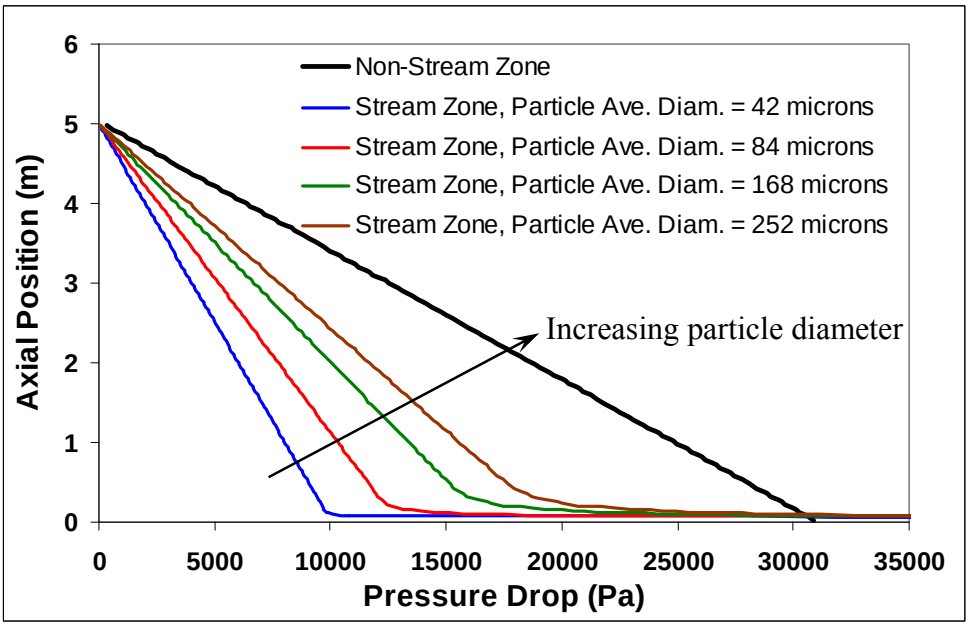

Figure 5.4. Axial profile of the pressure drop in the fluidized bed for different particle sizes, Bed depth = 5 m, Superficial gas velocity = 0.2 m/s

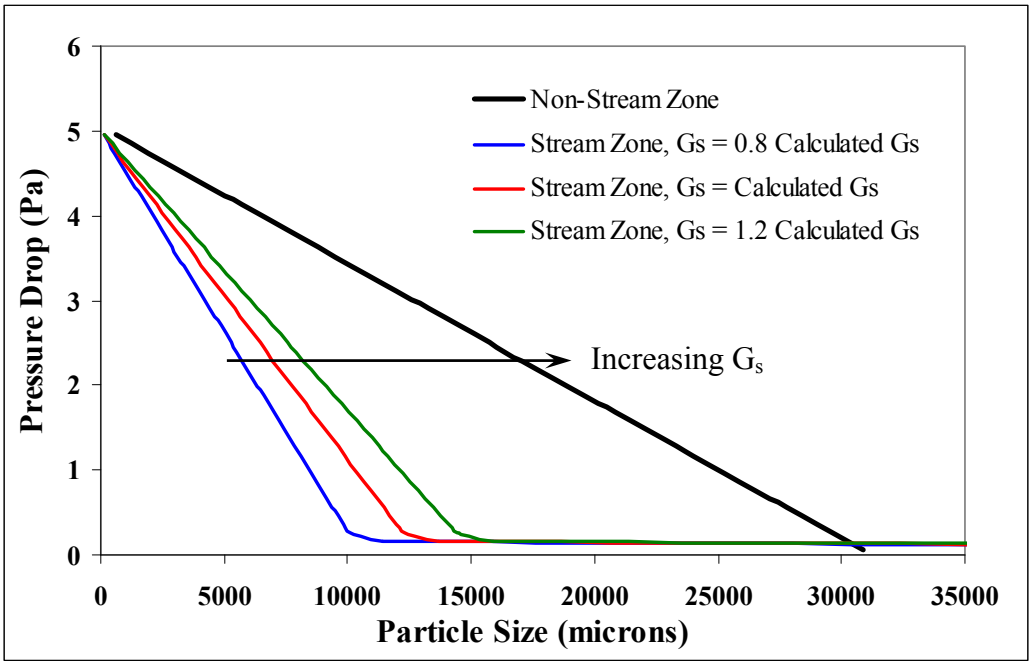

Figure 5.5. Effect of variation of Gs on the axial profile of pressure drop in the fluidized bed

CHAPTER 6 - Conclusions and Recommendations

6.1. Conclusions

The current project was designed and implemented to investigate the characteristics of gas-streaming phenomenon with a combination of experimental and modeling approaches. In the first phase of the experimental part, a series of experiments was conducted to study the effect of bed depth, superficial gas velocity, fines content, and distributor pressure drop on the streaming flow in a 0.3 m diameter fluidized bed. The analysis of the pressure fluctuations time series for bed depths ranging from 40 to 160 cm revealed that the normal bubbling fluidization is gradually compromised by increasing the bed depth. This conclusion is based on the gradual increase of the autocorrelation function, the decrease in the rate of decay of the autocorrelation function, and the disappearance of the dominant frequency in the PSD graph with increasing bed depth. The extent of streaming maldistribution was found to be non-uniform along the bed, with the quality of fluidization improving with increasing the distance above the distributor plate. Increasing the gas velocity from 10 to 50 U_{mf} was found to delay the streaming flow, likely due to the diffusion of additional gas into the poorly fluidized regions. This effect was observed to be more prominent at lower gas velocities. The analyses illustrated

that increasing the fines content from 3% to 20% can decrease the severity of the streaming flow. However, the improvement is not enough to solve the streaming problem. Finally, analyses did not show any significant effect of distributor design on the streaming phenomenon.

In order to further investigate the nature of streaming flow, several well-known configurations of gas flow into the fluidized bed (forced streaming, and jetting flows) was designed and compared to natural streaming flow in deep beds. The results of these studies revealed that there is no significant difference between the configurations for a fluidized bed with 40 cm bed depth. However, differences emerge by increasing the bed depth to 160 cm. It was found that natural streaming in a deep fluidized bed closely resembles the case of forced stream in which the gas flow is also present in the remaining regions of the distributor. The jet flows without the primary gas flow could be considered as the cases of severe streaming that might happen in very deep beds with possible formation of completely non-fluidized regions. Application of supporting jets with primary gas flow could enhance the fluidization quality to some extent. Increasing the primary gas velocity from 10 to 50 Umf was found to reduce the effect of supporting jets. It was also found that finer FCC particles provide a better fluidization quality. Wavelet analysis showed that even in deep fluidized beds that are dominated by the streaming flow, bubbling activity with the same dominant frequency as the shallow bed coexists, although with a minor contribution. These findings suggested that the streaming flow can be considered to form by increasing the relative importance of one of the available stream of bubbles compared to others as the bed depth increases.

Further study of the streaming flow was undertaken with computational fluid dynamic (CFD) simulations of the deep fluidized bed. In the present work, the commercial CFD codes FLUENT and MFIX were initially tested for the modeling of deep fluidized bed of Geldart A particles. However, simulation results did not show any sign of streaming flow in the fluidized bed. Subsequently, the commercial CFD code BARRACUDATM that has been claimed by the developers to be appropriate for this purpose, was tested. Due to the lack of data on the performance of this code, a simple case of modeling a freely bubbling fluidized bed of Geldart A particles was attempted first. For this purpose, four cases with three different grid sizes and two drag models have been simulated using the PIC approach. After simulating the bubbling fluidized bed, the bubble properties such as bubble size distribution, bubble rise velocity and bubble frequency as well as bed expansion and voidage profile have been calculated based on the simulation results. The results have been compared with commonly accepted correlations as well as experimental data provided in this work and from the literature. The results show a promising prediction capability of the multiphase PIC approach without any kind of modification in the drag model or other constituents of the model. The results indicate that although both grid size and drag model affect the simulation results, the effect of drag model is negligible compared to the effect of the grid size.

The BARRACUDA code was then used for simulating the deep fluidized bed of Geldart A particles. However, similar to the previous CFD codes tested, instead of streaming flow, bubbling fluidization was predicted. Therefore, a phenomenological model was

developed to better understand the streaming flow. According to the model results, the stream represents a low pressure drop region compared to other parts of the bed, which is the most likely reason for the formation and stability of the streaming flow. The influence of different parameters on the severity of the streaming flow is also evaluated with the model. The model results show that increasing the bed depth favors the streaming flow, while increasing the gas velocity increases the uniformity of the bed and decreases the streaming severity. Streaming flow was found to be less severe for larger particle sizes. All of these findings are in conformity with experimental investigations reported previously in the literature.

6.2. Recommendations

Many aspects of the gas streaming flow in deep fluidized beds of Geldart A particles have been studied in the context of the present project. However, several areas still exist that need to be investigated. Some of these proposed areas of research are:

- Providing a series of pressure transducers along the column in at least two angles and two radial positions. These arrangements enable us to simultaneously compare the hydrodynamics of several regions of the inside of the bed and detect possible non-uniformities. Also the pressure drop along the column in stream and non-stream areas can be calculated and used for a quantitative evaluation of the modeling results discussed in chapter 5.

- Equipping the column with more elaborate solid recycling equipment such as a series of external cyclones to be able to perform experiments at higher gas velocities.

- Repeating the experiments with other types of gas distributors, such as tuyers, bubble caps and Dutch weaves and evaluate their effects on streaming flow.

- One approach which is followed to enhance the flow of solids in stand-pipes is to consider several aeration nozzles along the column. The effectiveness of this approach and other approaches such as baffling in case of streaming flow can be tested.

- Fluidized beds have been frequently modeled by considering the emulsion and bubble phases as a series of CSTR and plug flow reactors, respectively, in the literature. This approach can be examined for modeling the streaming flow where the properties of these two phases will be determined from the non-fluidized and stream regions instead of emulsion and bubbles. The effect of streaming flow on the conversion rate in the fluidized bed reactors can be investigated.

- In the present study, only the pressure fluctuations measurement was used for investigating the fluidized bed hydrodynamics. Other types of measurement techniques which can provide more direct views of the hydrodynamic regimes in the fluidized bed such as ECT, fiber optic and capacitance probes can be tested.

- The CFD modeling of the streaming flow was followed as part of the present study. Different commercial CFD softwares such as FLUENT, MFIX and BARRACUDA in their original form were found to be unable to reveal the streaming flow in deep fluidized beds. Some types of modifications such as modifying the drag function and body force, as has been claimed by previous authors to be appropriate for accounting the effect of inter-particle forces, were attempted, but satisfactory results were not achieved. A separate project can be defined on seeking the appropriate method to consider the effect of inter-particle forces in one of the available CFD models to capture the streaming flow in deep beds.

- The effect of fines content of particles on the streaming flow was studied in the present work. The effect of adding coarse particles can also be studied. It is clear that coarser particles have a higher inter-particles pore size and voidage, thus gas can better diffuse into a bed of these particles. Adding some of these particles into the particle size distribution may enhance the uniform fluidization and decrease the streaming flow. This claim should be investigated in future studies.

- Effect of system pressure on the behavior of deep fluidized beds should be studied.